Politechnika Poznańska

Wydział Inżynierii Środowiska i Energetyki
Instytut Elektroenergetyki
Zakład Urządzeń Rozdzielczych i Instalacji Elektrycznych

Rozprawa doktorska

Karol Nowak

ELIMINOWANIE ŁUKU AWARYJNEGO I OGRANICZANIE SKUTKÓW ZWARCIOWYCH Z WYKORZYSTANIEM ŁĄCZNIKÓW HYBRYDOWYCH

Promotor: dr hab. inż. Jerzy Janiszewski, prof. PP

Promotor pomocniczy: dr inż. Grzegorz Dombek

Poznań, 2022

Spis treści

1. Streszczenie w języku polskim…… 3
2. Streszczenie w języku angielskim……... 4
3. Wykaz głównych publikacji naukowych stanowiących rozprawę doktorską……. 5
4. Wykaz dodatkowych prac związanych z rozprawą doktorską…… 7
5. Wykaz pozostałego dorobku naukowego…… 8
   5.1. Pozostałe publikacje……. 8
   5.2. Udział w konferencjach naukowych…… 8
   5.3. Inne osiągnięcia w działalności naukowej i organizacyjnej…… 9
6. Opis osiągnięcia naukowego……... 10
   6.1. Wprowadzenie…….. 10
   6.2. Cel i hipoteza badawcza pracy…….. 13
   6.3. Zakres i metodyka przeprowadzonych badań……... 14
      6.3.1. Autorska metoda rozwiązania problemu naukowego……..... 14
      6.3.2. Zakres prac prowadzących do rozwiązania problemu badawczego……..… 14
      6.3.3. Źródła zasilania i przyrządy pomiarowe stosowane podczas prac badawczych……..… 19
   6.4. Wyniki badań skuteczności działania łącznika hybrydowego……..… 21
      6.4.1. Ograniczanie oddziaływań elektrodynamicznych prądów zwarciowych w obwodach zabezpieczonych łącznikiem hybrydowym……..... 21
      6.4.2. Ograniczanie erozji torów prądowych poddanych działaniu łuku elektrycznego……...… 22
      6.4.3. Ograniczenie zagrożeń powodowanych akustycznym oddziaływaniem łuku elektrycznego……..…..... 24
      6.4.4. Ograniczenie zagrożeń powodowanych wzrostem ciśnienia w zamkniętych obudowach urządzeń elektrycznych…….……... 26
      6.4.5. Ograniczenie strefy rażenia łukiem elektrycznym……..…. 29
   6.5. Wnioski i praktyczne znaczenie pracy doktorskiej……. 31
   6.6. Literatura…… 32
7. Kopie publikacji naukowych stanowiących rozprawę doktorską ……... 35
   Oświadczenia o współautorstwie……. 113

1. STRESZCZENIE W JĘZYKU POLSKIM

Jedną z najczęściej spotykanych odmian zwarć elektrycznych stanowią zwarcia łukowe, w których palący się łuk określany jest mianem łuku zakłóceniowego lub łuku awaryjnego. Zwarcia te, z uwagi na bezpośrednie zagrożenie zdrowia lub nawet życia osób znajdujących się w pobliżu awarii, stanowią jedne z najpoważniejszych stanów awaryjnych w jakich mogą znaleźć się urządzenia rozdzielcze. Nie bez znaczenia są również ogromne straty materialne wywołane niszczącym działaniem łuku awaryjnego i niezbędnym przestojem naprawczo-konserwacyjnym.

Celem niniejszej pracy było opracowanie koncepcji eliminowania łuku awaryjnego i ograniczania skutków zwarciowych z wykorzystaniem łączników hybrydowych. Takie łączniki, stanowiące połączenie elementów półprzewodnikowych i zwiernika mechanizmowego, mogą zostać wykorzystane do budowy szybkiego eliminatora łuku elektrycznego o dużej obciążalności prądowej.

Opracowano autorski model łącznika hybrydowego, a następnie w oparciu o sporządzaną dokumentację techniczną podpartą symulacjami komputerowymi, zbudowano urządzenie prototypowe w kilku rozwiązaniach konfiguracyjnych. Wielkoprądowe badania eksperymentalne z wykorzystaniem zbudowanego urządzenia wykazały, że jest możliwe:

- gaszenie i skrócenie czasu palenia się łuku elektrycznego,
- zmniejszenie ilości energii wydzielanej w łuku,
- ograniczanie oddziaływań elektrodynamicznych prądów zwarciowych,
- ograniczanie erozji torów prądowych poddanych działaniu łuku elektrycznego,
- ograniczenie zagrożeń powodowanych akustycznym oddziaływaniem łuku elektrycznego,
- ograniczenie wzrostu ciśnienia gazów wewnątrz zamkniętych obudów urządzeń elektrycznych powstających w wyniku zapłonu łuku elektrycznego,
- znaczne skrócenie czasu oddziaływania skutków cieplnych w zabezpieczanym obwodzie,
- zmniejszenie niebezpiecznej strefy rażenia łukiem elektrycznym.

Uzyskane wyniki badań potwierdzają, że przez dobór odpowiedniej konfiguracji sekcji półprzewodnikowych i współpracującego z nimi łącznika mechanicznego możliwe jest wykonanie szybkiego łącznika hybrydowego, który pracując jako zwiernik skutecznie eliminującego łuk elektryczny oraz efektywnie ograniczającego skutki zwarciowe mogące występować w dotkniętych awarią wielkoprądowych obwodach elektroenergetycznych.

2. STRESZCZENIE W JĘZYKU ANGIELSKIM

One of the most common types of electrical short-circuits are arc faults, in which the burning arc is called the emergency arc or the interfering arc. These short-circuits are one of the most serious failure states in which switching devices can be found, due to the direct threat to the health or even life of people in the vicinity of the failure. The huge property losses caused by the destructive effects of the fault arc and the necessary downtime for repair and maintenance are also not insignificant.

The purpose of this work was to develop a concept for eliminating emergency arcing and reducing short-circuit effects using hybrid switches. Such switches are a combination of semiconductor elements and a mechanical short-circuiting switch, can be used to build a fast electric arc eliminator with high conduction current.

A proprietary model of the hybrid switch was developed, and then, based on the prepared technical documentation and computer simulations, a prototype device was made in several configuration solutions. High-current experimental tests using the built device showed that it is possible:

- extinguishing and shortening the burning time of the electric arc,
- reducing the amount of energy released in the arc,
- limiting electrodynamic effects of short-circuit currents,
- limiting the erosion of current paths as a result of the action of an electric arc,
- reduction of acoustic hazards as a result of the impact of an electric arc,
- limiting the increase in gas pressure inside the closed enclosures of electrical equipment resulting from arc ignition,
- significant reduction of the time of thermal effects in the protected circuit,
- reducing the danger zone of an electric arc.

The obtained test results confirm that by selecting the appropriate configuration of the semiconductor sections and the mechanical switch device cooperating with them, it is possible to make a quick hybrid short-circuiting switch that effectively eliminates the electric arc and effectively reduces the short-circuit effects that may occur in high-current power circuits affected by the failure.

3. WYKAZ GŁÓWNYCH PUBLIKACJI NAUKOWYCH STANOWIĄCYCH ROZPRAWĘ DOKTORSKĄ

Publikacja I: Karol Nowak, Jerzy Janiszewski, Grzegorz Dombek: „Thyristor Arc Eliminator for Protection of Low Voltage Electrical Equipment", *Energies 2019*, 12(14), 2749;

- liczba punktów zgodna z wykazem MEiN – 140 pkt.,
- Impact Factor w roku publikacji – 2.707,
- 5-letni Impact Factor – 3.333,
- liczba cytowań wg ResearchGate – 3,
- wkład indywidualny w pracę: 60%.

https://doi.org/10.3390/en12142749

Karol Nowak był odpowiedzialny za przygotowanie stanowiska badawczego, opracowanie koncepcji i metodyki badań. Przeprowadził indywidualnie większość zaplanowanych, laboratoryjnych prac badawczych. Zarejestrował wyniki badań, a następnie opracował je w postaci tabel i wykresów. Dokonał szerokiej analizy wpływu zmiany charakteru obciążenia na czas gaszenia łuku elektrycznego za pomocą tyrystorowego eliminatora łuku. Był odpowiedzialny za przegląd tematycznie związanych artykułów naukowych, opracowanie pierwszej wersji manuskryptu oraz udzielenie odpowiedzi na recenzje.

Publikacja II: Karol Nowak, Jerzy Janiszewski, Grzegorz Dombek: „A Multi-Sectional Arc Eliminator for Protection of Low Voltage Electrical Equipment", *Energies 2020*, 13(3), 605;

- liczba punktów zgodna z wykazem MEiN – 140 pkt.,
- Impact Factor w roku publikacji – 3.004,
- 5-letni Impact Factor – 3.333,
- liczba cytowań wg ResearchGate – 2,
- wkład indywidualny w pracę: 60%.

https://doi.org/10.3390/en13030605

Karol Nowak był odpowiedzialny za przygotowanie stanowiska badawczego, opracowanie koncepcji i metodyki badań. Przeprowadził indywidualnie większość zaplanowanych, laboratoryjnych prac badawczych. Dla kilku autorskich rozwiązań eliminatora łuku zarejestrował serie wyników badań, a następnie opracował je w postaci tabel i wykresów. Był odpowiedzialny za przegląd tematycznie związanych artykułów naukowych, opracowanie pierwszej wersji manuskryptu oraz udzielenie odpowiedzi na recenzje.

Publikacja III: Karol Nowak, Jerzy Janiszewski, Grzegorz Dombek: „The Possibilities to Reduce Arc Flash Exposure with Arc Fault Eliminators", *Energies 2021*, 14(7), 1927;

- liczba punktów zgodna z wykazem MEiN – 140 pkt.,
- Impact Factor w roku publikacji – 3.252,

- 5-letni Impact Factor – 3.333,
- liczba cytowań wg ResearchGate – 3,
- wkład indywidualny w pracę: 60%.

https://doi.org/10.3390/en14071927

Karol Nowak był odpowiedzialny za opracowanie sposobu rejestracji i metodyki badań oddziaływań łuku elektrycznego w awaryjnych stanach pracy sieci elektroenergetycznej. Przeprowadził indywidualnie większość zaplanowanych, laboratoryjnych prac badawczych, a także zebrał oraz dokonał analizy zarejestrowanych przebiegów i rejestracji fotograficznych. Wykonał obliczenia matematyczne związane z energią łuku elektrycznego i niebezpieczną strefą jego rażenia. Był odpowiedzialny za przegląd tematycznie związanych artykułów naukowych, opracowanie pierwszej wersji manuskryptu oraz udzielenie odpowiedzi na recenzje.

Publikacja IV: Karol Nowak, Jerzy Janiszewski, Grzegorz Dombek: „A New Short-Circuit Hybrid Device for the Protection of Low-Voltage Networks From the Effects of an Arc Fault", *IEEE Access 2022*, vol. 10, pp. 88678-88691;

- liczba punktów zgodna z wykazem MEiN – 100 pkt.,
- Impact Factor w roku publikacji – 3.476,
- 5-letni Impact Factor – 4.676,
- liczba cytowań wg ResearchGate – 0,
- wkład indywidualny w pracę: 80%.

https://doi.org/10.1109/ACCESS.2022.3199011

Karol Nowak był odpowiedzialny za opracowanie koncepcji i metodyki badań ograniczania skutków oddziaływania łuku awaryjnego i przepływu prądów zwarciowych. Przeprowadził indywidualnie większość zaplanowanych, laboratoryjnych prac badawczych. Zarejestrował wyniki badań, a następnie opracował je w postaci tabel i wykresów. Wykonał obliczenia matematyczne związane z elektrodynamiką torów prądowych, erozją materiałową oraz natężeniem dźwięku w otoczeniu wielkoprądowego łuku elektrycznego. Był odpowiedzialny za przegląd tematycznie związanych artykułów naukowych, opracowanie pierwszej wersji manuskryptu oraz udzielenie odpowiedzi na recenzje.

Sumaryczna liczba punktów - 520
Indywidualny wkład punktowy doktoranta - 332
Sumaryczny współczynnik oddziaływania IF - 12.439
Sumaryczna liczba cytowań - 8

4. WYKAZ DODATKOWYCH PRAC ZWIĄZANYCH Z ROZPRAWĄ DOKTORSKĄ

Artykuły naukowe, patent i zgłoszenie patentowe, które nie są częścią rozprawy, ale miały istotne znaczenie dla realizacji tematu rozprawy:

Praca V: Karol Nowak: „Mikroprocesorowy sterownik tyrystorowy", Poznan University of Technology Academic Journals. Electrical Engineering - 2018, Issue 95, pp. 77-86
http://dx.doi.org/10.21008/j.1897-0737.2018.95.0008

Praca VI: Karol Nowak, Jerzy Janiszewski, Andrzej Książkiewicz: „Wielkoprądowe syntetyczne źródło do badań zwarciowych", Kalejdoskop I, monografia konferencyjna 2021, wydawnictwo Cekona, s. 104-119
https://cekona.pl/myfiles/cogito1/monografia_cogito1.pdf

Praca VII: Andrzej Książkiewicz, Grzegorz Dombek, Karol Nowak: „Electrodynamic Contact Bounce Induced by Fault Current in Low-Voltage Relays", Energies 2019, 12(20), 3926
https://doi.org/10.3390/en12203926

Praca VIII: Andrzej Książkiewicz, Grzegorz Dombek, Karol Nowak: „Change in Electric Contact Resistance of Low-Voltage Relays Affected by Fault Current", Materials 2019,12(13), 2166
https://doi.org/10.3390/ma12132166

Praca IX: Karol Nowak, Jerzy Janiszewski, Łukasz Drużyński: „Półprzewodnikowy eliminator łuku elektrycznego w układach niskiego napięcia", Kalejdoskop I, monografia konferencyjna 2021, wydawnictwo Cekona, s. 120-146
https://cekona.pl/myfiles/cogito1/monografia_cogito1.pdf

Patent I: Jerzy Janiszewski, Karol Nowak: „Układ zwiernika hybrydowego", data zgłoszenia: 29.11.2018, **nr zgłoszenia P.427948**
https://ewyszukiwarka.pue.uprp.gov.pl/search/pwp-details/P.427948?lng=pl

Zgłoszenie patentowe I: Jerzy Janiszewski, Karol Nowak: „Układ zwiernika hybrydowego", data zgłoszenia: 29.11.2018, **nr zgłoszenia P.427947**
https://ewyszukiwarka.pue.uprp.gov.pl/search/pwp-details/P.427947?lng=pl

5. WYKAZ POZOSTAŁEGO DOROBKU NAUKOWEGO

5.1. Pozostałe publikacje

1. Jerzy Janiszewski, *Karol Nowak*: „Procesy cieplne w zestykach łączników próżniowych podczas przewodzenia prądów zwarciowych”, Poznan University of Technology Academic Journals. Electrical Engineering - 2017, Issue 90, pp. 125-136

2. *Karol Nowak*, Grzegorz Dombek, Andrzej Książkiewicz, Bartosz Bochenek, Piotr Nowaczyk, Paweł Pluta: „Zastosowanie przekaźników PLC do realizacji algorytmów sterowania ogrzewaniem”, Poznan University of Technology Academic Journals. Electrical Engineering - 2017, Issue 92, pp. 415-425

3. *Karol Nowak*: „Zastosowanie przekaźników programowalnych w automatyce budynkowej”, Poznan University of Technology Academic Journals. Electrical Engineering - 2017, Issue 92, pp. 427-438

5.2. Udział w konferencjach naukowych

1. *Karol Nowak*, Jerzy Janiszewski, Andrzej Książkiewicz, Wielkoprądowe syntetyczne źródło do badań zwarciowych. Interdyscyplinarna konferencja naukowa MIRATIO, 16.10.2021, CKN, Polska. Ustne wystąpienie autora

2. *Karol Nowak*, Jerzy Janiszewski, Łukasz Drużyński, Półprzewodnikowy eliminator łuku elektrycznego w układach niskiego napięcia. Interdyscyplinarna konferencja naukowa MIRATIO, 16 październik 2021, CKN, Polska. Ustne wystąpienie autora

3. *Karol Nowak*, Mikroprocesorowy sterownik tyrystorowy. XXIII Scientific Conference Computer Applications in Electrical Engineering ZKwE'2018, 23 – 24 wrzesień 2018, Poznań, Polska. Poster

4. *Karol Nowak*, Zastosowanie przekaźników programowalnych w automatyce budynkowej. XXII Scientific Conference Computer Applications in Electrical Engineering ZKwE'2017, 10 – 11 kwiecień 2017, Poznań, Polska. Poster

5. *Karol Nowak*, Grzegorz Dombek, Andrzej Książkiewicz, Bartosz Bochenek, Piotr Nowaczyk, Paweł Pluta, Zastosowanie przekaźników programowalnych w automatyce budynkowej. XXII Scientific Conference Computer Applications in Electrical Engineering ZKwE'2017, 10 – 11 kwiecień 2017, Poznań, Polska. Poster

6. Jerzy Janiszewski, *Karol Nowak*, Procesy cieplne w zestykach łączników próżniowych podczas przewodzenia prądów zwarciowych. XXII Scientific Conference Computer Applications in Electrical Engineering ZKwE'2017, 10 – 11 kwiecień 2017, Poznań, Polska. Poster.

5.3. Inne osiągnięcia w działalności naukowej i organizacyjnej

Osiągnięcia w działalności naukowej i organizacyjnej:

- złożenie wniosku o finansowanie projektu badawczego NCN Preludium 20 „Eliminacja łuku awaryjnego i ograniczenie skutków zwarciowych w układach zasilania niskiego napięcia przy wykorzystaniu wielosekcyjnego kaskadowego ultraszybkiego zwiernika hybrydowego", 2021,
- złożenie wniosku o finansowanie projektu badawczego NCN Preludium 19 „Eliminacja łuku awaryjnego i ograniczenie skutków zwarciowych w układach zasilania niskiego napięcia przy wykorzystaniu wielosekcyjnego kaskadowego ultraszybkiego zwiernika hybrydowego", 2020,
- złożenie wniosku o finansowanie projektu badawczego NCN Preludium 17 „Ograniczenie skutków prądu zwarciowego w układach niskiego napięcia z wykorzystaniem wielosekcyjnego kaskadowego ultraszybkiego zwiernika hybrydowego", 2018,
- Nagroda Rektora Politechniki Poznańskiej za osiągnięcia dydaktyczne przyznana przez Rektora PP prof. dr. hab. inż. Teofila Jesionowskiego w dniu 6 października 2021 r.,
- List gratulacyjny dla wyróżniającego się nauczyciela akademickiego przyznany przez Dziekana WIŚiE prof. dr. hab. inż. Zbigniewa Nadolnego w dniu 22 stycznia 2021 r.,
- w latach 2016 – 2019 pełnienie funkcji opiekuna koła naukowego Electronus działającego w Instytucie Elektroenergetyki,
- w latach 2019 – 2020 pełnienie funkcji opiekuna praktyk dla studentów kierunku Energetyka,
- udział w projektach badawczych:
  - „Procesy cieplne w zestykach podczas przewodzenia prądów zwarciowych", 04/41/DSMK/4305 - 2017,
  - „Ograniczanie skutków łukowych i zwarciowych w obwodach i urządzeniach elektroenergetycznych", 04/41/SBAD/4408 - 2019,
  - „Stany cieplne w torach prądowych łącznika hybrydowego", 0711/SBAD/4417 - 2020,
  - „Skutki energetyczne łuku awaryjnego", 0711/SBAD/4470 – 2021.

6. OPIS OSIĄGNIĘCIA NAUKOWEGO

6.1. Wprowadzenie

Jedną z najczęściej spotykanych odmian zwarć elektrycznych stanowią zwarcia łukowe, w których palący się łuk określany jest mianem łuku zakłóceniowego lub łuku awaryjnego. Zwarcia te stanowią jedne z najpoważniejszych stanów awaryjnych, w jakich mogą znaleźć się urządzenia rozdzielcze, z uwagi na bezpośrednie zagrożenie zdrowia lub nawet życia osób znajdujących się w bezpośrednim sąsiedztwie awarii oraz znaczne straty materialne wywołane niszczącym działaniem łuku awaryjnego [1-3].

Występowaniu elektrycznego łuku awaryjnego może towarzyszyć (nawet w odległości kilku metrów od źródła łuku) m.in. bardzo wysoka temperatura, oślepiający błysk światła, gwałtowne rozprzestrzenianie się plazmy i gorącego powietrza otaczającego wyładowanie, gwałtowna zmiana ciśnienia powietrza lub innego gazu izolacyjnego, fala dźwiękowa o dużym natężeniu (przekraczającym nawet 160 dB), emisja we wszystkich kierunkach gorących odłamków i stopionych drobin metalu, wydzielanie dużych ilości toksycznych gazów, czy też powstanie przewodzących warstw na powierzchniach materiałów [4-6].

Nie mniej istotne z punktu widzenia przepływu prądu o dużej wartości jest silne nagrzewanie torów prądowych, powstawanie dużych sił dynamicznych między elementami, w których płyną prądy zwarciowe, niszczenie konstrukcji wsporczych urządzeń elektroenergetycznych, powstanie zakłóceń elektromagnetycznych, a nawet możliwość utraty stabilności systemu (np. przez utratę synchronizacji generatorów) [7-9].

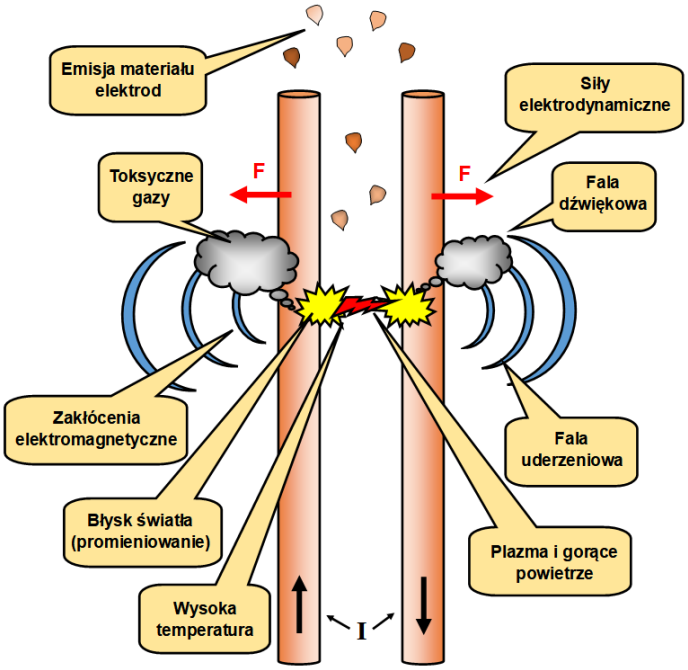

Rys. 1. Możliwe skutki zapłonu łuku elektrycznego i przepływu prądu zwarciowego.

Zobrazowanie zagrożeń jakie mogą wystąpić podczas zapłonu łuku elektrycznego i przepływie prądu zwarciowego przedstawiono na rysunku 1. Zagrożenie powodowane wyładowaniem łukowym zależy od energii zakłócenia. Na wartość energii łuku ma wpływ napięcie, prąd, czas trwania wyładowania łukowego, a także odległość od źródła łuku. Dla układów trójfazowych większość zwarć łukowych rozpoczyna się jako zwarcia jednofazowe, a następnie rozwija się w zwarcia trójfazowe, co powoduje znaczny wzrost uwalnianej energii. Podkreśla

to znaczenie wczesnego wykrycia łuku w celu szybkiego usunięcia zakłócenia łukowego i ograniczenia skutków zwarciowych [10].

Przyczyny wypadków związanych z łukiem elektrycznym są różne. Najczęściej występujące to: błędy ludzkie, złe połączenia, nieprawidłowo dobrane przyrządy, błędnie zaprojektowane urządzenia elektroenergetyczne, brak przeglądów i konserwacji, korozja elementów konstrukcji, starzenie materiałów izolacyjnych, przepięcia czy nawet udział zwierząt [11,12]. Do jednych z najczęstszych i najbardziej niebezpiecznych wypadków związanych z łukiem elektrycznym, dochodzi w sytuacji prac konserwacyjnych lub instalacji urządzeń w rozdzielnicy elektrycznej. Odbywa się to zwykle przy otwartych drzwiach szafy rozdzielczej [13]. W tej sytuacji nawet łukoochronna konstrukcja rozdzielnicy nie może spełniać swojego zadania.

Nie tylko w obwodach wielkoprądowych łuk elektryczny może stanowić zagrożenie dla osób i mienia. Równie niebezpieczne może okazać się zakłócenie łukowe, występujące w układach zasilania niskiego napięcia i „dostępnych" tam sieciowych prądach zwarciowych. Na rysunku 2 przedstawiono reprezentatywną sekwencję kadrów rejestracji filmowej dla łuku awaryjnego palącego się w instalacji elektrycznej o napięciu znamionowym 230/400 V. Opis przebiegu zdarzenia oraz analizę efektywności eliminacji łuku przedstawiono w **Publikacji III** rozprawy. W wyniku zapłonu łuku elektrycznego następuje wzrost ciśnienia wewnątrz obudowy elektrycznej puszki instalacyjnej (aż do jej rozszczelnienia), powstanie ogłuszającej fali akustycznej, gwałtowny wzrost temperatury, wyrzut do otoczenia produktów pierwotnych i wtórnych łuku awaryjnego w postaci par metali i kropli pochodzących z erozji elektrod. Zanik wyładowania elektrycznego w 25 ms nie oznacza wcale końca niebezpieczeństwa stworzonego wystąpieniem łuku awaryjnego. Eksplodujący materiał z elektrod stwarza realne zagrożenie oparzeniem i pożarem nawet po upływie ok 500 ms od chwili zgaszenia łuku elektrycznego, czego przykładem jest ostatnia klatka przedstawionej rejestracji, na której nadal widoczne są rozgrzane krople metalu.

Często stosowane praktyczne zasady ochrony łukowej, polegają na zwiększeniu odległości od miejsca wystąpienia wyładowania lub zapewnieniu mechanicznej bariery między operatorem (osobą), a łukiem oraz skróceniu czasu trwania zakłócenia lub zmniejszeniu prądu łuku [14,15]. W przypadku konieczności przebywania pracowników technicznych w pobliżu urządzeń narażonych na wystąpienie wyładowania łukowego (np. podczas prac konserwacyjnych rozdzielnic elektrycznych) dla zapewnienia ich bezpieczeństwa, stosuje się ochronę pasywną lub aktywną [14-16].

Pasywnymi środkami zmniejszającymi zagrożenie powodowane łukiem elektrycznym jest sprzęt ochrony osobistej, urządzenia wysuwne i rozdzielnice łukoodporne z urządzeniami obniżającymi ciśnienie. Z punktu widzenia bezpieczeństwa, rozdzielnica łukoodporna zapewnia ochronę personelu tylko w przypadku zamkniętych drzwi rozdzielnicy. Należy jednak mieć na uwadze, że podczas prac konserwacyjnych lub rozruchowych drzwi

rozdzielnicy elektrycznej są najczęściej otwarte, a więc nie ma ochrony przed skutkami łuku awaryjnego [17].

Aktywna ochrona polega na ograniczeniu prądu zwarciowego lub ograniczeniu czasu trwania wyładowania łukowego. Ograniczenie prądu w miejscu zwarcia, można zrealizować dobierając w obwodach zasilania transformatory o wysokiej wartości napięcia zwarcia lub stosując dławiki ograniczające prąd. Dużym mankamentem takiej ochrony jest zwiększony koszt wytwarzania tych elementów oraz straty energii. Szerzej stosowaną metodą jest instalowanie bezpieczników, które zapewniają nie tylko ograniczenie prądu, ale także szybką eliminację zakłócenia. Niestety, poważną wadą tego typu zabezpieczenia jest to, że ich szybkość działania uzależniona jest od wartości przepływającego prądu. Palący się łuk elektryczny przy prądach przeciążeniowych może doprowadzić do znacznego wydłużenia czasu zadziałania bezpiecznika, a przy prądzie znamionowym nawet do jego braku zadziałania [18].

Rys. 2. Kluczowe klatki rejestracji zapłonu i rozwoju wyładowania łukowego (I_m = 1250A, U = 400V) **[Publikacja III, fig. 10].**

Korzystnym rozwiązaniem z punktu widzenia obwodu zasilania jest metoda ograniczająca czas łukowy [19]. Eliminatory łuku wyposażone w energoelektroniczne łączniki wykonawcze, włączane do obwodu jako układy bocznikujące obwód elektryczny powyżej miejsca dotkniętego zakłóceniem, spełniają warunek skrócenia czasu łukowego i mogą być wykorzystane do efektywnej ochrony obwodów przed skutkami powstania łuku awaryjnego, zwarciowego, a także palącego się przy prądach roboczych i przeciążeniowych [20].

W przedstawianej dysertacji skupiono się głównie na wykorzystaniu innowacyjnego, autorskiego opracowania łącznika hybrydowego, który pracując w układzie bocznikującym miejsce dotknięte stanem awaryjnym ma za zadanie eliminację łuku awaryjnego i ograniczanie skutków zwarciowych.

6.2. Cel i hipoteza badawcza pracy

Celem niniejszej pracy było opracowanie koncepcji eliminowania łuku awaryjnego i ograniczania skutków zwarciowych z wykorzystaniem łącznika hybrydowego. Taki łącznik, stanowiący połączenie elementów półprzewodnikowych i zwiernika mechanizmowego, mógłby zostać wykorzystany do budowy szybkiego eliminatora łuku elektrycznego o dużej obciążalności prądowej.

Jednym z wielu rozwiązań konstrukcyjnych eliminatorów łuku są układy bocznikujące. Zaletą tych urządzeń, w porównaniu z układami wyłączającymi, jest duża szybkość działania. Opracowana konstrukcja łącznika hybrydowego jest układem bocznikującym zakłócenie powyżej miejsca jego wystąpienia. Stanowi ona połączenie wielu półprzewodnikowych gałęzi zwierających i łącznika mechanizmowego (zwiernika).

Spodziewane efekty celu badawczego związane z wykorzystaniem łącznika hybrydowego to:

- praktycznie bezzwłoczne eliminowanie łuku awaryjnego w uszkodzonym obwodzie,
- skrócenie czasu oddziaływania skutków cieplnych w zabezpieczanym obwodzie,
- ograniczenie oddziaływania elektrodynamicznego prądów zwarciowych,
- ograniczenie erozji torów prądowych poddanych działaniu łuku elektrycznego,
- ograniczenie zagrożenia powodowanego akustycznym oddziaływaniem łuku elektrycznego,
- ograniczenie wzrostu ciśnienia gazów wewnątrz zamkniętych obudów urządzeń elektrycznych powstającego w wyniku zapłonu łuku elektrycznego,
- zmniejszenie niebezpiecznej strefy rażenia łukiem elektrycznym.

Główna hipoteza badawcza przyjęta w dysertacji zakłada, że przy aktualnym stanie wiedzy, istnieją techniczne możliwości opracowania konstrukcji łącznika hybrydowego, pozwalającego na szybkie i skuteczne eliminowanie awaryjnego łuku elektrycznego oraz

efektywne ograniczanie skutków powodowanych wyładowaniami łukowymi i przepływami prądów zwarciowych.

W ramach realizacji wyżej przedstawionego celu rozprawy doktorskiej oraz weryfikacji postawionej hipotezy, przeprowadzone badania koncentrowały się na powiązanych ze sobą cząstkowych etapach badawczych:

- sprawdzenie możliwości wykorzystania przeciwsobnie połączonych tyrystorów i autorskiego rozwiązania programowalnego sterownika mikroprocesorowego w charakterze eliminatora łuku elektrycznego oraz analiza efektywności działania zabezpieczenia łukoochronnego dla zmiennego charakteru obciążenia. Zagadnienia te przedstawiono w **Publikacji I** i pracy V,
- zwiększenie możliwości prądowych eliminatora łuku elektrycznego (łącznika półprzewodnikowego) poprzez zastosowanie autorskiego opracowania układu kaskadowo połączonych i sekwencyjnie sterowanych wielu gałęzi półprzewodnikowych. Wyniki badań i pełną analizę przedstawiono w **Publikacji II,**
- sprawdzenie (w oparciu o wytyczne międzynarodowego standardu IEEE 1584) czy poprzez zastosowanie konstrukcji opracowanego wielosekcyjnego eliminatora łuku możliwe jest zmniejszenie strefy rażenia łukiem elektrycznym oraz obniżenie kategorii zagrożenia. Skuteczność tego rozwiązania przedstawiono w **Publikacja III**,
- zbadanie wpływu działania wielosekcyjnego eliminatora łuku na ograniczenie przyrostów ciśnienia wewnątrz zamkniętych obudów urządzeń elektrycznych dotkniętych zakłóceniem łukowym. Obszar oraz analizę wyników tych badań przedstawiono w **Publikacji III**,
- opracowanie kompletnego autorskiego rozwiązania łącznika hybrydowego, stanowiącego równoległe połączenie wielu sekcji półprzewodnikowych z łącznikiem mechanizmowym, który może zostać wykorzystany jako wielkoprądowy zwiernik hybrydowy, ograniczający skutki powstałego łuku awaryjnego i przepływu prądu zakłóceniowego. Zagadnienia te zostały przedstawione w **Publikacji IV oraz dwóch zgłoszeniach patentowych, z których jeden uzyskał pozytywną akceptację Urzędu Patentowego Rzeczypospolitej Polskiej.**

6.3. Zakres i metodyka przeprowadzonych badań

6.3.1. Autorska metoda rozwiązania problemu naukowego

Analiza literatury przedmiotu prowadzi do istotnego wniosku, że najbardziej efektywną metodą ograniczania skutków zwarciowych i łukowych jest skracanie czasu przepływu prądu w obwodzie dotkniętym awarią. Efekt ten można uzyskać przez bocznikowanie uszkodzonego obwodu urządzeniem o możliwe krótkim czasie zadziałania przy zachowaniu możliwe dużej obciążalności prądowej. Taki efekt, można uzyskać przez zastosowanie łącznika hybrydowego,

w którym sekcja półprzewodnikowa (o ograniczonej obciążalności prądowej) odpowiada za szybkość komutacji urządzenia, a część mechanizmowa (o zwłocznym zadziałaniu) pozwala na uzyskanie odpowiednio wysokiej obciążalności zwarciowej. W konsekwencji oczekuje się powstanie szybkiego hybrydowego zwiernika, współpracującego z działającymi ze znacznymi opóźnieniami, typowymi zabezpieczeniami sieciowymi.

6.3.2. Zakres prac prowadzących do rozwiązania problemu badawczego

Początkowy zakres prac obejmował budowę stanowiska badawczego półprzewodnikowego eliminatora łuku elektrycznego, będącego połączeniem dwóch przeciwsobnie połączonych tyrystorów **[Publikacja I]**. Rysunek 3 przedstawia uproszczoną wersję zaprojektowanego obwodu badawczego. Zadaniem przedstawionego układu bocznikującego jest szybka eliminacja łuku zakłóceniowego, zapobiegająca dalszemu rozwojowi wyładowania elektrycznego. Spadek napięcia na przewodzących półprzewodnikach jest mniejszy od napięcia palącego się łuku elektrycznego, czego efektem powinno być jego zgaszenie. Przeciwsobne połączenie tyrystorów pozwala na zastosowanie eliminatora łuku w sieciach prądu przemiennego o mogącym pojawiać się losowo stanie awaryjnym.

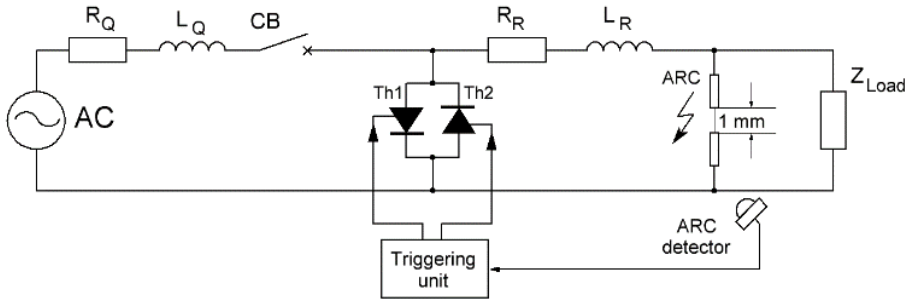

Rys. 3. Obwód testowy z półprzewodnikowym eliminatorem łuku **[Publikacja I, fig. 2]**.

Kolejny etap prac dotyczył problemu zwiększenia obciążalności prądowej półprzewodnikowej części eliminatora łuku przy zachowaniu jego skuteczności działania. Rozwiązaniem jest autorskie opracowanie stanowiące połączenie wielosekcyjnych półprzewodnikowych gałęzi bocznikujących wraz z ich sekwencyjnym sterowaniem **[Publikacje II** i **III]**. Na rysunku 4 przedstawiono schemat ideowy wielosekcyjnego tyrystorowego eliminatora łuku elektrycznego (*MSAE* ang. *Multi- Sectional Arc Eliminator*).

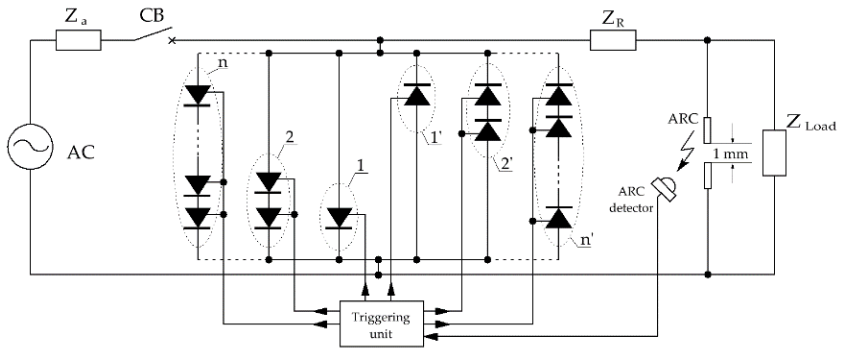

Rys. 4. Schemat ideowy wielosekcyjnego eliminatora łuku (*MSAE*) w wykonaniu tyrystorowym **[Publikacja II, fig. 2]**.

Poszczególne gałęzie bocznikujące wielosekcyjnego eliminatora łuku zbudowane są z wzrastającej liczby szeregowo połączonych elementów półprzewodnikowych (*1, 2, ..., n* oraz *1', 2', n'*). Aktywacja przedstawionego na rysunku 4 eliminatora łuku następuję przez wysterowanie tyrystorów w gałęzi bocznikującej najwyższego rzędu (*n* - dla polaryzacji dodatniej lub *n'* - dla polaryzacji ujemnej), a następnie w kolejnych gałęziach równoległych niższego rzędu *2, 1* lub *2', 1'*. Warunkiem przejmowania przewodzenia prądu przez kolejne gałęzie bocznika półprzewodnikowego *n, ..., 2, 1* lub *n', ..., 2', 1'* jest odpowiednie sterowanie bramkami tyrystorów. Zadaniem szeregowo połączonych tyrystorów w gałęziach bocznikujących wyższego rzędu jest utrzymanie w stanie ich przewodzenia spadku napięcia wystarczającego do wysterowania elementów sekcji rzędu niższego. Cała procedura zapewnia przejęcie prądu zakłóceniowego w obwodach półprzewodnikowych przez czas, który jest niezbędny do zgaszenia powstałego łuku elektrycznego. W ten sposób uzyskuje się praktycznie bezzwłoczne zadziałanie eliminatora łuku oraz sukcesywne odciążenie jego półprzewodnikowych elementów wykonawczych. Ta ostatnia funkcjonalność powoduje wydłużenie czasu dysponowanego na otwarcie styków wyłącznika głównego w przypadku ponownych zapłonów łuku oraz wzrost całkowitej wytrzymałości obciążeniowej łącznika półprzewodnikowego.

Skuteczność działania zaproponowanego eliminatora łuku elektrycznego została sprawdzona i potwierdzona dla kilku możliwych rozwiązań konstrukcyjnych. Wybrane przykłady przedstawiono na rysunku 5. Różnice w budowie eliminatora łuku (łącznika półprzewodnikowego) mają znaczący wpływ na charakterystyki przejmowania prądu przez część półprzewodnikową. Wynika to głównie z ilości i rodzajów zastosowanych tyrystorów w poszczególnych gałęziach półprzewodnikowych. Dodatkowo każdy z zaprezentowanych rozwiązań, ze względu na odmienną budowę, wymaga innego sposobu sterowania. Złożoność rozwiązania i ilość tyrystorów ma również wpływ na koszt budowy takiego eliminatora łuku.

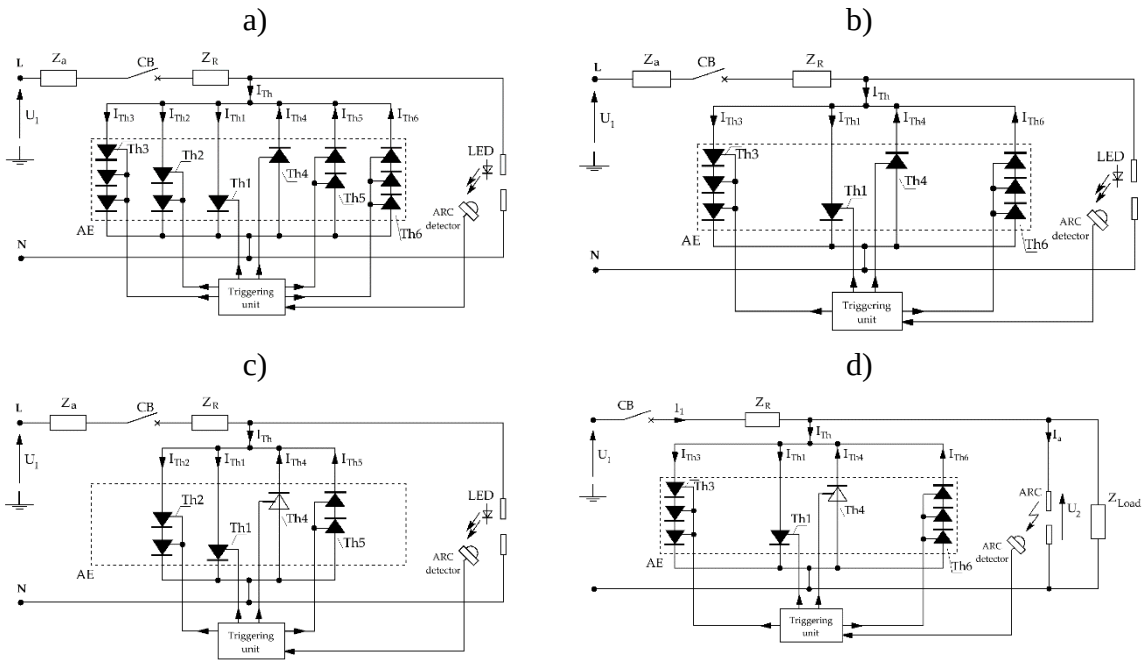

Rys. 5. Przykłady różnych rozwiązań konfiguracyjnych eliminatora łuku **[Publikacja II]:** a) trzysekcyjny **[fig. 3]**, b) dwusekcyjny **[fig. 6]**, c) dwusekcyjny z tyrystorem o mniejszym spadku napięcia (Th4) **[fig. 11]**, d) dwusekcyjny z tyrystorem o mniejszym spadku napięcia i większą ilością szeregowych tyrystorów w gałęzi najwyższego rzędu **[fig. 15]**.

Ostatnia część pracy dotyczyła możliwości wykorzystania innowacyjnego autorskiego opracowania łącznika hybrydowego (z dodatkowym zwiernikiem mechanicznym), który współpracując z czujnikami detekcji łuku elektrycznego lub detektorami zwarcia może efektywnie eliminować wielkoprądowy łuk elektryczny oraz ograniczać skutki przepływu prądu zwarciowego **[Publikacja IV, Patent I i Zgłoszenie patentowe I]**. Na rysunku 6 przedstawiono schemat blokowy zastosowania łącznika hybrydowego w roli eliminatora łuku elektrycznego.

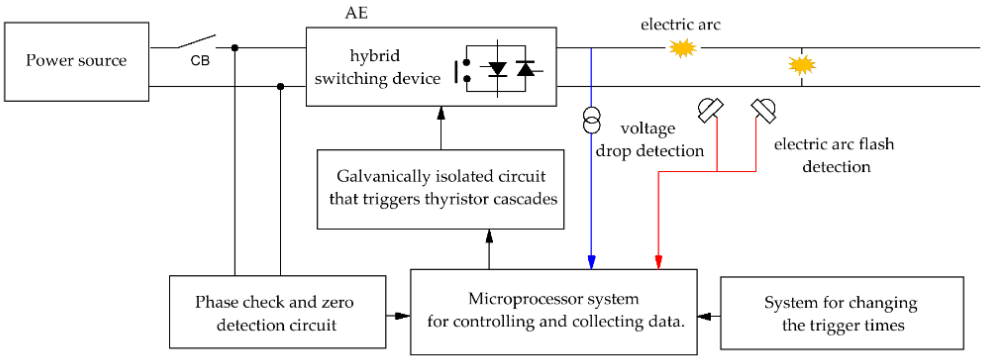

Rys. 6. Schemat blokowy zastosowania łącznika hybrydowego w roli eliminatora łuku elektrycznego **[Publikacja IV, fig. 2]**.

Zadaniem rozbudowanego mikroprocesorowego układu sterowania przedstawionego na rysunku 6 (autorski projekt), jest współpraca z układami: detekcji łuku elektrycznego, detekcji zera napięcia zasilającego i określenia polaryzacji półfali przepływającego prądu [praca V]. Precyzyjne określnie początku przepływu i polaryzacji przepływającego prądu, umożliwiają zaawansowane sterowanie wyzwalaniem tyrystorów i czasu załączenia zwiernika mechanizmowego.

Na rysunku 7 przedstawiono schemat ideowy autorskiego rozwiązania hybrydowego eliminatora łuku przeznaczonego dla obwodów zasilanych jednofazowo. Przedstawiony schemat ideowy posłużył do zbudowania prototypu urządzenia pokazanego na rysunku 8. Większość zaprezentowanych w pracy wyników badań została wykonana przy wykorzystaniu prototypu urządzenia zbudowanego w oparciu o schemat z rysunku 7.

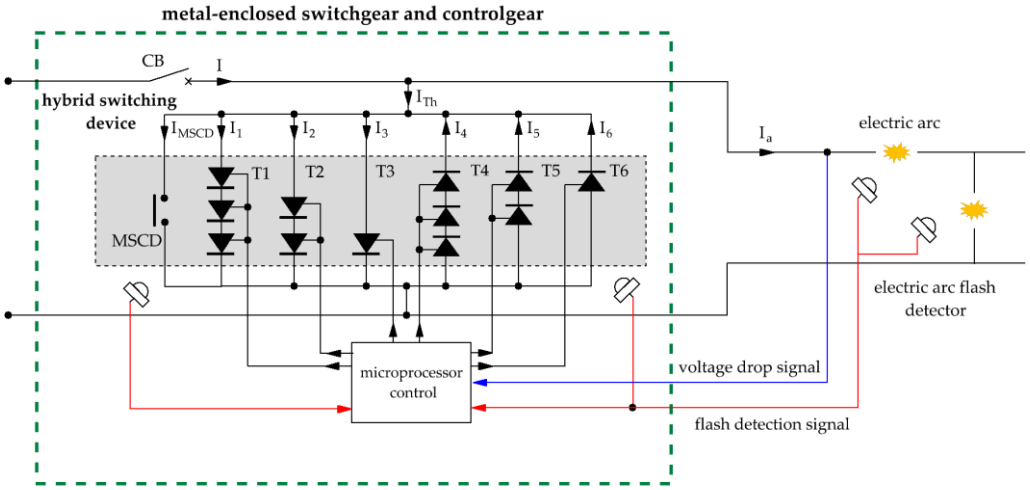

Rys. 7. Schemat ideowy eliminatora łuku w oparciu o łącznik hybrydowy **[Publikacja IV, fig. 3]**.

Układ łącznika hybrydowego stanowi połączenie jednej sekcji mechanizmowej MSCD (*ang. Mechanical Short-Circuit Device*) z sześcioma półprzewodnikowymi gałęziami tyrystorowymi, oznaczonymi kolejno T_1, T_2 *i* T_3 oraz T_4, T_5 *i* T_6. Aktywacja łącznika hybrydowego następuję w pierwszej kolejności przez wysterowanie gałęzi z największą liczbą szeregowo połączonych tyrystorów (T_1 dla polaryzacji dodatniej lub T_4 dla polaryzacji ujemnej). W dalszej kolejności następuje wysterowanie kolejnych gałęzi równoległych o zmniejszającej się liczbie szeregowo połączonych tyrystorów. Jako ostatnia zamyka się gałąź zwiernika mechanizmowego MSCD. Poprzez odciążenie, możliwe jest bezłukowe przejęcie prądu przez łącznik zestykowy.

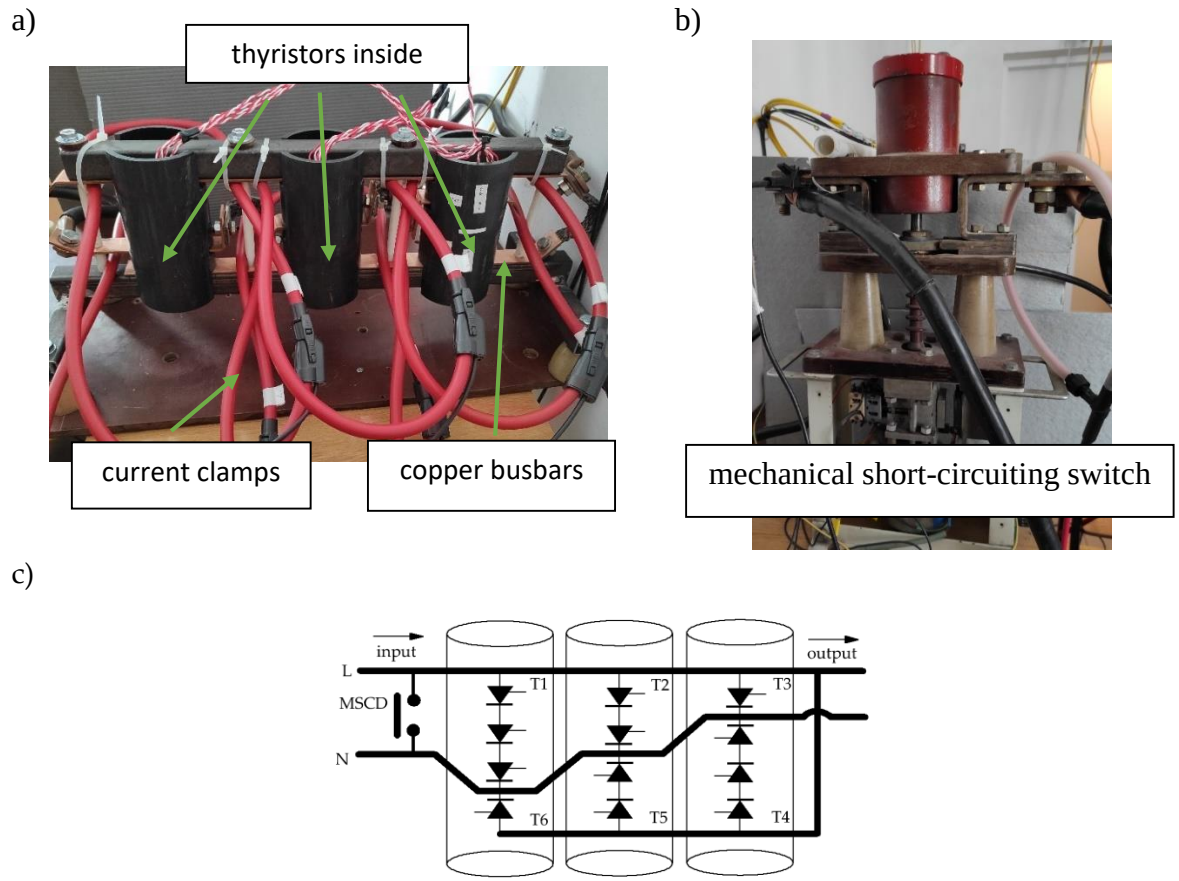

Rys. 8. Łącznik hybrydowy w rozwiązaniu praktycznym: a) półprzewodnikowa część łącznika hybrydowego, b) zwiernik mechanizmowy, c) sposób montażu tyrystorów **[Publikacja IV, fig. 6].**

Łącznik hybrydowy (rys. 8) zbudowany jest w oparciu o tyrystory DCR1910F14-1974 (Dynex Semiconductor) oraz zwiernik mechanizmowy ZZC-15. Wartość prądu ciągłego w stanie załączenia I_T dla pojedynczego tyrystora wynosi 2700 A. Zwiernik mechanizmowy charakteryzuje się zdolnością łączeniową na poziomie 30 kA. Z tego powodu oraz ze względów bezpieczeństwa i możliwych do wystąpienia niebezpiecznych skutków oddziaływania łuku elektrycznego, amplitudy prądów zakłóceniowych w badaniach eksperymentalnych zostały ograniczone do 30 kA.

6.3.3. Źródła zasilania i przyrządy pomiarowe stosowane podczas prac badawczych

Badania eksperymentalne realizowane w ramach pracy doktorskiej zostały przeprowadzone w laboratoriach urządzeń elektroenergetycznych Politechniki Poznańskiej. W zakresie prądów probierczych do ok 1,5 kA próby wykonano w obwodach zasilanych bezpośrednio z sieci energetycznej niskiego napięcia 230/400V. Na potrzeby prób łukowych i zwarciowych o prądach do 30 kA, pomieszczenia badawcze wyposażono w wielkoprądowe syntetyczne źródło zasilania. Do jego budowy wykorzystano 48 wysokonapięciowych (U_n =10 kV) kondensatorów impulsowych, połączonych równolegle w 6 sekcji (0,8 mF/sekcję) oraz dwa równolegle połączone transformatory zwarciowe TSX2-500. Spodziewane wartości

szczytowe prądów użytkowych (po stronie wtórnej transformatorów) wynoszą ponad 100 kA [praca VI]. Rysunek 9 przedstawia uproszczony schemat blokowy zaprojektowanego źródła wielkoprądowego, widok na pojedynczy transformator zwarciowy, bocznik prądowy i baterię kondensatorów impulsowych o energii magazynowanej 250 kJ.

a) b) c)

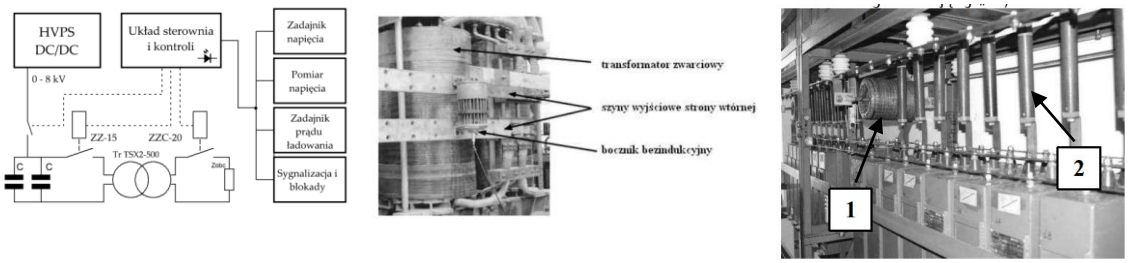

Rys. 9. Wielkoprądowe syntetyczne źródło zasilania: a) schemat blokowy, b) transformator zwarciowy TSX2-500, c) bateria kondensatorów impulsowych wraz z zabezpieczeniami zwarciowymi (1-2) [praca VI, rys. 2, 3 i 6].

Niezbędna podczas prac badawczych rejestracja wielu sygnałów pochodzących z różnych punktów pomiarowych wymagała opracowania, zbudowania i zsynchronizowania wielokanałowego stanowiska pomiarowego. Wiązało się to z koniecznością skompletowania m.in.:

- czterech oscyloskopów Volcraft DSO-1084,
- oscyloskopowych przystawek prądowych AC/DC PAC22 Chauvin Arnoux o zakresie pomiarowym do 1400 A,
- cewek Rogowskiego AmpFlex A110-120 o zakresie pomiarowym do 30 kA,
- cewek Rogowskiego CWT300 o zakresie pomiarowym do 60 kA,
- różnicowych sond wysokonapięciowych Pintek DP-50 o zakresie pomiarowym do 2300 V_{rms} AC i DC,
- napięciowych sond Voltcraft PP-350 o zakresie wejściowym 1500 V,
- czujników ciśnienia PA_21G firmy Keller o zakresie pomiarowym do 6 bar.

Graficzna rejestracja skutków przepływu prądu zwarciowego i zapłonu łuku elektrycznego została wykonana za pomocą szybkiej kamery Chronos 1.4 firmy Kron Technologies. Rejestracje do 40000 klatek/sekundę pozwoliły na dokładną analizę obserwowanych zjawisk w 25 μs przedziałach czasowych.

Pomiary natężenia dźwięku generowanego w wyniku zapłonu łuku elektrycznego wykonane zostały profesjonalnym miernikiem SW-1000 firmy Sauter o klasie dokładność 1, zakresie pomiarowym 136 dB oraz możliwością rejestracji dźwięku w trybie „Impuls”.

Pomiary masy elektrod wykonane przed próbą badawczą i jej ubytku po próbie, zrealizowano za pomocą analitycznej wagi AS 110/c/2 firmy Radwag, o zakresie do 110 g i błędzie pomiarowym ±0,4 mg.

6.4. Wyniki badań skuteczności działania łącznika hybrydowego

6.4.1. Ograniczanie oddziaływań elektrodynamicznych prądów zwarciowych w obwodach zabezpieczonych łącznikiem hybrydowym

Oddziaływania elektrodynamiczne w torach prądowych i układach stykowych łączników elektrycznych, są wywołane przepływającym przez nie prądem elektrycznym [21]. Siły elektrodynamiczne osiągają największe wartości podczas przepływu prądów zwarciowych. W czasie zwarcia płynący prąd może przekraczać setki razy prąd znamionowy, a więc siły elektrodynamiczne mogą być dziesiątki tysięcy razy większe od sił występujących w znamionowych warunkach pracy [praca VII].

Skutkiem działania siły elektrodynamicznej jest wystąpienie niebezpiecznych naprężeń, dodatkowych naciągów i wychyleń przewodów giętkich, a także odkształcenia przewodów szynowych. Najbardziej widoczne i destrukcyjne skutki działania prądów zwarciowych występują w rozdzielniach, gdzie odległości między przewodami są niewielkie [22].

Na rysunku 10 przedstawiono przykładowy efekt skuteczności ograniczania elektrodynamicznych skutków zwarciowych w układzie z łącznikiem hybrydowym **[Publikacja IV]**. Podczas eksperymentu wykorzystano dwa równoległe aluminiowe tory prądowe o długości l = 1000 mm, średnicy d = 8 mm, oddalone od siebie o a = 2 mm. Rysunek 10a przedstawia obiekt badań przed wykonaniem próby zwarciowej. Rysunek 10b to efekt skutków elektrodynamicznych podczas przepływu prądu zwarciowego o amplitudzie 10 kA i braku zabezpieczenia obwodu łącznikiem hybrydowym (AE OFF). W chwili największego oddziaływania siły elektrodynamicznej na tory prądowe, jej obliczona wartość wynosiła ponad 2 kN. Na skutek działania siły elektrodynamicznej, nastąpiło odkształcenie torów prądowych, a zmierzona odległość między środkami przewodów z początkowych 10 mm, wzrosła do 720 mm.

Dla tego samego obiektu badań i warunków zwarciowych, w układzie, w którym zadziałał łącznik hybrydowy (AE ON), obliczona wartość działającej siły wynosiła zaledwie 190 N. Zmierzona wartość odkształcenia przewodów między ich środkami z początkowych 10 mm, wzrosła do zaledwie 42 mm (rysunek 10c).

Z analizy wyników badań eksperymentalnych wynika, że zastosowanie łącznika hybrydowego pozwala na znaczne skrócenie czasu trwania zakłócenia zwarciowego. Powoduje to ograniczenie amplitudy prądu w obwodzie dotkniętym zakłóceniem, a tym samym zmniejszenie skutków oddziaływania elektrodynamicznego. Przeprowadzone dla omawianego przypadku obliczenia sił elektrodynamicznych, występujących podczas przepływu prądu zwarciowego 10 kA wykazały, że zastosowanie zaproponowanego przez autora rozwiązania ochrony z wykorzystaniem łącznika hybrydowego skutkuje zmniejszeniem oddziaływania elektrodynamicznego między torami prądowymi o prawie 90%. Podobnie, zmierzone wartości odkształcenia torów prądowych podczas przepływu prądu zwarciowego w układzie z łącznikiem hybrydowym zmalały o prawie 94%.

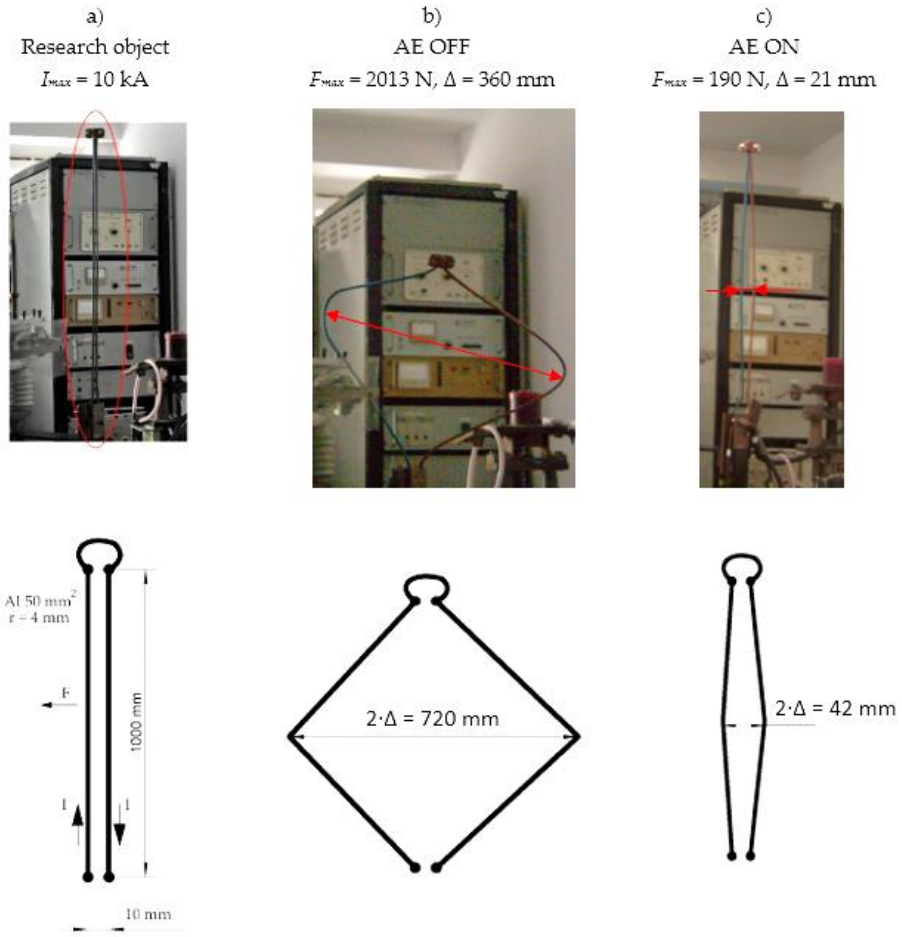

Rys. 10. Próba oceny skutków elektrodynamicznych podczas przepływu prądu zwarciowego o amplitudzie 10 kA w układzie równoległych aluminiowych torów prądowych: a) obiekt badań przed wykonaniem eksperymentu, b) obiekt badań po próbie zwarciowej, c) obiekt badań po próbie zwarciowej w układzie z łącznikiem hybrydowym, (Δ - strzałka ugięcia toru prądowego) **[Publikacja IV, fig. 7].**

Szczegółowy opis procesu badawczego i wyniki badań opisano w **Publikacji IV**.

6.4.2. Ograniczanie erozji torów prądowych poddanych działaniu łuku elektrycznego

Palący się łuk elektryczny i przepływający przez tory prądowe urządzeń i aparatów elektroenergetycznych prąd zakłóceniowy, powodują występowanie różnorodnych niebezpiecznych zjawisk fizycznych i chemicznych. Energia cieplna wydzielana w awaryjnym łuku elektrycznym, może powodować znaczne uszkodzenia urządzeń znajdujących się wewnątrz i na zewnątrz rozdzielnic, a także stanowić zagrożenie dla otoczenia [23]. Zwarcia łukowe i przepływy przez styki elektryczne prądu o znacznej wartości mogą wpływać na stan ich powierzchni, a tym samym na wartość rezystancji przejścia styku elektrycznego [praca VIII].

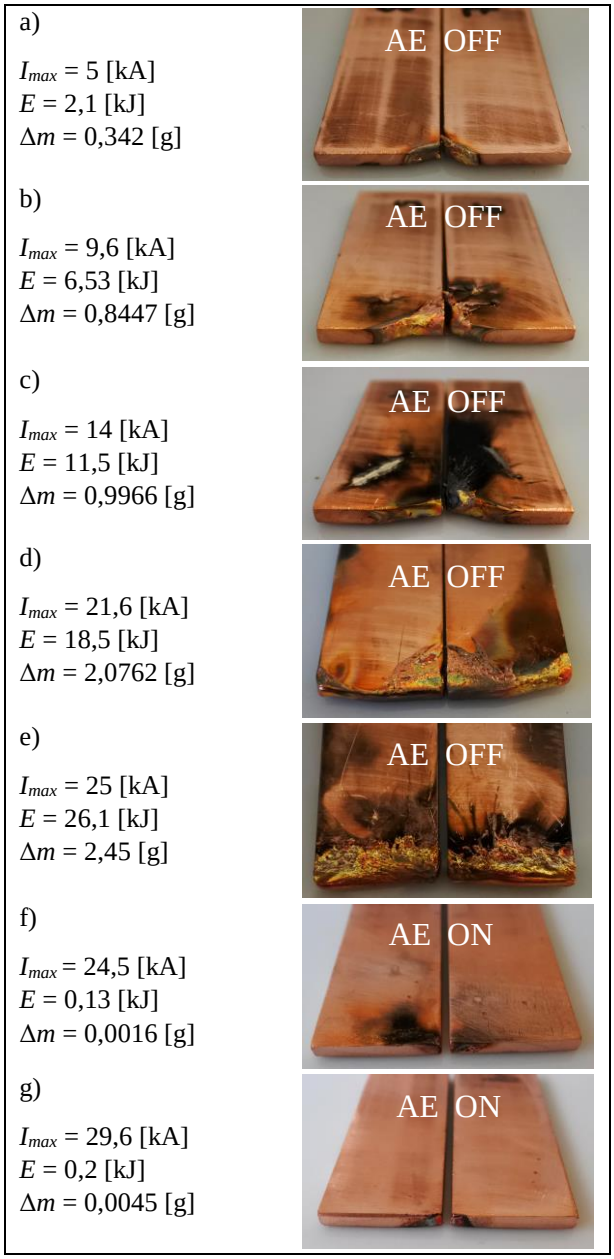

Rys. 11. Skutki erozji łukowej na miedzianych elektrodach w układzie bez aktywnego (AE OFF) i z aktywnym (AE ON) łącznikiem hybrydowym (Imax – zmierzona wartość prądu zakłócenia, E – obliczona energia łuku elektrycznego, Δm – wagowy ubytek masy elektrod) **[Publikacja IV, fig. 10].**

Pod pojęciem erozji łukowej materiału na ogół rozumie się wagowy lub objętościowy ubytek masy elektrod Δm oraz degradację i zmianę właściwości powierzchni elektrod wskutek różnych zjawisk i procesów związanych z występowaniem łuku elektrycznego.

Graficzne rejestracje (rys. 11a-g), przedstawiają erozję materiału miedzianych elektrod dla różnych wartości prądu zakłócającego, a tym samym różnych energii łuku **[Publikacja IV]**. Zaprezentowany eksperyment wykonano dla dwóch warunków probierczych: bez aktywnego łącznika hybrydowego (rysunki 11a-e, AE OFF) i z łącznikiem hybrydowym, wykorzystanym w roli eliminatora łuku elektrycznego (rysunki 11f-g, AE ON).

Należy dodać, że w obwodzie z zainstalowanym łącznikiem hybrydowym (AE ON), podczas zwarcia łukowego z prądem w zakresie od 5 do 20 kA, nie uwydatniły się widoczne uszkodzenia elektrod, a pomiar erozji mieścił się w granicach błędu przyrządu pomiarowego (±0,4 mg). Mierzalny i widoczny ubytek materiału, pojawia się dopiero przy amplitudzie prądu około 25 kA (rys. 11f). W obwodzie bez zainstalowanego łącznika hybrydowego (AE OFF), widoczne i mierzalne ubytki materiału, można było już zaobserwować dla prądów około 5 kA (rys.11a). Porównując, widoczne uszkodzenia i pomiary ubytku materiału dla elektrod przedstawionych na rysunku 11e (bez eliminatora łuku) i 11f (z eliminatorem łuku), można dostrzec skuteczność ograniczania erozji, która jest mniejsza o ponad 2 rzędy wielkości.

Rysunek 12 przedstawia graficzne porównanie obliczonej wartości ubytku objętości V materiału elektrod w układzie bez i z łącznikiem hybrydowym. Erozja materiału elektrod została przedstawiona w postaci kul o promieniu r (z zachowaniem wspólnej skali dla obu rysunków). Przyrównując ubytek objętościowy dla obu przykładów, otrzymujemy ponad 1500-krotnie mniejszą wartość erozji materiału w układzie z zastosowanym łącznikiem

hybrydowym. Krople płynnego metalu stanowią poważne zagrożenie pożarowe, dlatego ograniczenie ich ilości i masy, jest potwierdzenie istoty roli eliminatora łuku dla poprawy ochrony przeciwpożarowej.

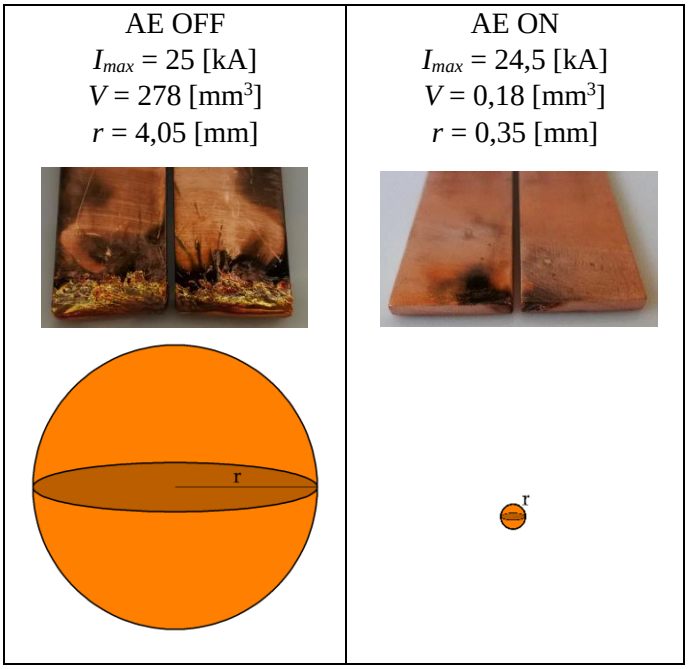

Rys. 12. Graficzne przedstawienie objętości materiału wyrzuconego z elektrod do otoczenia **[Publikacja IV, fig. 12].**

Reasumując, przeprowadzonych serii eksperymentów i analizy zebranych danych wynika, że zastosowanie łącznika hybrydowego powoduje znaczne zmniejszenie energii łuku (nawet 200 krotne), ograniczenie erozji materiału elektrod (w zakresie prądów probierczych do 30 kA nawet 1500 krotnie) oraz widoczne zmniejszenie degradacji powierzchni elektrod.

Opis przebiegu zdarzeń, wyniki badań i pełną analizę przedstawiono w **Publikacji IV**.

6.4.3. Ograniczenie zagrożeń powodowanych akustycznym oddziaływaniem łuku elektrycznego

Podczas zapłonu łuku elektrycznego i w jego dalszych etapach palenia się, następuje w otoczeniu wyładowania nagły wzrostu ciśnienia i powstaje fala dźwiękowa, której natężenie może prowadzić do uszkodzenia, a nawet utraty słuchu. Przeciętny łuk o natężeniu prądu rzędu kilku do kilkunastu kiloamperów i długości od kilkunastu do kilkudziesięciu centymetrów, generuje w odległości 1 m od łuku, ciśnienie akustyczne o wartościach dochodzących do 150 dB, czyli znacznie przewyższających poziom progu bólu, wynoszący 120 dB [24]. Jeszcze bardziej niebezpieczne są udary dźwiękowe, generowane w chwili zapłonu łuku w szczelnej obudowie lub osprzęcie kablowym.

Dla amplitud prądu łuku zakłóceniowego mieszczących się w zakresie od 5 do 20 kA, wykonano pomiary natężenia dźwięku w układzie bez łącznika hybrydowego (AE OFF) oraz z łącznikiem hybrydowym (AE ON). Rysunek 13 przedstawia sposób pomiaru natężenia dźwięku, pochodzącego od palącego się łuku elektrycznego. Pomiary natężenia dźwięku zostały wykonane w odległości 3 m od źródła dźwięku, ze względu na graniczny zakres pomiarowy zastosowanego miernika Sauter SW-1000.

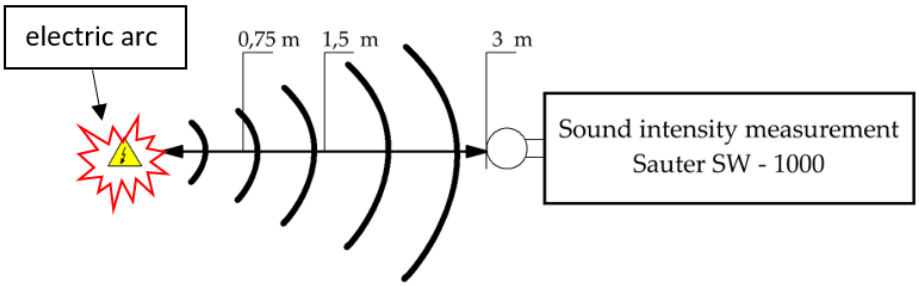

Rys. 13. Pomiar natężenia dźwięku pochodzącego od łuku elektrycznego **[Publikacja IV, fig. 14].**

Przy dookólnej propagacji dźwięku i zmierzonej wartość jego natężenia w odległości 3 m od źródła, można w pewnym uproszeniu obliczyć wartość natężenia w odległościach np. 1,5 m i 0,75 m. Odległości te, odpowiadają realnym odległościom pracy personelu technicznego od potencjalnego źródła łuku. Tabela 1 zawiera zmierzone (dla 3 m) i spodziewane (1,5 m) wartości natężenia dźwięku dla układu bez i z eliminatorem łuku w zakresie prądu łuku od 5 do 20 kA.

Tab. 1. Zmierzone i spodziewane wartości natężenia dźwięku w odległości 3 m i 1,5 m od źródła łuku w układach badawczych bez i z eliminatorem łuku **[Publikacja IV, tab. 4].**

$I_{a\,max}$ [kA]	AE OFF		AE ON	
	Measured value	Expected calculation values for a measuring distance of 1.5 m	Measured value	Expected calculation values for a measuring distance of 1.5 m
	$\beta_{AE\,OFF\,3m}$ [dB]	$\beta_{AE\,OFF\,1.5m}$ [dB]	$\beta_{AE\,ON\,3m}$ [dB]	$\beta_{AE\,ON\,1.5m}$ [dB]
5	121	127	110	116
10	123	129	113	119
15	124.5	130.5	116.5	122.5
20	126.5	132.5	119.5	125.5

W tabeli 1 zastosowano następujące oznaczania:

- $\beta_{AE\,OFF\,3\,m}$ / $\beta_{AE\,OFF\,1,5\,m}$ – wartość natężenia dźwięku w odległości 3 m/1,5 m od źródła łuku w układzie bez łącznika hybrydowego (AE OFF),
- $\beta_{AE\,ON\,3\,m}$ / $\beta_{AE\,ON\,1,5\,m}$ – wartość natężenia dźwięku w odległości 3 m/1,5 m od źródła łuku w układzie z łącznika hybrydowego (AE ON).

$I_{a\,max}$ [kA]	$\beta_{AE\,ON\,3\,m} - \beta_{AE\,OFF\,3\,m}$ [dB]	I_2/I_1
5	- 11	13
10	- 10	10
15	- 8	6,5
20	- 7	5

Tab. 2. Różnice poziomów natężenia dźwięku zmierzone w odległości 3 m od łuku elektrycznego i odpowiadające im stosunki natężeń dźwięków. (I_2/I_1 stosunek natężenia dźwięku) **[Publikacja IV, tab. 5].**

W tabeli 2 przedstawiono różnicę zarejestrowanych wartości natężenia dźwięku odległości 3 m od źródła dźwięku dla układu bez i z zainstalowanym łącznikiem hybrydowym. Zastosowanie łącznika hybrydowego w roli eliminatora łuku powoduje znaczną redukcję natężenia dźwięku. W zakresie prądów 5-20 kA natężenie dźwięku wytworzonego zapłonem łuku elektrycznego może być mniejsze o wartość z przedziału 7-11 dB. Reasumując, analiza zebranych danych pomiarowych wykazała, że możliwe jest nawet 13-krotne zmniejszenie natężenia dźwięku jaki towarzyszy zapłonowi łuku elektrycznego.

Opis procesu badawczego i wyniki badań opisano szczegółowo w **Publikacji IV**.

6.4.4. Ograniczenie zagrożeń powodowanych wzrostem ciśnienia w zamkniętych obudowach urządzeń elektrycznych

Przyrost ciśnienia wewnątrz zamkniętej obudowy (np. rozdzielnicy) jest przede wszystkim funkcją energii $e(t)$ pobieranej z sieci przez łuk elektryczny i przetwarzanej na ciepło. Część przeprowadzonych badań eksperymentalnych skupiona była na oszacowaniu przyrostu cieśnienia w osłonach szczelnych, niewyposażonych w klapy bezpieczeństwa, lecz posiadających membrany unoszące się w przypadku gwałtownego wzrostu ciśnienia wewnątrz przedziałów rozdzielnicy (obudowy) na skutek zwarć łukowych. Podjęto także próbę zweryfikowania zmierzonych przyrostów ciśnienia w odniesieniu do przyrostów obliczonych **[Publikacja III]**.

Na rysunku 14 przedstawiono budowę zaprojektowanego i wykonanego obiektu badań. Inicjacja łuku następowała w szczelnie zamkniętej obudowie puszki łączeniowej, pomiędzy dwoma miedzianymi elektrodami o średnicy ϕ = 2,21 mm. Układ zasilany był napięciem przemiennym o wartości skutecznej 230 V. Amplituda prądu w obwodzie została ograniczona ze względów bezpieczeństwa do wartości 1300 A.

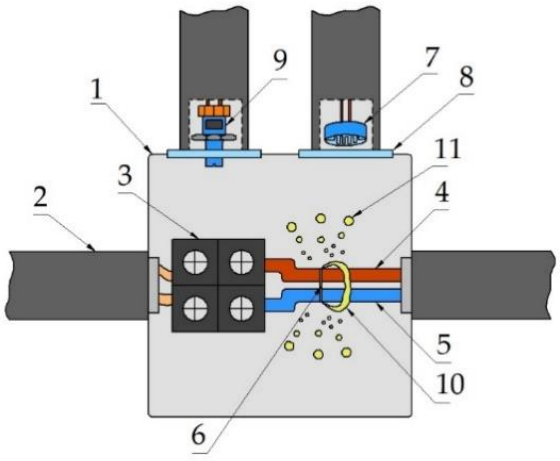

Rys. 14. Źródło łuku elektrycznego wewnątrz puszki łączeniowej: 1 – instalacyjna puszka natynkowa, 2 – rura PCV do wprowadzenia i wyprowadzenia przewodów zasilających, a także czujników pomiarowych, 3 – listwa zaciskowa umożliwiająca wymianę elektrod, 4 – przewód fazowy, 5 – przewód neutralny, 6 – element topikowy inicjujący zapłon łuku, 7 – detektor błysku łuku elektrycznego, 8 – szklana ochrona detektora błysku, 9 – czujnik ciśnienia gazów wewnątrz obudowy, 10 – łuk elektryczny, 11 – krople erodowanego materiału elektrod
[Publikacja III, fig. 2].

Reprezentatywne kadry z przykładowej rejestracji poklatkowej, wykonanej za pomocą szybkiej kamery Chronos, przedstawiono na rysunkach 15a-c. Rejestracja fotograficzna

pokazuje: moment zapłonu łuku w zamkniętej puszce łączeniowej, palący się łuk w rozszczelnionej obudowie oraz emisję gorącego materiału elektrod na zewnątrz puszki łączeniowej. Podobną sytuację przedstawiono wcześniej na rysunku 2.

a) b) c)

Rys. 15. Rejestracja fotograficzna skutków istnienia łuku w układzie bez i z eliminatorem łuku: a) zapłon łuku elektrycznego, b) rozwój łuku elektrycznego, c) emisja gorącego materiału elektrod na zewnątrz puszki łączeniowej (I_m = 1300A, U =230V, elektrody *Cu-Cu*) **[wybrane kadry z Publikacji III, fig. 5].**

Dzięki synchronizacji szybkiej kamery filmowej Chronos z pozostałymi urządzeniami rejestracyjnymi, kadry zdjęciowe z rysunku 15 są skorelowane z przebiegami przedstawionymi na rysunku 16. Pierwszy zapłon łuku elektrycznego wewnątrz szczelnie zamkniętej puszki instalacyjnej jest powodem wzrostu ciśnienia w jej wnętrzu. W chwili t_3 = 2,3 ms zmierzone ciśnienie gazów wewnątrz puszki łączeniowej osiąga maximum ok 15 kPa. Dla tej samej chwili czasowej, obliczeniowa wartość ciśnienia wynosi 20 kPa, a krzywa tego przebiegu pokrywa się z krzywą zmierzonego ciśnienia (rysunek 16b). Znając charakterystykę energii łuku i wiedząc, że przyrost ciśnienia jest przede wszystkim funkcją tej energii, można z dużą dokładnością wyznaczyć krzywą ciśnienia wewnątrz szczelnej obudowy. Obliczony p_{obl} i zmierzony p_a przyrost ciśnienia dla przeprowadzonego eksperymentu został przedstawiony na rysunku 16b. Przebieg przyrostu ciśnienia obliczonego i zmierzonego przestają się pokrywać w miarę upływu czasu od chwili otwarcia obudowy (dla przedstawionego eksperymentu po czasie 2,3 ms). Dalsza próba porównywania obu wielkości nie daje miarodajnych wyników. Na skutek otwarcia obudowy puszki łączeniowej, ciśnienie w jej wnętrzu zaczyna się obniżać. Gdyby nie doszło do rozszczelnienia obudowy puszki łączeniowej, obliczeniowy przyrost ciśnienia może osiągnąć wartość 94 kPa.

Dla tych samych warunków badawczych przeprowadzono eksperyment porównawczy, w którym wykorzystano łącznik hybrydowy jako eliminator łuku elektrycznego. Przebiegi istotnych wielkości pomiarowych pokazuje rysunek 17.

Na rysunku 17b przedstawiono przyrost ciśnienia zmierzonego p_a i obliczonego p_{obl} wewnątrz puszki instalacyjnej, w której doszło do zapłonu łuku. Podczas przepływu prądu w obwodzie (chwila t_1 = 0 ms) następuje zapłon łuku elektrycznego. W chwili t_2 = 0,05 ms następuje detekcja błysku, a w chwili t_3 = 0,69 ms zaczyna przewodzić bocznikujący układ łącznika hybrydowego. Od momentu pojawienia się łuku do momentu jego całkowitego zgaszenia mija czas łukowy t_a = 0,9 ms. W trakcie trwania eksperymentu nie stwierdzono rozszczelnienia puszki instalacyjnej.

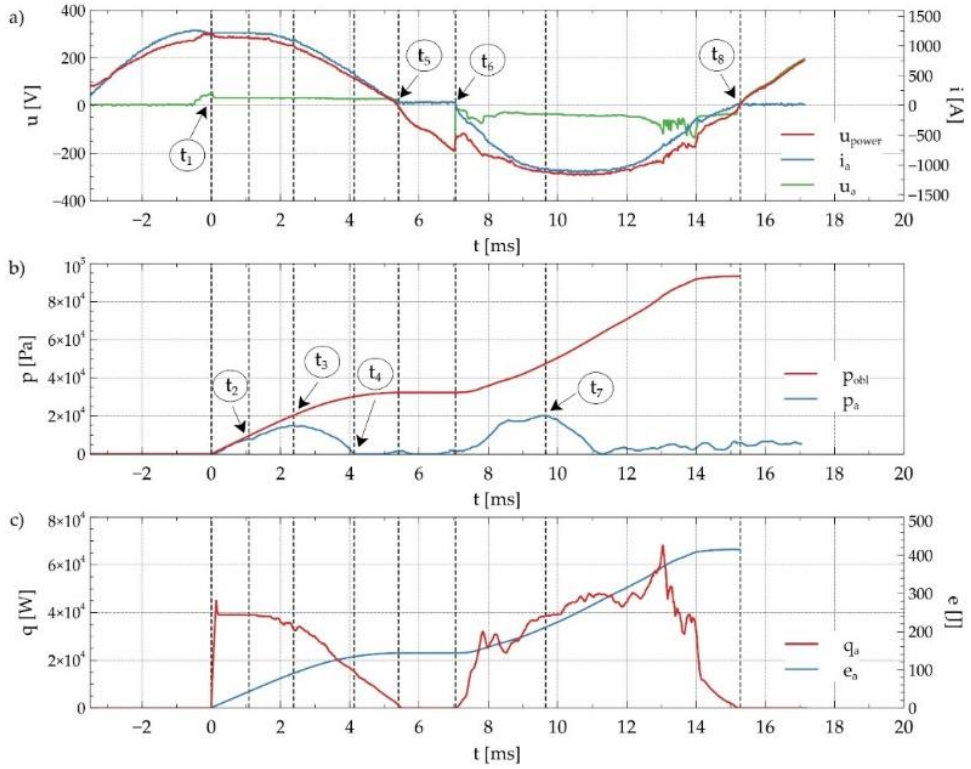

Rys. 16. Przebiegi czasowe zakłócenia łukowego w obwodzie bez łącznika hybrydowego: a) napięcie zasilania u_{power}, napięcie łuku u_a, prąd łuku i_a, b) zmierzone p_a i obliczonego p_{obl} ciśnienia wewnątrz puszki łączeniowej, c) energia e_a i moc q_a pobierana przez łuk **[Publikacja III, fig. 4].**

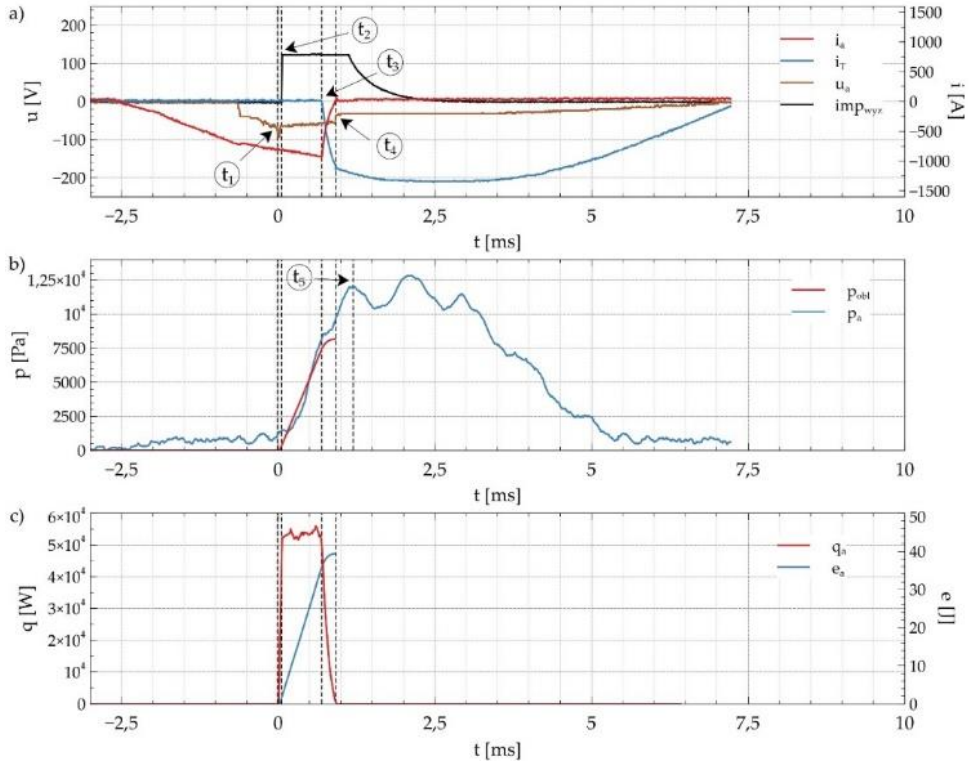

Rys. 17. Przebiegi czasowe zakłócenia łukowego w obwodzie z łącznikiem hybrydowym: a) napięcie na łuku u_a, prąd w gałęzi łuku i_a, prąd w gałęzi eliminatora łuku i_T, impuls detekcji błysku łuku imp_{wyz}, b) zmierzone p_a i obliczone p_{obl} ciśnienie wewnątrz puszki instalacyjnej, c) moc pobierana przez łuk q_a i energia e_a wydzielana w łuku **[Publikacja III, fig. 12].**

Przyrost zmierzonego ciśnienia Δp_a wewnątrz zamkniętej obudowy puszki instalacyjnej, od momentu zapłonu łuku (t_1 = 0 ms) do całkowitego przejęcia przewodzenia przez bocznikujący układ łącznika hybrydowego (t_4 = 0,9 ms), jest współliniowy z przyrostem wartości obliczonej Δp_{obl} (rysunek 17b). W chwili całkowitego przejęcia przewodzenia przez łącznik i zgaszenia łuku elektrycznego, wartość zmierzonego ciśnienia wynosi p_a = 9,7 kPa, a obliczonego p_{obl} = 8,1 kPa. Zgaszony łuk elektryczny nie powoduje dalszego wzrostu ciśnienia wewnątrz puszki instalacyjnej. W układzie bez łącznika hybrydowego, obliczona wartość ciśnienia wskazywała przyrosty do 94 kPa. Zastosowanie szybkiego eliminatora łuku, w postaci łącznika hybrydowego, powoduje prawie dwunastokrotne zmniejszenie spodziewanego ciśnienia wewnątrz zamkniętej puszki łączeniowej.

Reasumując, zastosowanie łącznika hybrydowego znacząco skraca czas palenia się łuku elektrycznego, co w konsekwencji zmniejsza energię łuku i ciśnienie wewnątrz obudowy. Brak rozszczelnienia obudowy podczas palenia się łuku, skrócenie czasu łukowego oraz zmniejszenie energii powodują:

- ograniczenie ubytku materiału elektrodowego,
- ograniczenie przyrostu temperatury wewnątrz obudowy,
- brak wyrzutu do otoczenia plazmy, gorących gazów, dymu i kropli metali,
- brak ogłuszającej fali dźwiękowej.

Poruszone zagadnienia w sposób szczegółowy zostały opisane i przedstawione w **Publikacji III**.

6.4.5. *Ograniczenie strefy rażenia łukiem elektrycznym*

Kategoria zagrożenia rażeniem łukiem elektrycznym jest ściśle związana z wartością energii łuku. Istnieje kilka metod [25-27] za pomocą których można oszacować wartość tej energii oraz innych parametrów charakteryzujących skutki łuku w miejscu analizy. Jedną z najbardziej uniwersalnych jest metoda opisana w opracowaniu "IEEE 1584 Guide for Performing Arc-Flash Hazard Calculations" [28-30]. Wynikające z tego opracowania kategorie (od 0 do 4) pozwalają zaproponować środki ochrony pracownika, adekwatne do poziomu zagrożenia. Opierając się na metodzie IEEE 1584, można również obliczyć odległość granicy strefy rażenia łukiem elektrycznym.

W celu określenia wpływu zadziałania eliminatora łuku na kategorię zagrożenia i strefę rażenia przeprowadzono eksperymenty w układzie zbliżonym do przedstawionego na rysunku 6 **[Publikacja III]**. Założono, że dla przeprowadzonego eksperymentu układ zasilany będzie jednofazowo napięciem 230 V, prąd łuku zostanie ograniczony do 1,3 kA, a odległość części ciała osoby od źródła łuku wynosie 50 mm (osoba znajduje się w bezpośrednim kontakcie z puszką instalacyjną, np. wykonując czynności sprawdzające). Dla tak przyjętych założeń i obwodu niewyposażonego w układ łącznika hybrydowego (witch out MSAE) zasięg

strefy rażenia D_B sięga prawie 90 mm od miejsca zapłonu łuku elektrycznego. Zastosowanie zabezpieczenia łukoochronnego (MSAE) w postaci łącznika hybrydowego znacznie skraca zasięg niebezpiecznej strefy rażenia *HRC* do zaledwie 9,45 mm. Zastosowanie układu łącznika hybrydowego zmniejszyło prawie dziesięciokrotnie strefę możliwego zagrożenia ze strony łuku elektrycznego dla personelu technicznego. Na rysunku 18 zobrazowano zasięg niebezpiecznej strefy rażenia podczas wyładowania łukowego w układzie bez i z zainstalowanym łącznikiem hybrydowym.

Dla rozpatrywanego przypadku, analiza zagrożenia w układzie, w którym doszło do zakłócenia łukowego wyposażonego w urządzenie łukoochronne (łącznik hybrydowy), wykazała, że mieści się on w kategorii zagrożenia 0. Dla tej kategorii, ze względu na znikomą wartość energii łuku nie ma konieczności stosowania specjalistycznych środków ochrony osobistej z wyjątkiem rękawic i okularów ochronnych. Brak eliminatora łuku, wydłużenie czasu palenia i wzrost energii łuku powoduje podwyższenie kategorii do 1. Dla tej kategorii zagrożenia konieczne jest stosowanie odzieży odpornej na łuk elektryczny, specjalnych skórzanych rękawic i ochraniaczy na nogi oraz używanie hełmów ochronnych z przyłbicą.

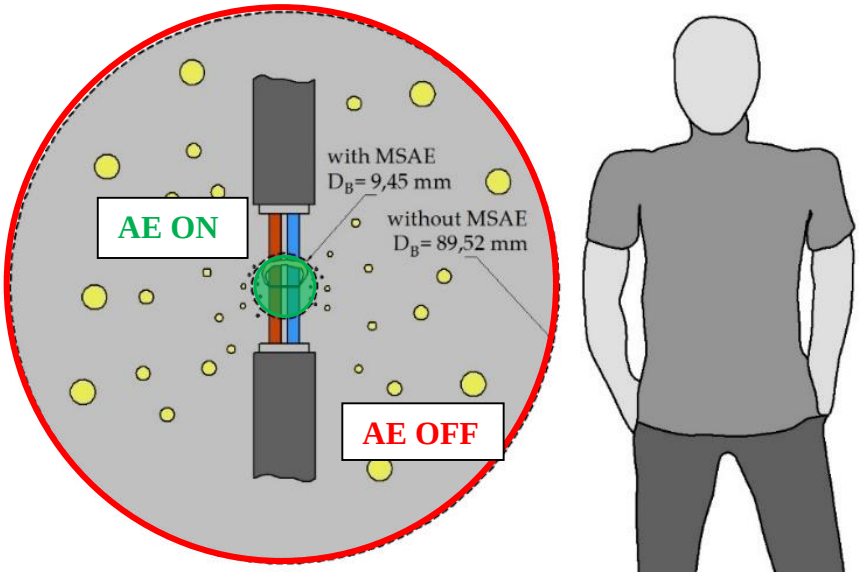

Rys. 18. Strefa rażenia awaryjnym łukiem elektrycznym w obwodzie z i bez MSAE (amplituda prądu łuku 1300 A) **[Publikacja III, fig. 14].**

W tabeli 3 (dla porównania) oprócz obliczonych wartości strefy rażenia D_B i kategorii zagrożenia *HRC* dla prądu łuku 1,3 kA (wg. IEEE 1584), przedstawiono spodziewane parametry obliczeniowe D_B i *HRC* dla prądów 10 i 20 kA. Dla tak dużych amplitud prądów (10 i 20 kA) w obwodzie bez łącznika hybrydowego, rozwijające się w czasie zakłócenie łukowe, powoduje przekroczenie bezpiecznej wartości energii łuku (wg. IEEE 1584 [28-30]) w wyniku czego niedopuszczalne jest przebywanie personelu technicznego w obszarze urządzenia, w którym doszło do zapłonu łuku elektrycznego. Natomiast dla tych samych wartości prądów (10 i 20 kA), szybkie zadziałanie łącznika hybrydowego (rzędu 1 ms)

powoduje znaczne ograniczenie energii łuku, a wartość kategorii zagrożenia pozwala na dobranie odpowiedniego ubrania ochronnego i wyznaczenie bezpiecznej strefy poza strefą rażenia.

Wyniki badań i pełną analizę przedstawiono w **Publikacji III**.

Tab. 3. Spodziewane parametry obliczeniowe (wg. IEEE 1584) stref i kategorii zagrożenia trzech wartości prądu łuku **[Publikacja III, tab. 6]**.

t_a [s]	I_a = 1,3 kA				I_a = 10 kA				I_a = 20 kA			
	D_B [mm]		*HRC*		D_B [mm]		*HRC*		D_B [mm]		*HRC*	
	MSAE ON	MSAE OFF	MSAE ON	MSAE OFF	MSAE ON	MSAE OFF	MSAE ON	MSAE OFF	MSAE ON	MSAE OFF	MSAE ON	MSAE OFF
0,001	22,5	22,5	0	0	67,7	67,7	1	1	98,4	98,4	2	2
0,005	NO ARC FAULT	50,2	NO ARC FAULT	1	NO ARC FAULT	151,3	NO ARC FAULT	3	NO ARC FAULT	220,0	NO ARC FAULT	3
0,010		71,0		1		214,0		3		311,2		DANGEROUS!
0,020		100,4		2		302,6		DANGEROUS!		440,1		
0,030		123,0		2		370,6				539,0		
0,040		142,0		3		427,9				622,4		
0,050		158,8		3		478,4				695,8		
0,060		174,0		3		524,1				762,3		
0,070		187,9		3		566,1				823,3		
0,080		200,9		3		605,2				880,2		
0,090		213,1		3		641,9				933,6		
0,100		224,6		3		676,6				984,07		

6.5. Wnioski i praktyczne znaczenie pracy doktorskiej

W rozprawie doktorskiej zostały przedstawione procedury i efekty eliminacji zagrożeń powodowanych pojawieniem się w obwodach zasilających zdarzeń awaryjnych w postaci zapalenia się łuku elektrycznego lub zaistnienia stanów zwarciowych. Do zbadania poprawności idei oraz postawionych założeń, wynikających z tematu i hipotezy badawczej rozprawy, wykorzystano autorski projekt łącznika hybrydowego pracującego w roli zwiernika. Jest to urządzenie umożliwiającym bardzo szybkie zbocznikowanie obwodu elektrycznego dotkniętego zakłóceniem łukowym, mające na celu stworzenie alternatywnej – uprzywilejowanej drogi dla przepływu prądu. Efektem tego jest bardzo szybka eliminacja powstałego łuku elektrycznego lub przepływu prądu zwarciowego w dotkniętym awarią obwodzie i zmniejszenie powstałych szkód na skutek rozwijającego się stanu awaryjnego.

Badania eksperymentalne z wykorzystaniem łącznika hybrydowego wykazały, że jest możliwe:

- gaszenie i skrócenie czasu palenia się łuku elektrycznego,
- zmniejszenie ilości energii wydzielanej w łuku,
- ograniczanie oddziaływań elektrodynamicznych prądów zwarciowych,
- ograniczanie erozji torów prądowych poddanych działaniu łuku elektrycznego,

- ograniczenie zagrożeń powodowanych akustycznym oddziaływaniem łuku elektrycznego,
- ograniczenie ciśnienia gazów wewnątrz zamkniętych obudów urządzeń elektroenergetycznych,
- znaczne skrócenie czasu oddziaływania skutków cieplnych w zabezpieczanym obwodzie,
- zmniejszenie niebezpiecznej strefy rażenia łukiem elektrycznym.

Przedstawione przez doktoranta wyniki badań i obliczeń w cyklu publikacji, dotyczących eliminacji łuku elektrycznego i ograniczania skutków zwarciowych z wykorzystaniem łączników hybrydowych, potwierdzają skuteczność działania autorskiej konstrukcji łącznika hybrydowego. Zaproponowane urządzenie w rozwiązaniu przemysłowym, może przyczynić się do ochrony zdrowia lub życia osób narażonych na działanie łuku elektrycznego, ale również w znacznym stopniu zminimalizuje straty materialne, wynikające z uszkodzeń powodowanych przepływem prądu zwarciowego lub zapłonem łuku elektrycznego.

Zrealizowany cel i uzyskane wyniki badań pozwoliły na **potwierdzenie postawionej hipotezy badawczej.**

Przy aktualnych cenach i dostępności komponentów, opracowana konstrukcja wielkoprądowego łącznika hybrydowego jest konstrukcją dość drogą. Potencjalne obszary jej wykorzystania będą zatem dotyczyły:

- obiektów o znaczeniu strategicznym (np. militarnym),
- obiektów o znacznej wartości materialnej,
- rozwijającej się gałęzi pojazdów elektrycznych,
- układów trakcyjnych,
- obiektów, w których można spodziewać się podwyższonego ryzyka eksploatacyjnego (górnictwo).

W zabezpieczeniach obwodów prądu stałego przedstawione rozwiązanie można uprościć do wersji unipolarnej. Skuteczność działania takiego układu, w tym także zdolność łączeniowa i szybkość działania będą celem dalszych prac badawczych.

6.6. Literatura

[1] Kaźmierczak M.: „Zwarcia łukowe – doświadczenia eksploatacyjne w polskiej energetyce zawodowej i przemysłowej”, Elektroenergetyka – współczesność i rozwój, nr 2 (8), 2011.

[2] Volger J.: „Arc fault protection as seen by employers’ liability insurance associations”, The arc-fault demonstration in the head office of the Moeller GmbH, Bonn 2008.

[3] ABB, Protection against electric arc Integration between Arc Guard System™ TVOC-2 and SACE Emax 2, online: https://library.e.abb.com/public/fc33af751d664dad932e9c7344cffec0/1SDC007407G0203_revB_Protection%20against%20electric%20arc%20.pdf , available 17.02.2022r.

[4] Lu, Q.; Ye, Z.; Zhang, Y.; Wang, T.; Gao, Z. Analysis of the Effects of Arc Volt–Ampere Characteristics on Different Loads and Detection Methods of Series Arc Faults. Energies 2019, 12, 323, doi:10.3390/en12020323.

[5] Yin, Z.; Wang, L.; Zhang, Y.; Gao, Y. A Novel Arc Fault Detection Method Integrated Random Forest, Improved Multi-Scale Permutation Entropy and Wavelet Packet Transform. Electronics 2019, 8, 396, doi:10.3390/electronics8040396.

[6] Paul, S.; Jewell, W. Optimization Methodology for Minimizing the Arc Flash Incident Energy; 2018; p. 6;.

[7] J.C. Das: „Power System Analysis - Short-Circuit Load Flow and Harmonics", https://doi.org/10.1201/9780203908952

[8] Kasikci, Ismail. Short circuits in power systems: A practical guide to IEC 60909-0. John Wiley & Sons, 2018.

[9] Tleis, Nasser. Power systems modelling and fault analysis: theory and practice. Elsevier, 2007.

[10] H.B. Land, C.L Eddins, J.M. Klimek, 2004, "Evolution of Arc Fault Protection Technology at APL", Johns Hopkins APL Technical Digest, Volume 25, Number 2, 2004.

[11] Kaźmierczak M.: „Zwarcia łukowe – doświadczenia eksploatacyjne w polskiej energetyce zawodowej i przemysłowej", Elektroenergetyka – współczesność i rozwój, nr 2 (8), 2011.

[12] Volger J.: „Arc fault protection as seen by employers' liability insurance associations", The arc-fault demonstration in the head office of the Moeller GmbH, Bonn 2008.

[13] Szadkowski, M., Warachim, A., Dekarz, K., „Minimalizacja skutków zwarć łukowych w stacjach wnętrzowych SN", Energetyka, 2015, nr 12, str. 791—797

[14] PA Scarpino, A. Reatti i F. Grasso, „AC Arc Flash Analysis: a new derivation method", 2018 AEIT International Annual Conference , 2018, s. 1-4, doi: 10.23919/AEIT.2018.8577341.

[15] Kumpulainen, Lauri & Dahl, Samuel. (2009). Selective arc-flash protection. 1 - 4. 10.1049/cp.2009.0900.

[16] Ghulam Amjad Hussain, „Methods for Arc-Flash Prediction in Medium Voltage and Low Voltage Switchgear", Aalto University publication series DOCTORAL DISSERTATIONS 221/2015

[17] R.A. Jones, D.P. Liggett, M. Capelli-Schellpfeffer, T. Macalady, L.F. Saunders, R.E., Downey, B. McClung, A., Smith, S., Jamil, V. Saporita, 2000, "Staged tests increase awareness of arc-flash hazards in electrical equipment", IEEE Transactions on Industry Application, Vol. 36, No 2, March/April 2000.

[18] T. Dugan, 2007, “Reducing the arc flash hazard”, IEEE Industry Applications Magazine, p. 51-58, May/June 2007.

[19] J. A. Kay, L. Kumpulainen, „Maximizing Protection by Minimizing Arcing Times in Medium -Voltage Systems”, IEEE Transactions on industry applications, vol. 49, no. 4, july/august 2013

[20] Ghulam Amjad Hussain, „Methods for Arc-Flash Prediction in Medium Voltage and Low Voltage Switchgear”, Aalto University publication series DOCTORAL DISSERTATIONS 221/2015

[21] J. Turowski, „Elektrodynamika Techniczna”. WN-T, Warszawa, 1993

[22] S. Kulas, „Tory prądowe i układy zestykowe, OWPW, Warszawa, 2008

[23] Królikowski C.: Inżynieria łączenia obwodów elektrycznych wielkiej mocy. WPP, Poznań 1998.

[24] Bohdan Koch, Jan Maksymiuk, „Łukoodporność rozdzielnic osłoniętych i symulacja zwarć łukowych”, Oficyna Wydawnicza Politechniki Warszawskiej, Warszawa 2007.

[25] Mohla, D.; Lee, W.; Phillips, J.; Marroquin, A. Introduction to IEEE Standard. 1584 IEEE Guide for Performing Arc-Flash Hazard Calculations- 2018 Edition. In Proceedings of the 2019 IEEE Petroleum and Chemical Industry Committee Conference (PCIC); September 2019; pp. 1–12.

[26] Mohla, D.; Lee, W.-J.; Phillips, J.; Marroquin, A. Introduction to IEEE Standard 1584: Guide for Performing Arc-Flash Hazard Calculations, 2018 Edition. *IEEE Industry Applications Magazine* 2020, *26*, 64–76, doi:10.1109/MIAS.2020.2982574.

[27] Gammon, T.; Matthews, J. Conventional and Recommended Arc Power and Energy Calculations and Arc Damage Assessment. *IEEE Transactions on Industry Applications* 2003, *39*, 594–599, doi:10.1109/TIA.2003.811775.

[28] IEEE Guide for Performing Arc-Flash Hazard Calculations. IEEE Std 1584-2018 (Revision of IEEE Std 1584-2002) 2018, 1–134, doi:10.1109/IEEESTD.2018.8563139.

[29] IEEE 1584-2018 - IEEE Guide for Performing Arc-Flash Hazard Calculations Available online: https://standards.ieee.org/standard/1584-2018.html (accessed on 17 January 2021).

[30] Mohla, D.; Lee, W.-J.; Phillips, J.; Marroquin, A. Introduction to IEEE Standard 1584: Guide for Performing Arc-Flash Hazard Calculations, 2018 Edition. IEEE Industry Applications Magazine 2020, 26, 64–76, doi:10.1109/MIAS.2020.2982574.

7. KOPIE PUBLIKACJI NAUKOWYCH STANOWIĄCYCH ROZPRAWĘ DOKTORSKĄ

Publikacja I

Karol Nowak, Jerzy Janiszewski, Grzegorz Dombek: „Thyristor Arc Eliminator for Protection of Low Voltage Electrical Equipment". *Energies 2019*, 12(14), 2749; https://doi.org/10.3390/en12142749

energies

MDPI

Article

Thyristor Arc Eliminator for Protection of Low Voltage Electrical Equipment

Karol Nowak *, Jerzy Janiszewski and Grzegorz Dombek

Institute of Electric Power Engineering, Poznan University of Technology, Piotrowo 3A, 60-965 Poznan, Poland
* Correspondence: karol.nowak@put.poznan.pl; Tel.: +48-61-665-2584

Received: 5 June 2019; Accepted: 17 July 2019; Published: 18 July 2019

Abstract: The paper presents the layout of two opposing thyristors working as an Arc Eliminator (AE). The presented solution makes it possible to protect an electrical apparatus against the effects of an arcing fault. An Arc Eliminator is assumed to be a device cooperating with the protected apparatus. Thyristors were used because of their speed of operation and a relatively lower cost compared to other semiconductors with the same current-carrying capacity. The proposed solution, as one of the few currently available, makes it possible to eliminate the fault arc—both at short-circuit currents and current values to which overcurrent protections do not react. A test circuit was designed and made to study the effectiveness of the thyristor arc eliminator. A series of tests was carried out with variable impedance in the arc branch, including the influence of circuit inductance on arc time. It was found that the thyristor arc eliminator effectively protects devices powered from a low voltage power network against the effects of a fault or arc fault. The correctness of system operation for a wide range of impedance changes in the circuit feeding the arc location was demonstrated.

Keywords: arc eliminator; arc fault; arc protection; low voltage; thyristor

1. Introduction

1.1. Motivation

Most arcing faults in a power system can be described as large discharges of electrical energy between conductors. The occurrence of short circuits can be indirectly conditioned by many factors, such as mechanical damage [1], insulation aging [2], overvoltages [3] and surface discharges [4]. In addition, arching faults in a power system that are associated with erroneous switching activities, accidental rapprochement or touching of active parts, as well as fatigue, insufficient concentration, and haste at work may contribute to short circuits directly [5]. The occurrence of the electric arc phenomenon is accompanied by the release of significant energy, the effects of which may be the heating and destruction of the power equipment, as well as a sharp growth of pressure inside the enclosed elements. In addition to hazards to the devices (both in the switchgear and near the location of short circuit), this energy can also be a threat to people in close proximity to the arcing (glare, burn) [6–8].

Improving the operational safety of receiving and power circuits requires (sometimes on a compulsory basis) a reduction of the effects of fault currents and occurrence of a fault arc. From the existing methods of elimination of the effects of arcing fault, two main ones [9] can be distinguished – limitation of the electric current value and limitation of arc discharge duration. The limitation of the current value is achieved by connecting series impedance to the powered circuit. However, it can have a negative effect on the activation time of overcurrent protection, thus leading to a longer arc discharge time and increased energy released in the electric arc. Consequently, the time-limitation approach is usually preferred [6]. Switches equipped with power electronics actuators (semiconductor switches) meet the condition of shortening the arc time and can be used to effectively protect circuits against the

effects of an arc fault, short-circuit arcing, and arc burning at operating and overload currents [9]. The use of a semiconductor arc eliminator enables obtaining virtually instantaneous elimination of the arc fault in the damaged circuit, commutation of short-circuit current without an arc in the branch of the arc eliminator, shortening the time of influence of thermal effects in the protected circuit, and even (when faults are detected before the first amplitude of short-circuit current) reducing the effects of electrodynamic interactions [10].

Extinguishing the arc fault with the use of an arc eliminator is based on the fact that as soon as a flash (coming from the arc) appears in the affected circuit, it is detected and one of the parallel semiconductor devices is triggered [11]. The voltage of the burning arc is usually greater than 20 V. Such a voltage value is sufficient for the semiconductor to switch to the conduction state, which results in a very fast bypassing of the electric circuit affected by the failure, aimed at creating an alternative (privileged) path for the current flow. In this way, current is immediately eliminated in the protected circuit. The voltage of the conductive semiconductors is much smaller than the voltage of the burning arc, which in turn makes it possible to extinguish the arc fault.

1.2. Literature Review

The Arc Eliminator (AE) belongs to the family of bypass system of the electric circuits above the place affected by the failure. Its task is to quickly eliminate the arc fault, preventing the further development of an electric discharge. Operation of the system relies on commutating the current in the branch of the AE at the moment of failure in the protected electrical circuit. The bypass system can be used in a wide range of applications such as:

- motor drive systems using frequency converters (inverters), in which an arc fault may not be eliminated by the protection system [12],
- industrial manufacturing facilities where capacitors play a role of reactive power compensation [13],
- power systems using photovoltaic panels, where the bypass system can suppress overvoltages, which can induce excessive overheating of cells and, as a result, cause permanent damage to photovoltaic cells [14],
- a hybrid circuit breaker, which is a combination of a mechanical switch and a semiconductor bypass branch, where the bypass system plays the role of un-arc circuit current commutation [15],
- a hybrid vacuum switch, where the vacuum chamber is bypassed by a semiconductor circuit, which commutates the flow of the electric current without an arc [16],
- an arc protection system in electric vehicles powered with constant voltage [17].

There are many solutions for the construction of drive systems and branches of bypass circuits. One of them is a mechanical switch whose drive is based on Thomson's electromagnetic coil [18,19]. The advantage of this solution is a mechanical bypass system characterized by appropriate speed and high current-carrying capacity. However, the disadvantage of the solution is the complexity of the drive mechanism and the cost of its implementation. Another solution is spring mechanisms accelerated by electromagnetic systems [6,20,21]. In contrast to the drive built on the basis of the Thomson coil, these mechanisms are characterized by simpler construction and lower cost of execution. Yet, the disadvantage of this solution is a longer operating time. Ultra-fast earthing switches based on the vacuum chamber are also used as drive systems for bypass branches [22]. It permits commutation of the current without an arc in the circuit affected by the failure. The most unfavourable switching operation of the vacuum chamber is short circuit closure, which can cause the working contacts to bond. The pyrotechnic charge explosion systems are also used to interrupt the fault arc [23]. This solution offers a high response speed. Nevertheless, each operation of the limiter requires the replacement of detonators and explosive charges, which entails additional costs and downtimes in the supply of electricity. One of the most promising solutions for elimination of the fault arc is semiconductor bypass systems [10]. With regard to the aforementioned solutions, they are characterized by much

faster activation (from the moment of arc detection to the time of full shunting of the place affected by the failure), ease of making the complete arc-protecting device, and a low cost of production. One disadvantage of this solution is the limited possibility of using the protection in medium voltage networks, which requires the serial connection of semiconductor devices in order to obtain the required voltage strength.

1.3. Contributions and Paper Organization

Research into the use of the arc eliminator semiconductor is based on the application of bypass thyristor branch [10]. However, the authors of these tests present only the results obtained through trials in a system fed from capacitor batteries. The effect of this is the course of a single half-wave of current starting in the amplitude of the supply voltage. In addition, Zhang and others in reference [10] only focused on two circuit inductance values. Therefore, in this paper, the authors present the results of research from an attempt to extinguish the electric arc using two thyristors connected in opposition supplied with alternating current of frequency of 50 Hz, for over a dozen values of the circuit inductance. This solution made it possible to confirm the effectiveness of protection of power circuits against the effects of an electric arc in devices fed from AC mains under resistive and inductive loads. The traditional overcurrent protections do not eliminate the electric arc with currents below their response currents. The proposed system accomplishes both the extinguishing of the arc and the forcing switch-off by the main overcurrent protection in the supply circuit. The system of two oppositely connected thyristors, presented and examined in this paper, was proposed due to the expected speed of action.

The paper has been organized in the following way. The second chapter explains the principle of the arc eliminator. The designed and built-in test circuit is also presented in detail. The third chapter presents the results of experimental investigations on the ability to extinguish the arc in AC low voltage networks using the thyristor arc eliminator. The results of the study were analyzed and discussed in the fourth chapter. The last, fifth chapter contains a summary and final conclusions.

2. Thyristor Arc Fault Eliminator

2.1. Principle of Operation

The thyristor arc eliminator (AE) is a protective device connected in parallel to the load (it can be placed in e.g., the electrical switchboard). A substitute diagram of the low voltage network circuit is shown in Figure 1.

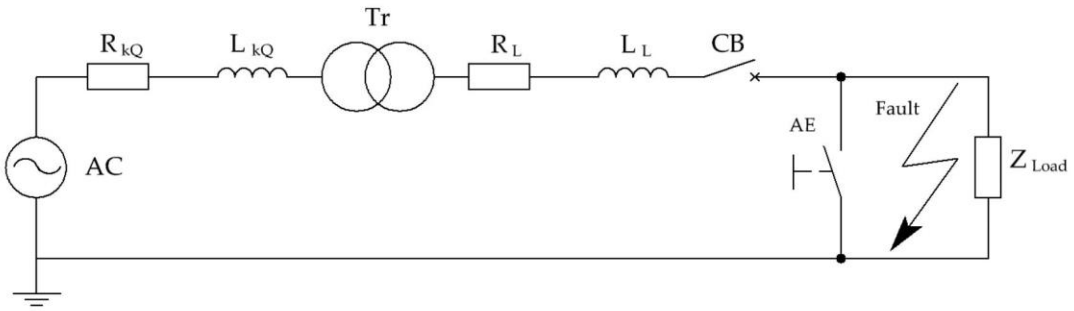

Figure 1. Scheme of using the Arc Eliminator to protect low voltage network devices; R_{kQ}—resistance of the power system [Ω], L_{kQ}—inductance of the power system [H], Tr—transformer with resistance R_{Tr} and reactance X_{Tr} [Ω], R_L—resistance of the power line [Ω], L_L—inductance of the power line [H], CB—circuit breaker, Z_{Load}—load with resistance R_{LOAD} and reactance X_{LOAD} [Ω], AE—arc eliminator, I, i—effective and instantaneous current values at characteristic points of the circuit, U, u—effective and instantaneous voltage values at characteristic points of the circuit.

Assuming that the supply voltage at the moment of fault has the instantaneous value described by this equation:

$$u = U_m \cdot \sin(\omega \cdot t + \psi), \tag{1}$$

at the moment of the appearance of the electric arc, the instantaneous value of short-circuit current i flowing through the secondary winding of the transformer is the sum of the instantaneous values of alternating-current component i_{AC} and direct-current component i_{DC} of the short-circuit current:

$$i = i_{AC} + i_{DC} = \sqrt{2} \cdot I''_K \left[\sin(\omega t + \psi - \varphi_Z) - e^{-\frac{R}{L}t} \cdot \sin(\psi - \varphi_Z) \right], \tag{2}$$

where ω is a voltage pulsation, φ_Z is the short-circuit impedance argument, Ψ is the phase angle of voltage at the moment of short-circuit, I''_K is the effective value of the initial short circuit current [A], and L and R are the elements of the fault circuit impedance.

An electric arc may ignite during the fault current flow. Activation of the electric arc detector generates a signal that controls the arc eliminator (AE). A virtually immediate activation of AE commutes the flow of fault current in the bypass (AE) until the main switch is activated or the electric arc is put out. Because the voltage drop on the thyristor arc eliminator (AE) is negligible compared to the arc voltage, the arc is extinguished in a very short time, often without the main circuit protection being switched off.

In the absence of an arc eliminator (AE), the total time of turning off the arc fault is influenced by fault detection time and time of tripping the circuit breaker (CB). Apart from the time needed to activate the disturbance detector (activation of the optical, voltage, current component, etc.) and send control signals, the decisive aspect is the time of delay of tripping the circuit breaker, which ranges between 20 ms and 60 ms for various protection devices in the low-voltage network. During this time, a burning electric arc, which is generating heat energy, may cause a complete destruction of the electrical apparatus, undermine the insulation of power supply cables, or damage the inside of the electrical switchgear.

Arc energy W_a is described by the following dependence:

$$W_a = \int_0^{T_a} u_a \cdot i_a \cdot dt, \tag{3}$$

where u_a is the instantaneous value of the arc voltage [V], i_a is the instantaneous value of arc current [A], and T_a is the duration of the electric arc [s].

The energy of a 20 ms arc for the rms value of 1 kA current and 80 V voltage is 1.6 kJ. Extending the arc fault duration to 60 ms results in an increase of the arc energy to 4.8 kJ. Assuming the arc voltage which does not undergo any significant changes, the arc energy increases in direct proportion to the arc time and the value of the fault current. It is assumed that for arc energy values lower than 100 kJ, repairs of electrical equipment mainly boil down to their cleaning [24]. The task of the arc eliminator is to shorten the arc time, whereby the amounts of energy emitted on the arc will be reduced.

The arc eliminator (AE) is only activated when an electric arc occurs. The solution can protect electrical equipment installed in e.g., a switchgear. The bypass branch of the arc eliminator can force the flow of a large fault current, therefore it is necessary to provide additional protection for the transformer in the switchgear station.

The thyristor shunt branch may in the least favorable case conduct through the time of a half-wave of the flowing current (10 ms). This time does not result from the difficulty to extinguish the arc with the AE but from switching off the thyristor, which stops conducting when the current passes through zero. In order not to damage the thyristors during the flow of the fault current, their limit parameters must be properly selected and the thyristor itself must be equipped with a heat sink to dissipate the heat.

2.2. Circuit Design

At the moment of detecting a flash of an electric arc, the short circuit is bypassed by a system of two reciprocally connected thyristors, which commutate the flow of current in the branch bypassing the place where the interference has occurred. The voltage drop on the conductive thyristors is lower than the voltage of the burning arc. The electric arc is extinguished. The test used TR51-80-12-76 (Unitra-Lamina, Poland) thyristors. The parameters of the thyristors are presented in Table 1.

Table 1. Parameters of the Unitra-Lamina TR51-80-12-76 thyristors (Adapted from [25]).

Parameter	Value
Surge current I_{TSM} [A]	1260
Repetitive peak reverse voltage U_{RRM} [V]	1200
I^2t value [A^2s]	7900
Rate of rise of on-state current repetitive di/dt [A/µs]	50
Critical rate of raise of off-state voltage du/dt [V/µs]	1000
Circuit commutated turn-off time (typical) t_q [µs]	20
Turn-on time (typical) t_{ON} [µs]	4
Operating junction temperature T_i [°C]	125

In order to test the effectiveness of two oppositely connected thyristors operating as an arc eliminator (AE) in low-voltage networks and powered by the available power system, the test electrical circuit shown in Figure 2 was built.

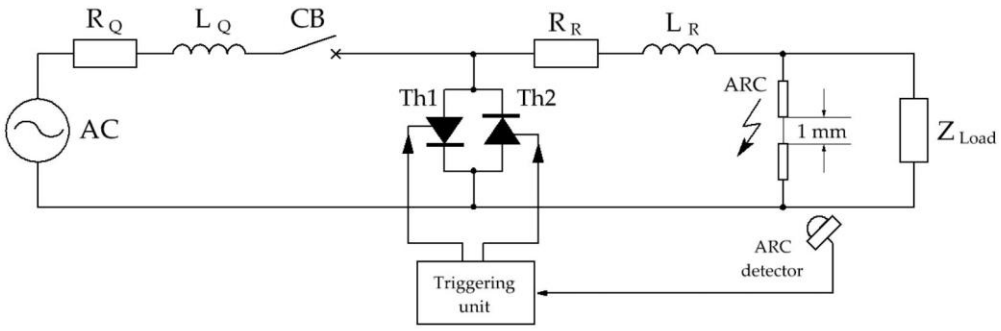

Figure 2. Arc eliminator test circuit (AE).

The triggering unit works on the basis of arc detector signals (ARC detector), activate the arc eliminator (AE), which consists of oppositely connected Th1 and Th2 thyristors. Such connection allows its use in alternating current networks with a possible random emergency state. Thyristor Th1 conducts for the positive half-wave of current, and thyristor Th2 takes over to conduct for the negative half-wave.

The arc source is a pair of cylindrical carbon electrodes with a diameter of 5.76 mm, facing each other and separated by 1 mm. A fusible element is inserted between the electrodes, which after a preselected time delay (resulting from the diameter of the fusible element) initiates the ignition of the electric arc. For safety reasons, the arc generating system (electrode with a fuse and flash detector) is enclosed in an insulating casing.

The test circuit shown in Figure 2 is powered from an AC electrical network with an effective voltage of 230 V. The measured impedance of the Z_Q short circuit loop of the power supply circuit is 0.197 Ω. It is the sum of resistances (R_Q = 0.196 Ω) and inductance (L_Q = 0.148 mH). The expected amplitude of the short-circuit current I_k directly at the terminals of the power source is 1650 A. In series in the arc generator circuit there is variable impedance Z_R (R_R, L_L), enabling the arc current to be regulated. The impedance Z_{Load} is the load of the tested system, where $Z_{Load} >> Z_Q + Z_R$.

3. Experiments Results

Figure 3 shows a fragment of the test circuit of the arc eliminator together with the marked points of measurement signal registration. The supply voltage is recorded in relation to the PE protective conductor. The arc voltage has been registered using a differential voltage probe DP-50 (Pintek Electronics Co. Ltd., Shulin, New Taipei City, Taiwan). The measuring probes of the differential voltage probe were placed as close as possible to the electrodes of the arc generator. The value of current in the branches of the arc eliminator (AE) and load, as well as the current drawn from the source, were registered using the model current clamps PAC22 (Chauvin Arnoux, Paris, France).

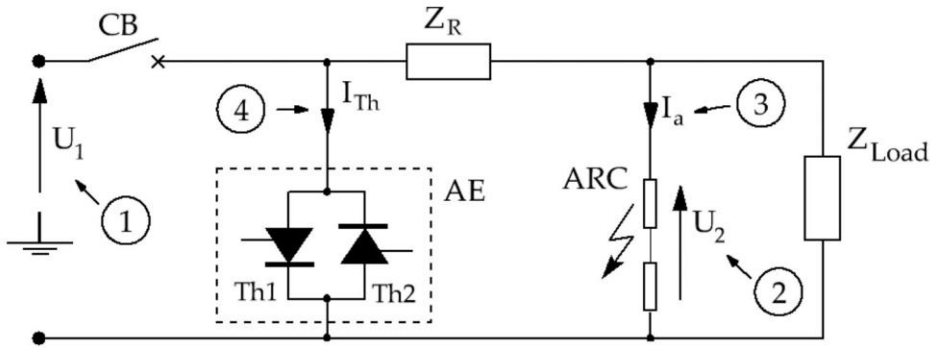

Figure 3. Part of the arc eliminator test circuit (AE) with marked measurement points: 1—supply voltage (U_1), 2—voltage on the electrodes of the arc source (U_2), 3—current in the branch of the arc source (I_a), 4—current in the thyristor branch (I_{Th}).

Figure 4a shows the current curve i_a, supply voltage U_1 and voltage measured on the electrodes of the arc generator U_2, registered in the system without the arc eliminator (AE). The presented experiment corresponds to a short circuit occurring close to the arc elimination system (regulatory impedance Z_R is practically negligible). The current flow is maintained for 47 ms until the main short-circuit protection is activated. The course of the short-circuit current contains the periodic component AC and a small non-periodic component DC hence the amplitude of the current I_a is decreasing. The peak current value is 1250 A. In order to facilitate readings, the moment t = 0 s, was adopted at the moment of arc ignition. During the current flow exceeding the permissible value for the fusible element, after a time of approx. 0.6 ms, arc ignition occurs between the electrodes. Then the arc burns between the carbon electrodes for approximately 47 ms. The arc voltage at the moment of ignition reaches 75 V. When the current passes through zero, the arc voltage drops to zero and the arc is extinguished. However, the favorable thermal conditions and the short distance between the electrodes cause re-ignition of the fault arc between the measuring electrodes.

Figure 4b shows the waveform of currents and voltages at a load inductance of 163 µH. An increase in the serial inductance L_R increases the value of the time constant τ for the LR circuit to approximately 2.9 ms. It is noticeable in the form of a phase shift between voltage and current, hence the effect of a burning arc at the moment when the supply voltage has already reached the zero value and is heading towards the negative values. The arc extinguishes when the arc current passes through zero.

A series of tests are aimed at checking the ability of a system of two oppositely connected thyristors to extinguish arcs in low-voltage AC circuits. A variable element in the tested circuit was serial L_R inductance, with constant values of the Z_Q power circuit.

Figures 5 and 6 show the test results at different moments of ignition and extinguishing of the electric arc. In each case, the load impedance is negligibly low in relation to the impedance of the entire circuit. This is due to bypassing by a branch with an electric arc. This action made it possible to reproduce a short circuit close to the arc eliminator system.

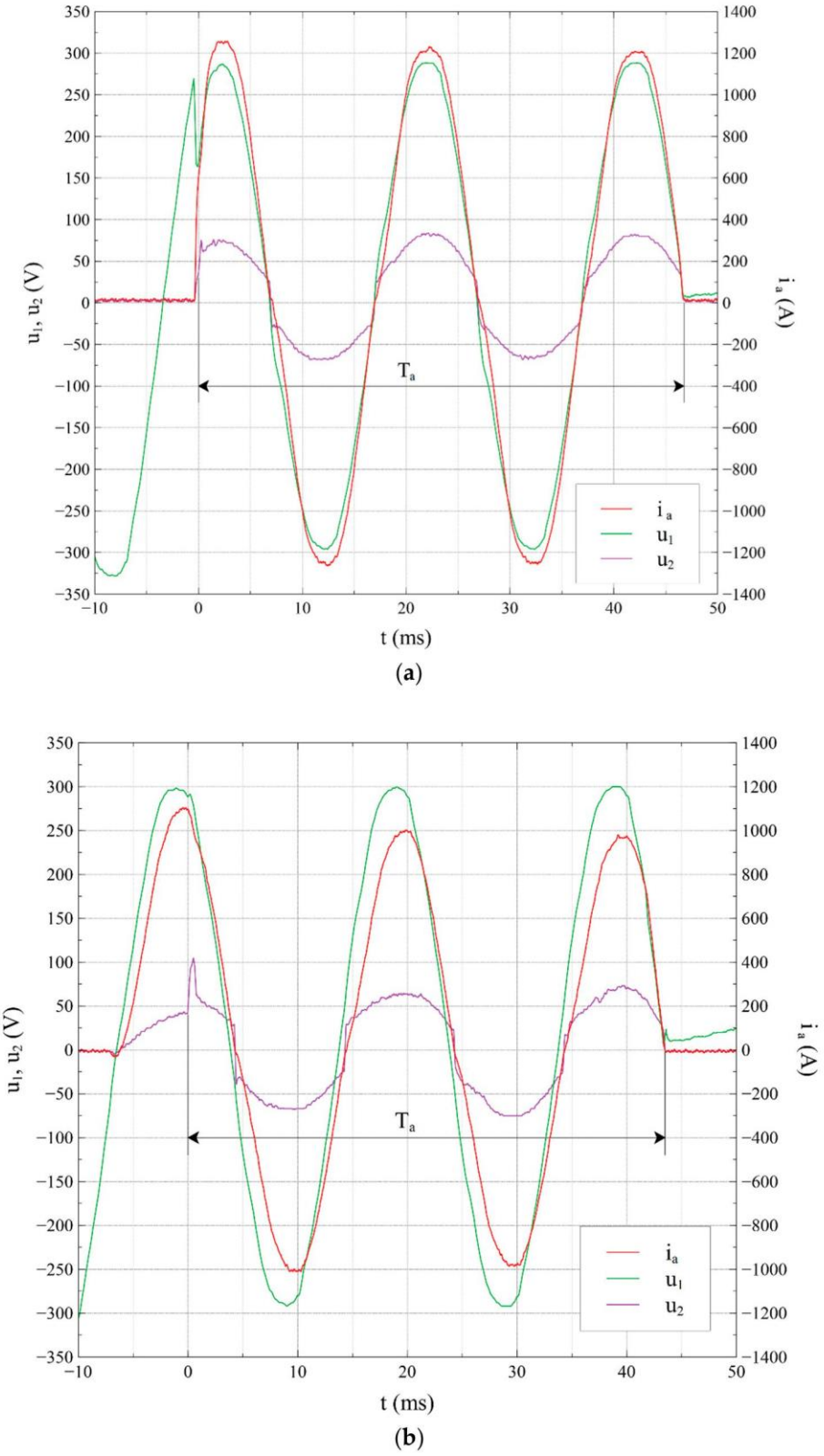

Figure 4. Arc current waveforms (i_a) and supply voltage (u_1) and voltage measured on the arc source electrodes (u_2) in a circuit in which thyristor Th1 and thyristor Th2 are not triggered: (**a**) L_R = 0 μH, arc time T_a = 47 ms; (**b**) L_R = 163 μH, arc time T_a = 43.5 ms.

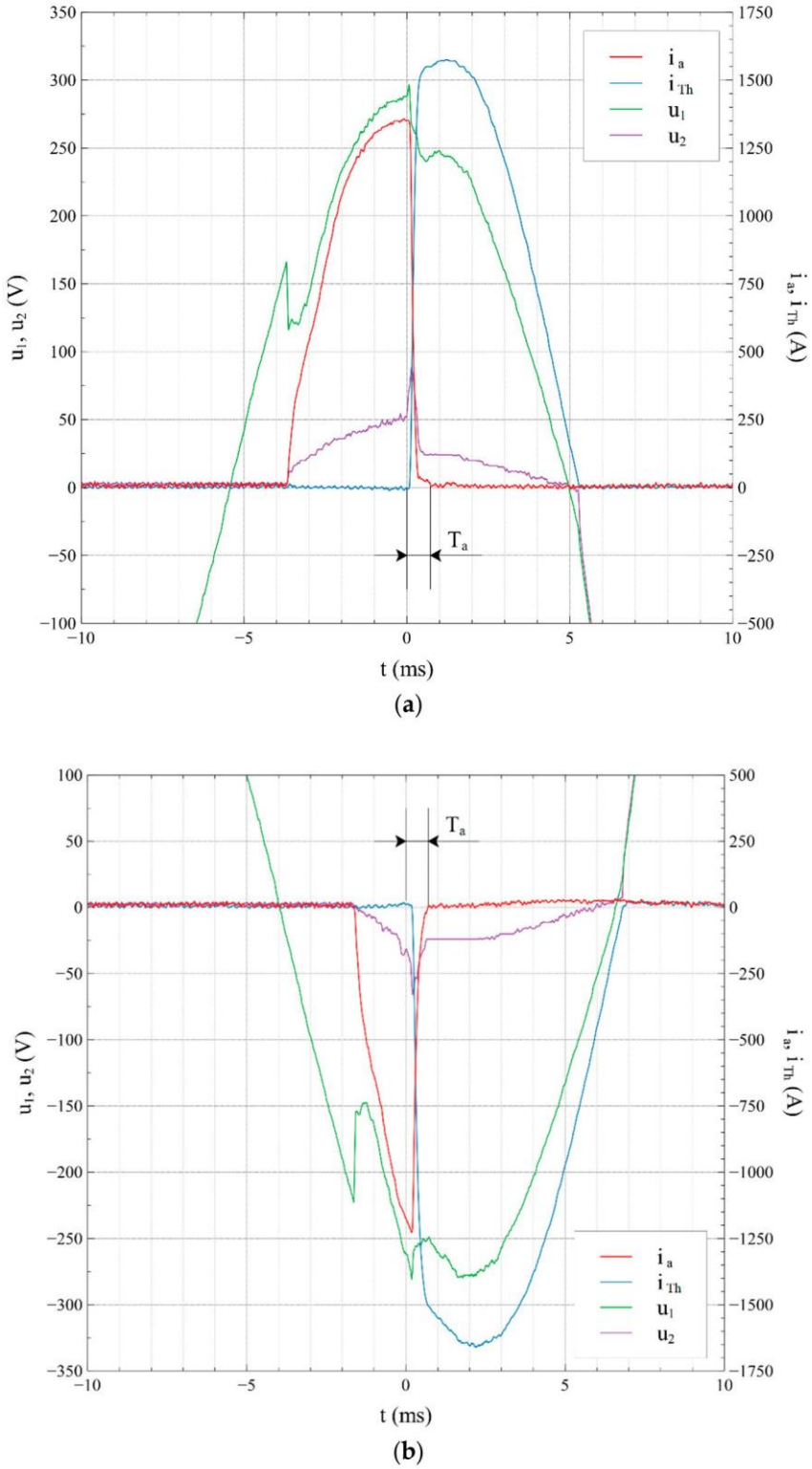

Figure 5. Current waveforms in the load (i_a) branch and current in the thyristor branch (i_{Th}) and supply voltage (u_1) and voltage measured on the arc source electrodes (u_2) in the arc eliminator system: (**a**) Arc eliminator switched on when an electric arc flash was detected for a positive half-wave of flowing current, L_R = 0 µH, arc time T_a = 0.72 ms; (**b**) Arc eliminator switched on when an electric arc flash was detected for a negative half-wave of flowing current L_R = 0 µH, arc time T_a = 0.7 ms.

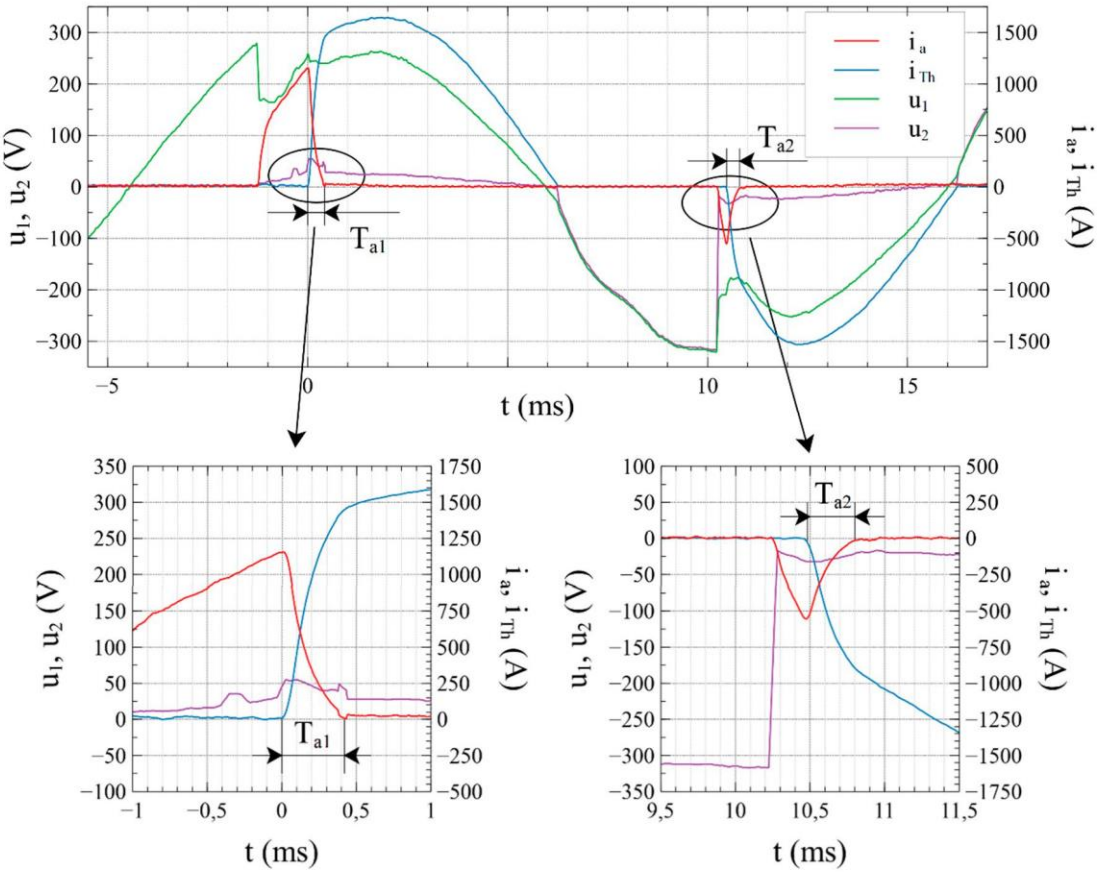

Figure 6. Current waveforms in the load branch (I_a), current in the thyristor branch (i_{Th}), supply voltage (u_1) and voltage measured on the arc source electrodes (u_2) at subsequent arc ignitions (T_{a1} = 0.42 ms, T_{a2} = 0.32 ms).

Figure 5a shows the elimination of the arc for the positive semi-wave of the flowing current. In turn, Figure 5b shows the elimination of the arc for the negative semi-wave of the flowing current. At the moment of arc ignition, the current and voltage in the branch of the arc source reach maximum values. The peak value of the current is 1600 A and the arc voltage at the moment of arc ignition is 80 V. When the explosion of a fusible element is detected by a detector, one of the thyristors of the arc eliminator is triggered. The voltage U_2 decreases to about 25 V, i.e., to the voltage of the conductive semiconductor branch of the arc eliminator. The commutation of the current by the thyristor branch I_{Th} causes the arc voltage U_a to be lowered below the minimum value of the burning arc, and as a result the arc is extinguished and the I_a current is reduced to zero. When the current passes through zero, the thyristor stops conducting and the current in the eliminator branch stops flowing. In the case of a positive half-wave of supply voltage, the arc time T_a from the moment of electric arc detection to taking over the full conduction through the thyristor in branch AE is 0.65 ms. In turn, in the case of a negative half-wave of the supply voltage, the arc time T_a is 0.52 ms.

When analyzing the voltage waveform on the U_2 arc generator electrodes, it can be interpreted in the following way: at the moment of the arc fault, this waveform is shown by the voltage on the arc. However, at the moment when the arc eliminator is activated, this waveform represents voltage on the conductive thyristors. In turn, when the arc is extinguished and the thyristors are not conducting, it represents the voltage of the mains supply.

Figure 6 shows the course of arc ignitions in the positive and negative half-wave of the supply voltage together with enlarged pieces for each of the ignitions. The first arc ignition, initiated by the disintegration of the fusible element, occurs during a positive half-wave of the supply voltage. The

elapsing time, from the moment of arc detection to the complete electric conduction over of the current conductivity by the Th1 thyristor, is 0.42 ms. When the current passes through zero, the conductive thyristor of the arc eliminator is switched off. Because of favorable conditions of electric arc formation, in the negative half-wave of power supply voltage the gap between electrodes is broken and another electric arc ignition occurs. The current in the branch affected by the arc fault disappears after 0.32 ms from the moment of detection and after triggering the Th2 thyristor in the branch of the arc eliminator.

Figure 7 shows the waveforms of currents and voltages recorded with variable regulatory inductance L_R ranging from 5 µH to 426 µH. The increase in serial inductance of L_R extends the time needed to turn off the arc. The term "arc extinguishing time T_a" should be understood as the interval from the moment of taking over the conductivity by the bypassing thyristor branch to the moment of current disappearance in the branch affected by the fault arc.

Analyzing Figure 7e, it can be seen that the arc ignition occurs in a positive half-wave of the supply voltage. Activation of the arc eliminator causes arc extinguishing in time T_a = 4.6 ms. Residues of the heated metallic material of the fuse excite the arc detector and the AE system reactivates again for a negative half-wave of the supply voltage. Thyristor Th1 conducts during the positive half-wave of the supply voltage, and thyristor Th2 takes over the conduction for the negative half-wave. The I_{Th} current is the sum of the currents of the thyristor branches.

The inductance of the power supply network resulting from the measured impedance of the short circuit loop is 148 µH. Figure 7f shows the situation in which the serial regulatory inductance L_R is three times as high as the inductance of the supply network. With such a large L_R value, the arc will not be put out even when the supply voltage goes through zero and then changes to the opposite sign. The arc is extinguished in the second half-wave of the flowing current after 4.6 ms from the moment of its detection. This is because the value of current in the arc branch decreases exponentially and the increase in inductance increases the value of the time constant.

Table 2 shows the elimination times of the electric arc for variable arc current regulation parameters. It shows that the inductive nature of the circuit extends the time of full commutation of the current through the bypass branch. In addition, it can also be noted that with the increase in serial inductance in the arc branch, the arc time increases its value. It means that the time needed to effectively extinguish the arc is increased. It is therefore advisable to place the arc eliminator as close as possible to the protected device or to minimize the inductance of the line feeding the receiver.

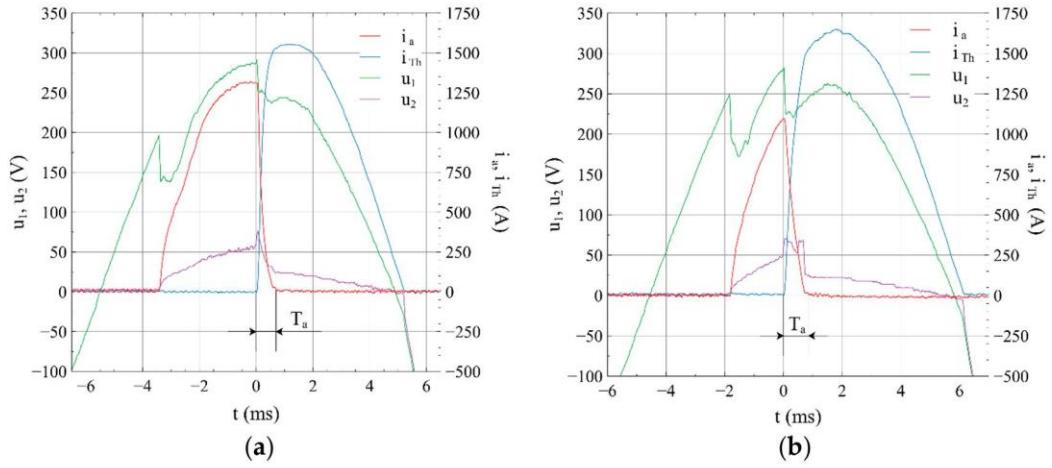

Figure 7. *Cont.*

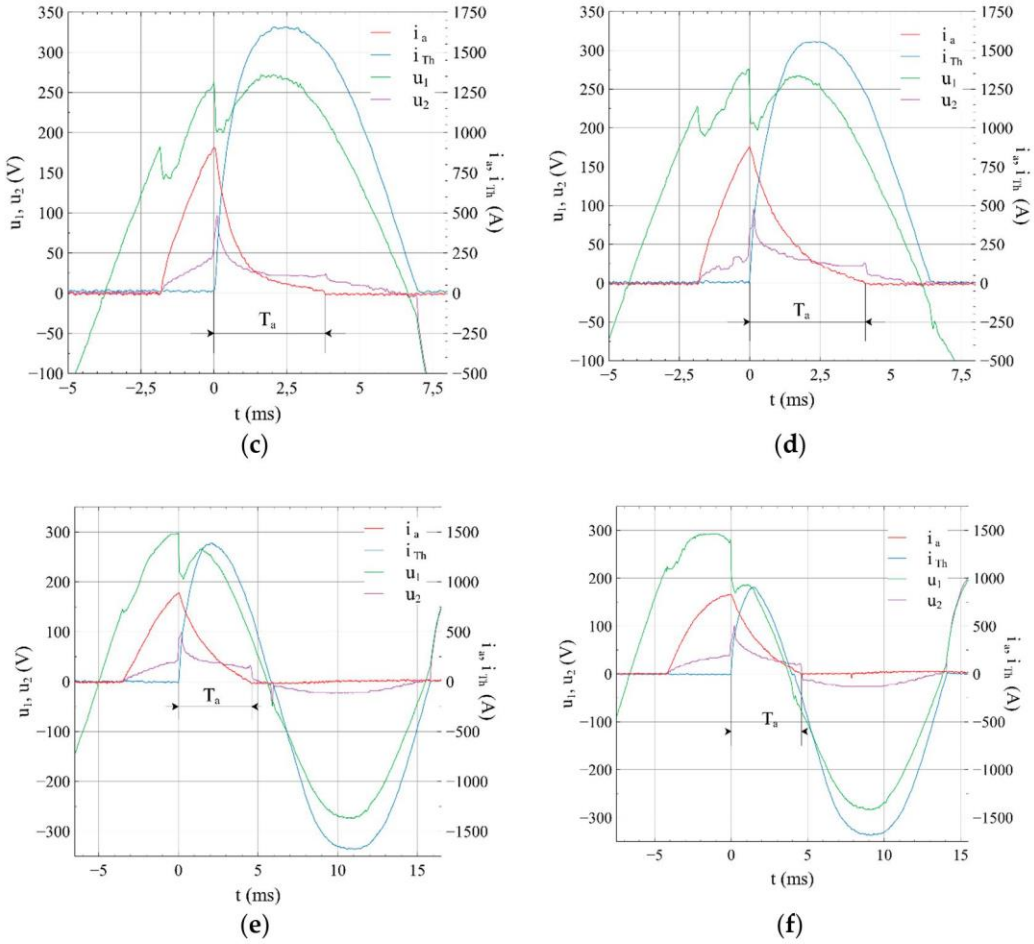

Figure 7. Current waveforms in the arc branch (i_a) and current in the thyristor branch (i_{Th}) and supply voltage (u_1) and voltage measured on the arc source electrodes (u_2) for various parameters of the current: (**a**) L_R = 5 µH, T_a = 0.7 ms; (**b**) L_R = 34 µH, T_a = 0.85 ms; (**c**) L_R = 76 µH, T_a = *3.8* ms; (**d**) L_R = 160 µH, T_a = 4.1 ms; (**e**) L_R = 286 µH, T_a = *4.6* ms; (**f**) L_R = 426 µH, T_a = 4.6 ms.

Table 2. Effect of serial inductance of arc branches on arc time.

No	Load L_R [µH]	Arc Time T_a [ms]
1	0	0.32–0.72
2	5	0.7
3	8.4	0.7
4	18	0.72
5	34	0.85
6	42	1.8
7	50	2
8	76	3.8
9	160	4.1
10	286	4.6
11	426	4.6

Figure 8 shows a graphical representation of the results in Table 2. The dependence of the influence of serial inductance with arc on the value of arc time is shown. Activation of the arc eliminator in time up to 0.7 ms can be observed for L_R inductance in the range from 0 µH to 34 µH. The next L_R increase

to 160 µH causes a rapid increase of arc time from 0.7 ms to 4.1 ms. After exceeding 160 µH, you can see a clear stabilization of arc time at the level of 4.6 ms.

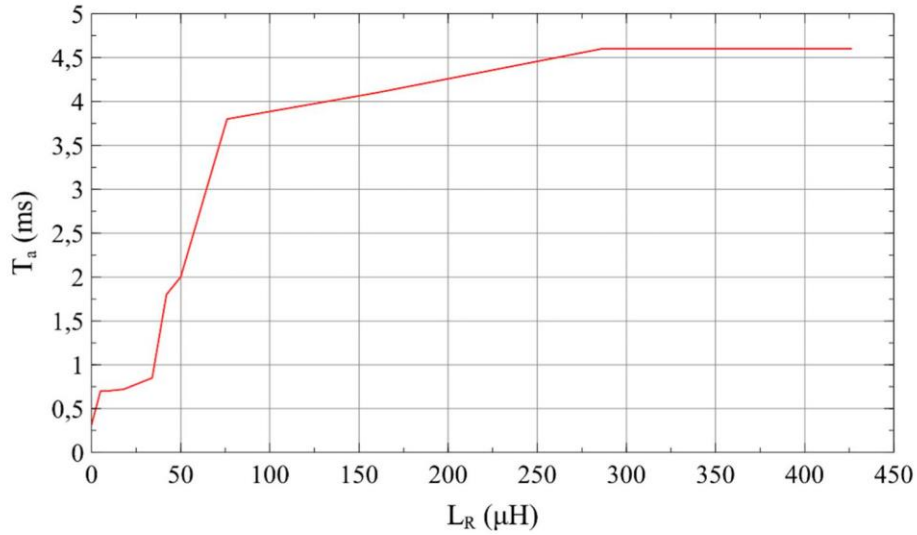

Figure 8. The dependence of series inductance in the L_R arc branch from the arc time T_a.

4. Discussion

The available literature contains little work addressing the use of controlled semiconductor devices to eliminate electric arc and reduce short-circuit effects in electrical power circuits. Authors Zhang and others in reference [10] stated that a thyristor can work as an arc eliminator in circuits of a resistive or capacitive-resistance character. Based on their research, they concluded that the arc eliminator would not fulfill its task (quick elimination of the arc) in inductive circuits or in a situation where the arc is formed at a large distance from the location of the arc eliminator. Their assumption may be correct in a situation where the protected object is powered from capacitor banks, which results in a single half-wave of current starting in the amplitude of the supply voltage. The authors of this paper, carrying out a series of tests for variable inductance of the circuit supplied from the AC power grid, demonstrated the effectiveness of the electric arc eliminator both in resistive and inductive circuits. An increase in load inductance extends the time of arc eliminator activation but does not disqualify it as an arc protection device. It should be noted that in the context of protecting distant objects powered from low voltage AC power networks, the resistance of the circuit significantly exceeds its reactance. At the current stage of research, thyristors parameters, stemming from diversified technologies of their production, including, for example conduction voltage (several volts), are less important from the point of view of extinguishing an electric arc with a voltage exceeding 20 V. Diversified switching times for thyristors can be an optimization parameter, but are less important for the very nature of the eliminator operation.

5. Conclusions

The object of the above experiments was to check the possibility of using two oppositely connected thyristors as an emergency arc eliminator (AE). The semiconductor bypass system allows very fast bypassing of an electric circuit affected by arc disturbance, aimed at creating an alternative, privileged path for the current flow. In this way, the resulting electric arc is immediately eliminated. If the arcing fault occurred before reaching the maximum value of the flowing current, the elimination time of the arc fault affects the amplitude of the current in the affected branch. The shortening of the arc fault duration will reduce the amplitude of the fault current and the value of the arc energy released.

Experimental research has shown that in circuits with predominant resistance in relation to reactance, two oppositely connected thyristors can act as an arc eliminator, which will extinguish the

arc in less than 0.7 ms. The work of thyristors as arc eliminators becomes more difficult in circuits where high inductance occurs between the power source and the place of emergence of the fault arc. The arc extinguishing time increases with the increase of serial inductivity to the value of 4.6 ms. Despite the large serial inductance of the object affected by the arc disturbance and the significant extension of the time needed to extinguish the arc, the arc eliminator fulfills its purpose, even if the longer arc burning time causes its re-ignition in the next half-wave of electricity.

An interesting area for observation may be the work of the arc eliminator in a configuration similar to autoreclosing known in protection automation (automatic reclosed). At the moment of the arc detection, the eliminator thyristors are triggered, and the arc is extinguished. After the disappearance of arc interference, the thyristors cease to conduct in the next half-wave of current, and the voltage at the receiver terminals reaches the value of the mains voltage. In such cases, quick elimination of the arc does not trigger the main power switch.

Author Contributions: Section 1 was prepared by K.N. and G.D. Section 2 (Thyristor arc fault Eliminator) was described by K.N. and J.J. All the authors jointly planned the experiment, described by K.N in Section 3. Section 4 was prepared by K.N., G.D. and J.J. The experiment was conducted by K.N. and J.J. Conclusions (Section 5) were prepared jointly by all the authors.

Funding: This research was funded by the Ministry of Science and Higher Education, grant number 04/41/SBAD/4408.

Conflicts of Interest: The authors declare no conflict of interest.

Nomenclatures

Abbreviations

AE	arc eliminator
AC	power source (Alternating Current)
Tr	transformer
CB	circuit breaker
Th1, Th2	thyristors

Parameters

R_{kQ}	resistance of the power system
R_{Tr}	resistance of the transformer
R_L	resistance of the power line
R_{LOAD}	resistance of load
R	resistance of the fault circuit
R_Q	the measured resistance of the short circuit loop
R_R	serial resistance in the circuit of the arc generator
L_{kQ}	inductance of the power system
L_L	inductance of the power line
L	inductance of the fault circuit
L_Q	the measured inductance of the short circuit loop
L_R	serial inductance in the circuit of the arc generator
Z_{Load}	impedance of load
Z_Q	the measured impedance of the short circuit loop
Z_R	serial impedance in the circuit of the arc generator
X_{Tr}	reactance of the transformer
X_{LOAD}	reactance of load
I, i	effective and instantaneous current values at characteristic points of the circuit
I''_K	the effective value of the initial short circuit current
I_a	current in the branch of the arc source
I_{Th}	current in the thyristor branch
i_{AC}	alternating-current component
i_{DC}	direct-current component
i_a	the instantaneous value of arc current
U, u	effective and instantaneous voltage values at characteristic points of the circuit

U_m	supply voltage amplitude
U_a	the value of the arc voltage
U_1	supply voltage
U_2	voltage on the electrodes of the arc source
u_a	the instantaneous value of the arc voltage
u_1	the instantaneous value of the supply voltage
u_2	the instantaneous voltage value on the electrodes of the arc source
ω	pulsation voltage values or current values
ψ	phase angle of voltage at the moment of short circuit
φ_z	the short circuit impedance argument
W_a	arc energy
T_a	the duration of the electric arc

References

1. Yang, L.; Qiu, W.; Huang, J.; Hao, Y.; Fu, M.; Hou, S.; Li, L. Comparison of conductor-temperature calculations based on different radial-position-temperature detections for high-voltage power cable. *Energies* **2018**, *11*, 117. [CrossRef]
2. Lu, Q.; Ye, Z.; Zhang, Y.; Wang, T.; Gao, Z. Analysis of the effects of arc volt-ampere characteristics on different loads and detection methods of series arc faults. *Energies* **2019**, *12*, 323. [CrossRef]
3. Yang, Q.; Wang, J.; Sima, W.; Chen, L.; Yuan, T. Mixed over-voltage decomposition using atomic decompositions based on a damped sinusoids atom dictionary. *Energies* **2011**, *4*, 1410–1427. [CrossRef]
4. Yin, Z.; Wang, L.; Zhang, Y.; Gao, Y. A novel arc fault detection method integrated random forest, improved multi-scale permutation entropy and wavelet packet transform. *Electronics* **2019**, *8*, 396. [CrossRef]
5. Whittingham, R.B. *The Blame Machine. Why Human Error Causes Accidents*, 1st ed.; Elsevier Butterworth Heinemann Linacre House: Burlington, MA, USA, 2004; pp. 237–242.
6. Kay, J.A.; Kumpulainen, L. Maximizing protection by minimizing arcing times in medium-voltage systems. *IEEE Tech. Ind. Appl.* **2013**, *49*, 1920–1927. [CrossRef]
7. Dugan, T. Reducing the flash hazard. *IEEE Ind. Appl. Mag.* **2007**, *13*, 51–58. [CrossRef]
8. Hodder, M.; Vilchek, W.; Croyle, F.; McCue, D. Practical arc-flash reduction. *IEEE Ind. Appl. Mag.* **2006**, *12*, 22–29. [CrossRef]
9. Hussain, G.A. Method for Arc-Flash Protection in Medium Voltage and Low Voltage Switchgear. Ph.D. Thesis, Aalto University, Helsinki, Finland, 2015.
10. Zhang, Z.; Ma, B.; Friberg, A. Thyristor working as arc eliminator protecting electrical apparatus in low voltage power system. In Proceedings of the IEEE International Conference on Industrial Technology (ICIT), Seville, Spain, 17–19 March 2015; pp. 1216–1219.
11. Yang, K.; Zhang, R.; Yang, J.; Liu, C.; Chen, S.; Zhang, F. A novel arc fault detector for early detection of electrical fires. *Sensors* **2016**, *16*, 500. [CrossRef] [PubMed]
12. Boren, S.G. Intelligence Automatic Bypass for a Motor Control Device Fault. U.S. Patent US20040252423A1, 16 December 2004.
13. Bhargava, B.; Haas, R.G. Thyristor protected series capacitors project at Southern California Edison Co. In Proceedings of the IEEE Power Engineering Society Summer Meeting (PESS), Chicago, IL, USA, 21–25 July 2002; pp. 241–246.
14. Pulvirenti, F.; La Scala, A.; Pennisi, S. Low voltage-drop bypass switch for photovoltaic applications. In Proceeding of the IEEE International Symposium on Circuits and Systems (ISCAS), Seoul, Korea, 20–23 May 2012; pp. 2283–2286.
15. Backman, M.; Demetriades, G.; Shukla, A. Hybrid Circuit Breaker. European Patent Patent No. EP2465129B1, 24 April 2013.
16. Liu, L.; Zhuang, C.; Wang, Z.; Jiang, Z.; Wu, J.; Chen, B. A hybrid DC vacuum circuit breaker for medium voltage: Principle and first measurements. *IEEE Tech. Power Deliv.* **2015**, *30*, 2096–2101. [CrossRef]
17. Naidu, M.; Schoepf, T.J.; Gopalakrishnan, S. Arc fault detection scheme for 42-V automotive DS networks using current shunt. *IEEE T. Power Electr.* **2006**, *21*, 633–639. [CrossRef]
18. Hatsagi, B. Electromagnetic Modelling and Testing of a Thomson Coil Based Actuator. Master's Thesis, KTH Royal Institute of Technology, Stockholm, Sweden, 2017.

19. Pei, X.; Smith, A.C.; Shuttleworth, R.; Vilchis-Rodriguez, D.S.; Barnes, M. Fast operating moving coil actuator for vacuum interrupter. *IEEE Tech. Energy Convers.* **2017**, *32*, 931–940. [CrossRef]
20. Bissal, A.; Eriksson, A.; Magnusson, J.; Engdahl, G. Hybrid multi-physics modeling of an ultra-fast electro-mechanical actuator. *Actuators* **2015**, *4*, 314–335. [CrossRef]
21. Peng, C.; Husain, I.; Huang, A.Q. Evaluation of design variables in Thompson coil based operating mechanisms for ultra-fast opening in hybrid AC and DC circuit breakers. In Proceedings of the IEEE Applied Power Electronics Conference and Exposition (APEC), Charlotte, NC, USA, 15–19 March 2015; pp. 2325–2332.
22. Oeberg, A.; Chimento, F.; Qin, J.; Wang, L.; Jeppsson, O. Bypass Switch Assembly. U.S. Patent US9099268B2, 4 August 2015.
23. Tirmizi, A.A. Pyrotechnic Circuit Breaker. U.S. Patent US7239225B2, 3 July 2007.
24. Partyka, R. *Investigation of Fault-Arcs Effects in Enclosed Switchgear*, 1st ed.; Gdansk University of Technology Publisher: Gdansk, Poland, 2008; pp. 22–96. (In Polish)
25. The Catalogue of Power Semiconductor Devices. Thyristors. Available online: http://delibra.bg.polsl.pl/Content/30503/BCPS_34289_1986_Tyrystory---przyrzad.pdf (accessed on 3 July 2019).

Publikacja II

Karol Nowak, Jerzy Janiszewski, Grzegorz Dombek: „A Multi-Sectional Arc Eliminator for Protection of Low Voltage Electrical Equipment”. *Energies 2020*, 13(3), 605; https://doi.org/10.3390/en13030605

energies

MDPI

Article

A Multi-Sectional Arc Eliminator for Protection of Low Voltage Electrical Equipment

Karol Nowak *, Jerzy Janiszewski and Grzegorz Dombek

Institute of Electric Power Engineering, Poznan University of Technology, Piotrowo 3A, 60-965 Poznan, Poland; jerzy.janiszewski@put.poznan.pl (J.J.); grzegorz.dombek@put.poznan.pl (G.D.)

* Correspondence: karol.nowak@put.poznan.pl; Tel.: +48-61-665-2584

Received: 11 December 2019; Accepted: 28 January 2020; Published: 30 January 2020

Abstract: The paper presents a system of two oppositely connected multi-sectional thyristor branches. The system works as a multi-sectional arc eliminator (MSAE), protecting low-voltage electrical apparatus against the effects of an arcing fault. MSAE is designed to serve as a device cooperating with protected and secured electrical equipment. The use of thyristors in the proposed solution allows to obtain a high speed of operation, while multi-sectional thyristor branches significantly increase the permissible current load of the arc eliminator. A test circuit was designed and made to test the performance effectiveness of the multi-sectional thyristor arc eliminator. A number of tests were carried out with variable current values in the arc branch, taking into account the influence of thyristor conduction voltage and different thyristor gate release times. It was found that the multi-section thyristor arc eliminator system effectively protects devices powered from low voltage power network against the effects of interference or arc fault.

Keywords: arc eliminator; arc protection; current bypass

1. Introduction

Short circuits and accompanying electric arcs are the most difficult operating conditions in power circuits. Limiting the negative effects of these factors is an important element in improving the operational safety of power systems. One way to reduce these effects is by bypassing the affected circuit. For this purpose, contact jacks with relatively long switching times [1] and limited contact capacity are usually used. The long delay in tripping the bypass circuit is accompanied by a significant emission of heat energy from the arc burning in the affected circuit and its power supply current circuits.

Interference current shunting devices and systems are used in many protective applications. They can be found, for example, in motor-drive systems exposed to arcuate interference [2], reactive power compensation devices [3], photovoltaic panel protection systems [4], hybrid circuit breakers [5,6], electric vehicle protection systems [7], and circuit breaker systems used to prevent electric fires [8]. Bypassing circuits are built based on Thomson's electromagnetic coil [9,10], spring mechanisms accelerated by electromagnetic systems [11,12], circuits interrupted by an explosive charge [13] or containing compressed gas [14], and also on semiconductor devices [15,16].

One of the most common types of electrical short circuit is arc fault. Most often, an arc occurs as a result of improper operation of distribution devices, bad design solutions or environmental conditions in which electric devices work [17,18]. Among the many available methods for eliminating the effects of arc faults, two groups are interesting [19,20]:

- limitation of the current value by adding supplementary (higher) impedance to the power supply circuit,
- limitation of the arcing discharge duration.

The preferred solution from the power supply point of view is the arc time limitation method [21]. This effect can be achieved by bypassing the damaged circuit with semiconductor short circuiting elements. The use of a thyristor arc eliminator causes a virtually instantaneous elimination of the arc fault in the affected circuit [15,16]. An additional advantage of the arc eliminator (AE) is arc-free short-circuit current commutation in AE branches and a shorter duration of thermal effects in the protected circuit.

Little research has been done on the use of semiconductor components as short-circuit switches or arc eliminators [3,5,16,22,23]. The available works deal with currents ranging from hundreds to several thousand amperes. Short-circuit currents expected in many power circuits today exceed tens of thousands of amperes and no commercial thyristors with this current capacity have not been available so far. The thyristor multi-sectional arc eliminator (MSAE) presented in this paper is a way to solve this problem. A number of experiments described in publications [15,16] confirm the justifiability of using two counter-connected thyristors as an AE. This current research has been carried out for a multi-sectional semiconductor module, which is an improved version of the AE presented in paper [15]. This solution significantly extends the usability of the version presented in [15]. Ultimately, the multi-sectional semiconductor module can work in the hybrid short-circuiting switch, a subject of an original solution submitted in a patent application [24,25].

The use of two oppositely connected thyristors as an arc eliminator can be limited by the permissible forward current for each thyristor [26,27]. AE semiconductor elements must be selected in such a way as to allow the flow of the interference current as long as it is required to eliminate the interference or trip the master circuit breaker. It makes it more difficult to choose semiconductor elements and increases of the construction costs of an arc protection device. The current-carrying capacity of an arc eliminator can be increased through parallel connection of semiconductor components. However, this connection arrangement has several disadvantages. It requires careful selection of semiconductors, assurance of simultaneous control of all gates and alignment of current values in thyristor branches.

The purpose of this work is to solve the issue of increasing the current-carrying capacity of the semiconductor arc eliminator while maintaining its operational efficiency, i.e., arc elimination and the shortening of current flow time in the protected circuit. Unlike in works [15,16], an AE study based on multi-sectional thyristor shunt branches was performed. The system allows for a sequential (in each half-wave) takeover of the disturbing current by individual bypass sections, which enables the shortening of the time of current flow in subsequent branches of the device, until the electric arc goes out or the contacts of the main switch open. Consequently, an increase in short-term current carrying capacity is achieved in individual semiconductor branches of the arc eliminator as well as an increase in its total switching capability.

2. Methodology and Research Object

2.1. Methodology

MSAE tests were performed in a circuit fed from a 400/230 V AC power network with a maximum short-circuit current I_{RMS} = 2500 A. The arc current was regulated by means of an additional series impedance. Current and voltage waveforms were recorded using the Voltcraft 1084E and Voltcraft 1084F oscilloscopes (Conrad Electronic International GmbH & Co KG, Wels, Austria). The tests were performed in a system with arc simulation (using an arc detector stimulated by an LED light pulse) and in a real system, where the detector was stimulated by the arcing light. Arcs were initiated with the use of a fuse element in the arc generator system presented in [15].

The MSAE design uses two- and three-section thyristor shunt branches for each half of the flowing current. In thyristor branches, semiconductors characterized by different conduction voltages were used. For the triggering of semiconductor elements, a microprocessor controller was used which allowed any selection of initiation and conduction times for individual thyristor branches.

2.2. Multi-sectional Thyristhor Arc Fault Eliminator

The thyristor arc eliminator is a protective device connected in parallel to the load. A substitute diagram of the low-voltage power grid is shown in Figure 1.

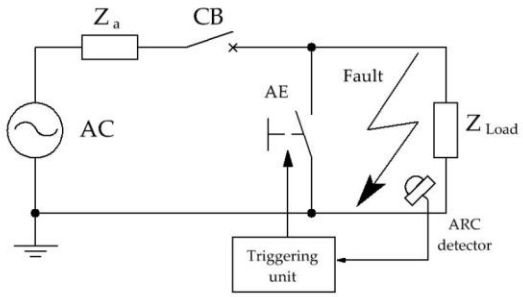

Figure 1. The idea of using the arc eliminator to protect low-voltage network equipment; CB—circuit breaker, Z_{Load}—load (Ω), AE—arc eliminator, Z_a—impedance of the power line (Ω).

If an electric arc is ignited during current flow in the AE-protected circuit will be retained by the activation of the arc detector causes a practically immediate activation of AE and the commutation of disturbance current flow in the bypass branch (AE) until the main switch (CB) is activated or the electric arc is switched off. The voltage of the conductive eliminator is significantly lower than that of the arc, so the arc is extinguished in a short time without causing the main electrical circuit protection to turn off (provided that the AE is switched off). A source of electric arc (arc generator) was used in the research, the structure and essence of which is presented in paper [15].

Having conducted a series of studies the authors found that a semiconductor system of two oppositely connected semiconductor elements allowed very fast bypassing of an electric circuit affected by arcuate interference, aimed at creating an alternative, privileged path for current flow. Such AE operation forces the immediate elimination of the resulting arc fault, and the shortening of arc fault duration simultaneously reduces the values of fault current and arc energy.

In order not to damage the thyristors during the flow of interference current, it is necessary to select their limit parameters properly, particularly the absolute maximum surge current I_{Tsm}, whose catalog value is given, as a rule, for the flow time of 10 ms. In the case of parameters defined as unique, the condition is that the value cannot be repeated until the thermal effects of its previous occurrence have ceased. Consequently, in the event of subsequent ignition of the arc in successive half-waves of current flow, in principle, the previously used thyristor cannot be turned on to eliminate the interference. The thermal effects of successive semi-waves of the flowing current can lead to damage to the semiconductor. A measure of the sensitivity of a semiconductor valve to its short circuit heat can be its Joule integral. The I^2t value is called the overload parameter of the semiconductor element [28].

One of the solutions to the above problem is the use a thyristor with much higher parameters of current overload capacity without changing its properties in a specified time. Unfortunately, this is linked to a significant increase in the price of the arc eliminator. By analyzing the prices of semiconductors [29] as a function of the maximum surge current, it can be seen that the increase follows an exponential curve.

It may be problematic when the load current is higher than the limit maximum surge current of a single thyristor. The solution to this issue is to connect thyristors in parallel. When two or more thyristors are connected in parallel, the following conditions must be met:

- all thyristors should belong to the same group and have the same forward voltage,
- the highest value of the load current flowing through a group of thyristors connected in parallel should be less than the sum of the limit currents of the individual thyristors,
- a simultaneous switching-on time of all thyristors should be ensured by the use of a quick trigger unit which sends, at one moment, appropriately formed pulses to each thyristor gate,

- equalization of current distribution in individual branches.

Such a connection of semiconductor elements is burdened with the dispersion of voltage-current characteristics in the conduction state and a need to select semiconductor elements. Incorrect selection results in an uneven distribution of currents in the steady state in individual branches. In order to obtain a sufficiently uniform current distribution, thyristors are selected to match the voltage-current characteristics in the conduction state. It is usually sufficient to match the thyristor forward voltage value at the limiting current [30]. The dispersion of thyristor characteristics may not be the main cause of the uneven current distribution in a parallel connection. Current distribution is significantly affected by impedance distribution in individual branches and elements (connections, wires), usually connected in series with each thyristor.

In the case of excessive irregularity of current distribution (in parallel thyristor branches), it is necessary to use equalizing elements. This solution gives good results when working in steady states, however, it reduces the efficiency of the whole system and requires the use of equalization impedance with appropriate current-carrying capacity, at least equal to the thyristor used in series. Uneven current distribution is also associated with unfavorable transition states in thyristors, especially with the switching state [30]. The thyristor with the shortest switching time initially conducts the total load current of the system.

The solution to the problem of increasing the current load capacity of the arc eliminator while maintaining its effectiveness described in [15] is to use a multi-sectional bypass branch made of semiconductor elements. Figure 2 shows a diagram of a multi-section thyristor electric arc eliminator in a thyristor design.

The use of a multi-sectional branch bypassing the electrical interference allows for sequential take-up of short circuit current by individual bypass tracks, which shortens the current flow time in subsequent sections of the device until the electric arc is switched off or the contacts of the master switch are open. Consequently, an increase is achieved in current carrying capacity in individual semiconductor branches of the arc eliminator as well as a growth in its total current load capacity.

The schematic diagram in Figure 2 shows the configuration of a Multi-Sectional Electric Arc Eliminator (MSAE) for direct and alternating current. Thyristor or diode-thyristor blocks of bypass cascades are turned on, respectively, for positive or negative polarity (half sine wave) of the flowing current. To facilitate the description of the arc eliminator, the following abbreviations have been adopted:

- MB—semiconductor bypass module for the positive half-wave of the flowing current, which consists of semiconductors *1*, *2*, ..., *n*,
- MB′—semiconductor bypass module for the negative half-wave of the flowing current, which consists of semiconductors *1′*, *2′*, ..., *n′*.

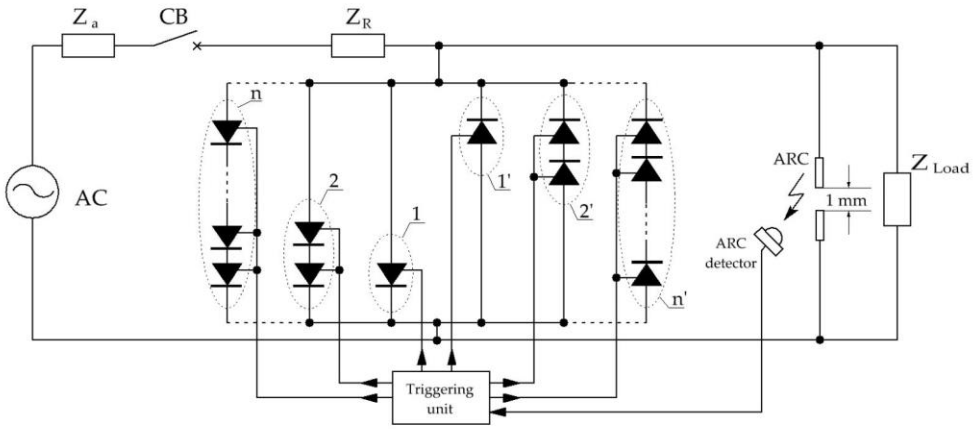

Figure 2. Schematic diagram of the Multi-Section Arc Eliminator MSAE made by the thyristor.

For each half-wave of the sinusoid supplying the presented system, it is a set of the ARC detector (common for both current polarizations) and cascading semiconductor bypassing tracks (branches) *1*, *2*, ..., *n* or respectively *1′*, *2′*, ..., *n′*. Individual bypassing branches are composed of an increasing number of serially connected semiconductor valves, of which at least one is a thyristor in each branch. From the operational perspective, it is beneficial for the system to contain only thyristor shunt branches (Figure 2), but it may be economically advantageous to use a diode-and-thyristor design. Along with arc flash detection, the activation of the arc eliminator takes place by controlling the thyristors in the last bypassing branch (*n*—for positive polarization or *n′*—for negative polarization respectively) and then in subsequent parallel branches (*n*−*1*), (*n*−*2*), etc., or respectively (*n′*−*1*), (*n′*−*2*), etc. The condition for taking over current conduction by successive branches of the semiconductor shunt *n*, (*n*−*1*) ... *2*, *1* of the MB bypass module (or *n′*, (*n′*−*1*)...*2′*, *1′* for MB′) is proper control of thyristor gates. The task of serial thyristors and diodes in higher-order semiconductor branches is to maintain in their conduction state a voltage drop sufficient to switch on the elements of the lower-order sections. The whole procedure ensures that the fault current or arc current in the semiconductor circuits is taken over for the time that is necessary to extinguish the resulting electric arc or open the contacts of the main switch. In this way, it achieves virtually instantaneous operation of the AE and gradually relieves its semiconductor elements.

Thanks to the application of the solution according to Figure 2, the following technical and utility effects have been achieved:

- increased current load capacity of the arc eliminator,
- practically immediate elimination of the arc fault in the damaged circuit,
- extended time available to open the main switch contacts in the case of re-ignition of the arc in subsequent half-waves of the flowing arc current,
- shorter time of impact of thermal effects in the circuit to be protected,
- reduced electrodynamic effects,
- ability to optimize the thermal load of individual semiconductor branches,
- possible cooperation with arc protection devices available on the market,
- reduced costs of implementation in diode-thyristor solutions.

Figure 3 shows part of a test circuit of a multi-sectional arc eliminator with marked measurement signal registration points. The supply voltage is registered in relation to the protective conductor PE. The arc voltage was registered with the DP-50 voltage differential probe (Pintek Electronics Co. Ltd., Shulin, New Taipei City, Taiwan). The differential probe terminals are located as close as possible to the electrodes of the arc generator. The value of the current in the branches of the AE and the load, as well as the current taken from the source were recorded using current probes PAC22 (Chauvin Arnoux, Paris, France).

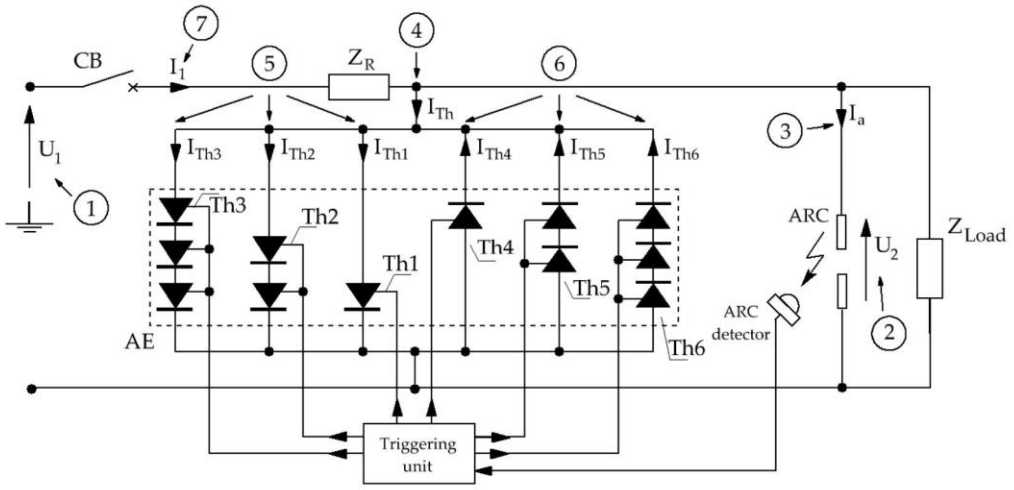

Figure 3. Part of the arc eliminator test circuit MSAE with marked measurement points: 1—supply voltage (U_1), 2—voltage on the electrodes of the arc source (U_2), 3—current in the branch of the arc source (Ia), 4—current in the thyristor branch (I_{Th}), 5—current for the positive half-wave of the flowing current MB (I_{Th1}, I_{Th2}, I_{Th3}), 6—current for the negative half-wave of the flowing current MB' (I_{Th4}, I_{Th5}, I_{Th6}), 7—power source current (I_1).

3. Thyristor Triggering Procedure

The exemplary solution of the current circuit of a multi-sectional arc eliminator shown in Figure 3 contains two MB and MB' modules, each containing three semiconductor branches bypassing a place affected by arc disturbance (ARC). The individual components of the semiconductor cascade are switched on in a sequence of $T_{h3}\rightarrow T_{h2}\rightarrow T_{h1}$, followed by $T_{h6}\rightarrow T_{h5}\rightarrow T_{h4}$, when the detected initial fault current polarity is positive or, when the detected current has negative polarity it runs in the order of $T_{h6}\rightarrow T_{h5}\rightarrow T_{h4}$, and then $T_{h3}\rightarrow T_{h2}\rightarrow T_{h1}$,. Subsequent switching on of thyristor branches in each of the MB and MB' modules run in accordance with the decreasing voltage drop in the individual bypass sections. Sequential closing of semiconductor circuits allows the fault current to be taken over by individual branches of the short-circuiting switch in the way shown as an example in Figure 4.The sequence of taking over the current by successive branches of the arc eliminator shown in Figure 4 is connected with the appropriate triggering of subsequent thyristors. The control unit for thyristor modules (MB and MB') consists of systems enabling the following:

- generation of gating pulses,
- appropriate time modulation, synchronization and distribution of these pulses,
- input control signal conversion and adaptation (regardless of signal source),
- operation of the system of interlocks and safeguards affecting the triggering pulses,
- elimination or limitation of external influences such as: temperature, voltage changes, power supply, interference, etc.

The requirements for thyristor triggering systems include [31]:

- ensuring an appropriate value of the tripping current and gate voltage. These requirements also include the optimization of rise steepness and trigger pulse duration,
- minimizing the trigger delay in relation to the moment the signal triggering the trigger pulse occurs,
- ensuring the maximum operational reliability,
- galvanic separation of output circuits supplying the gates of individual thyristors.

The above requirements are met by the thyristor microprocessor controller described in detail in [32]. The device was expanded with the ability to independently control six thyristor sections

(T_{h1}, T_{h2}, T_{h3}, T_{h4}, T_{h5}, T_{h5}) and an external trigger input, which, based on the signal from the arc detector, initiates the process of controlling thyristor sections. The microprocessor thyristor controller can be used with commercial arc interference detectors. In the experimental tests presented below, the controller was activated from a simple arc flash detector based only on light detection of a burning arc. The occurrence of arc interference in the initial or final phase of the supply voltage half-wave has no effect on the operation and control of the appropriate section of arc eliminator thyristors.

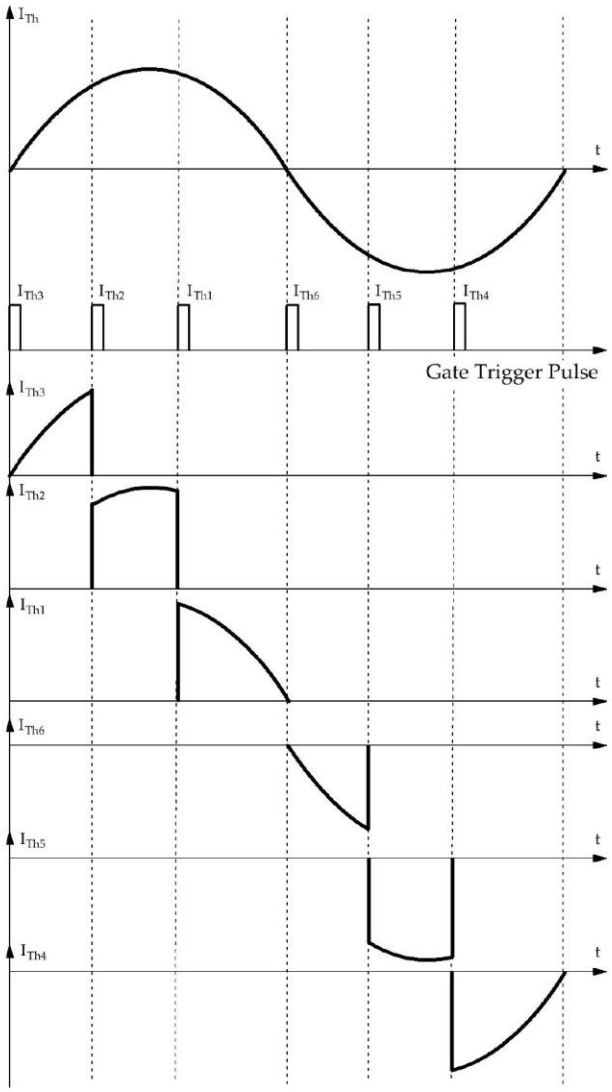

Figure 4. An example of sequential taking over of current by shunting paths in the order in which thyristors are triggered T_{h1}, T_{h2}, T_{h3}, T_{h4}, T_{h5}, T_{h6}.

Figure 5 shows the recorded gating pulses of the individual thyristor sections. In each of the four presented oscillograms, supply voltage U_1 and gate voltage impulses triggering the thyristors T_{h1}, T_{h2}, T_{h3}, T_{h4}, T_{h5} and T_{h6} were recorded. For the positive half-wave, the supply voltages are sequentially T_{h3}, T_{h2}, and T_{h1}, and for the negative half-wave the supply voltages are T_{h6}, T_{h5}, and T_{h4}. Figure 5a shows the arc ignition moment during a negative supply voltage semi-wave and Figure 5b shows the arc ignition moment during a positive supply voltage semi-wave. The test circuit was designed in such a way as to create favorable conditions for subsequent arc ignitions. Detection of the electric arc and identification of the direction of the disturbed current flow causes the generation of the control pulse

and the sequential triggering of the appropriate group of thyristors. Successive electric arc flashes trigger the detection system and cause subsequent triggering of the thyristor groups.

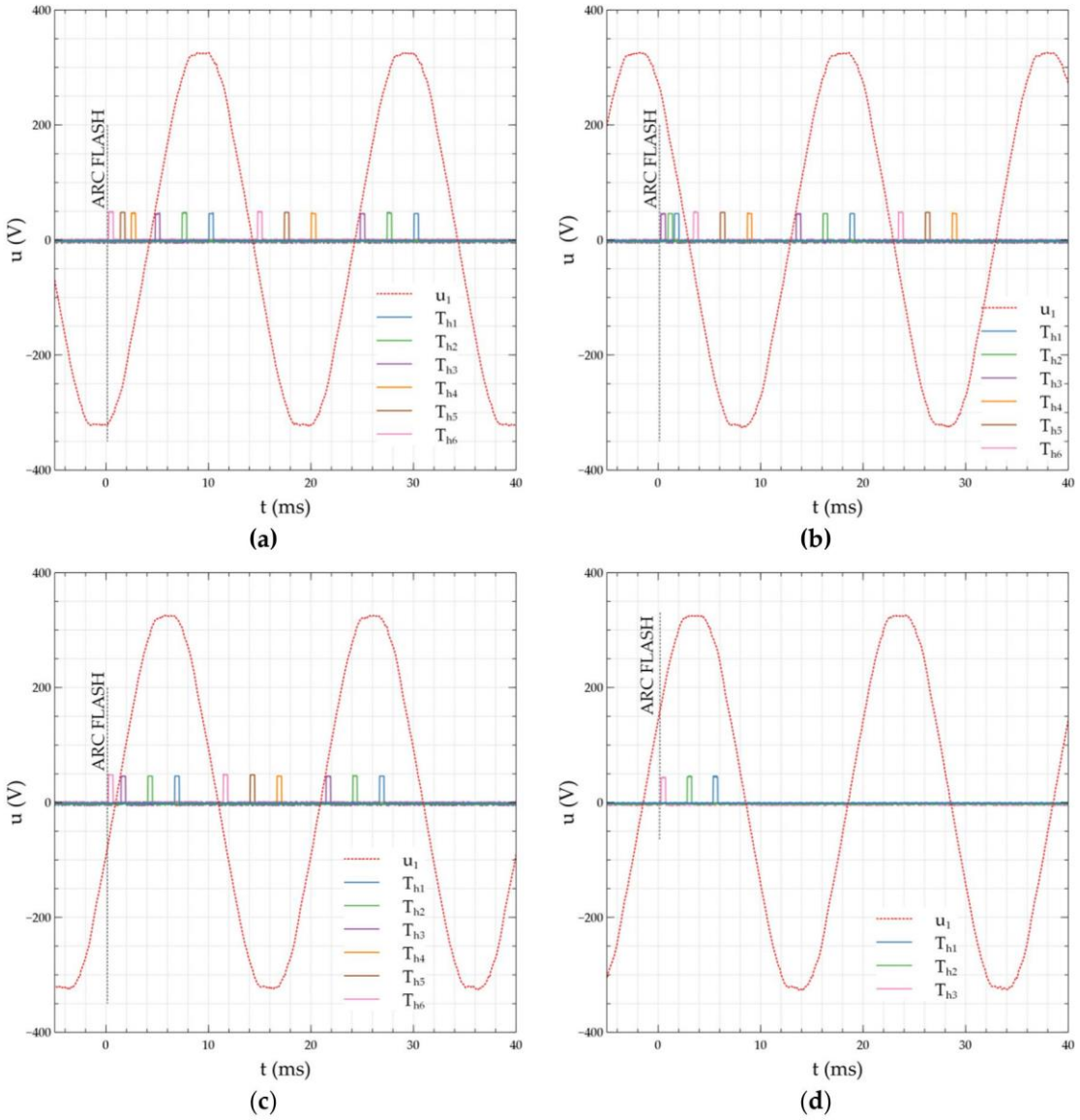

Figure 5. Pulses triggering thyristors T_{h1}, T_{h2}, T_{h3}, T_{h4}, T_{h5}, and T_{h6} in the MSAE control system in relation to supply voltage u_1: (**a**) arc flash in the negative voltage half-wave; (**b**) arc flash in the positive voltage half-wave; (**c**) arc flash at the end of the positive half-wave voltage, the algorithm generates only one triggering pulse; (**d**) the arc extinguishes in the first half wave of voltage.

In the oscillograms in Figure 5a, and Figure 5b, it can be clearly seen that only one group of thyristors is triggered for a given supply voltage half-wave. Figure 5c shows the moment of appearance of an electric arc flash in the final part of the supply voltage half-wave. Flash detection takes place about 0.8 ms before the time of voltage transition through zero, which determines the natural extinguishing of the electric arc in resistive circuits typical of low-voltage electrical installations. In such a short time that remains until $u_1(t) = 0$ V only one of the thyristors is triggered.

At the moment of a programmed arc flash detection, the microprocessor controller calculates the t_p time left before the half-wave current passes through zero. Depending on the remaining time, one, two or three thyristor sections are triggered:

For the three bypass branch sections, the following trigger times were determined:

- the flash detection moment is the beginning of the countdown of time t_p remaining to the end of the half-wave current,
- when the flash is detected, the section with the highest number of thyristors is triggered,
- after, for example, 30% of t_p time, the lower order semiconductor section is triggered,
- after, for example, 60% of t_p time, the lowest order semiconductor section is triggered.

For the t_p time of 1 ms < t_p < 2 ms, two thyristor sections of the highest order are triggered with a conductive time division of 50% of the t_p. For times t_p < 1 ms, one top-level section is triggered.

The microprocessor algorithm is the decision system in this case. In the applied controller, there is a possibility to create any algorithms in making decisions about the optimal load on the thyristor section. This configuration freedom allows to change:

- the duration of the trigger pulse,
- the time between successive trigger pulses,
- decisions on the number of triggered sections in a given half-wave of current flow.

The oscillogram in Figure 5d was recorded in a system with an arc extinguishing itself after a time of T_a < 10 ms. T_a is the duration of the electric arc. The trigger of the appropriate group of thyristors that can conduct current, occurs when the electric arc is detected. Because the electric arc appeared in the positive half-wave of the flowing current, T_{h3}, T_{h2} and T_{h1} thyristors were triggered. The arc is extinguished during the first half-wave of power supply voltage, so there are no further gating impulses.

4. Investigations of Currents and Voltages in the Multi-Sectional Arc Eliminator System

The schematic diagrams in Figures 6 and 7 show the solution of the arc eliminator in the following systems:

- two-sectional—containing two branches bypassing the arc fault: T_{h3} and T_{h1} for the positive half-wave supply voltage and the corresponding T_{h6} and T_{h4} for the negative. Higher-order sections (T_{h3} and T_{h4}) are made of more semiconductor components than lower-order sections (T_{h1} and T_{h4}),
- three-sectional—containing two branches bypassing the arc fault: T_{h3}, T_{h2} and T_{h1} for the positive half-wave supply voltage and corresponding T_{h6}, T_{h5} and T_{h4} for the negative. Each of the lower-order sections contains in its connection one semiconductor element less than the preceding higher-order section.

Due to the short circuit conditions at the measuring point, the value of the I_{Th} was limited by means of additional impedance Z_R to the maximum value I_{Thmax}. The circuit has a resistive character, and the insignificant inductance included in the impedance results from the parameters of the power supply circuit and the connections inside the AE. The preliminary test in the systems shown in Figures 6 and 7 was carried out at triggering the T_{h3} thyristor sections at the moment of passing the voltage half-wave through zero. They were made in a circuit with a simulation of arc by means of an LED diode turned on at the moment $u_1(t)$ = 0 V. This method of control allows to register the possibility of dividing the full half-wave of the flowing current into fragments and show conduction through individual thyristor sections.

Current flows in the solutions presented are shown in Figures 8 and 9. Figure 8 shows the current and voltage waveforms in the two-section arc eliminator circuit (Figure 6), recorded in the duration of the interference for two periods of the supply voltage. The first T_{h3} thyristor section is triggered when $u_1(t)$ = 0 V (about 0.137 ms). The activated thyristors allow the flow of I_{Th3} current. The higher number of series semiconductors in the higher order bypass branch T_{h3} in the conduction state causes the voltage to drop sufficiently enough to trigger the elements of the lower order section Th1. After

the period resulting from the division of the voltage half-wave duration into two (not necessarily equal) parts (two semiconductor sections) the impulse triggering the Th1 lower order section is given. Triggering the Th1 branch causes the I_{Th1} current to flow. A smaller number of working semiconductors in the lower order bypass branch T_{h1} lowers the voltage drop, making it impossible to maintain the conduction in elements of the higher section T_{h3}. The group of thyristors from the T_{h3} section ceases to conduct I_{Th3} current, which results in the complete taking over of the conductivity by the T_{h1} section. The current I_{Th} registered with a current probe and shown in Figure 8 is the sum of the currents flowing in the subsequent sections of the arc eliminator. Continuity of the I_{Th} current flow indicates the state of activity of the arc eliminator.

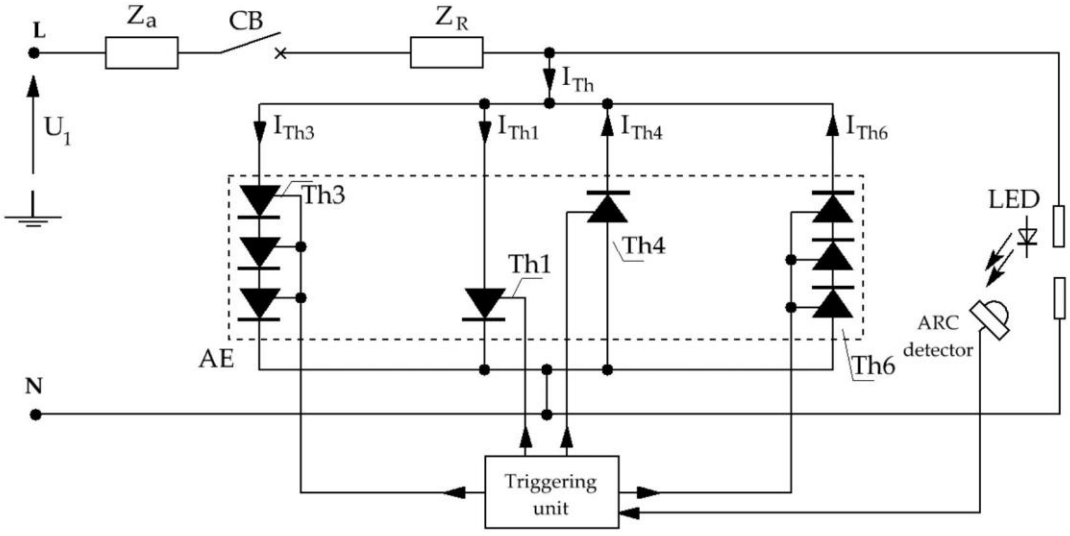

Figure 6. Schematic diagram of the test circuit in a two-sectional MSAE system.

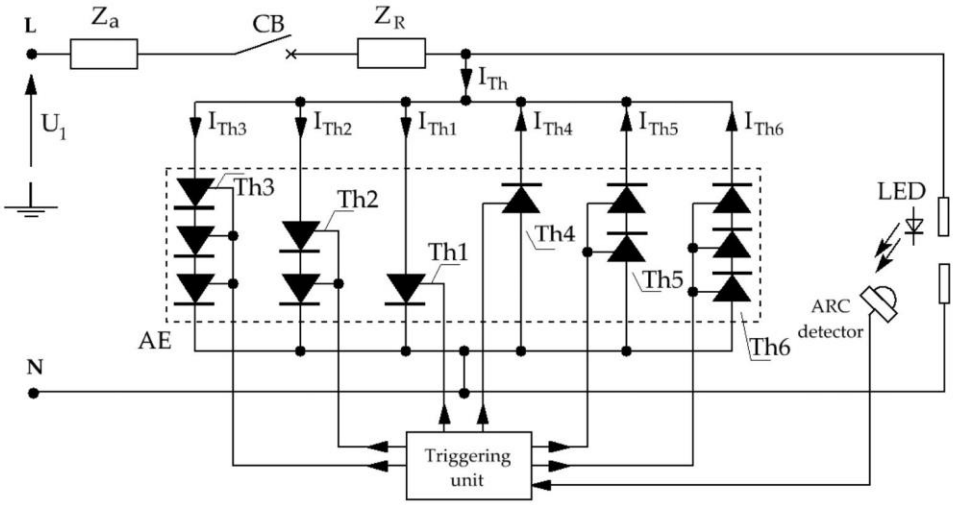

Figure 7. Schematic diagram of the test circuit in a three-sectional MSAE system.

Figure 9 shows the current and voltage waveforms in the three-sectional arc eliminator circuit shown in Figure 7. The recorded waveforms are limited to two periods of supply voltage. At the moment when the supply voltage $u_1(t) = 0$ V (about 0.138 ms) the first T_{h3} thyristor section is triggered. Current I_{Th3} flows through the controlled thyristors. A larger number of serial semiconductor elements in the higher order bypass branch T_{h3} in the conduction state, maintains a sufficient voltage drop to trigger the elements of the lower order T_{h2} section, built of a smaller number of in series connected semiconductor elements.

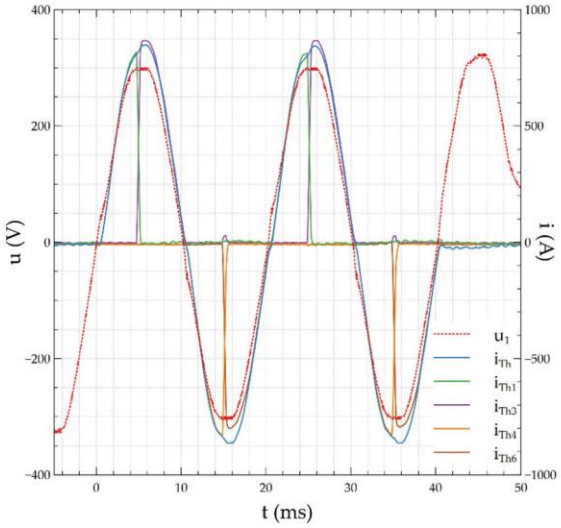

Figure 8. Current and voltage waveforms in a two-sectional MSAE system.

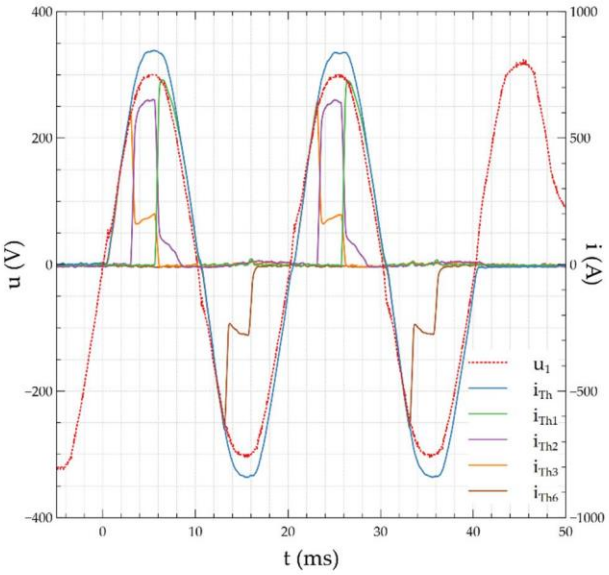

Figure 9. Current and voltage waveforms in a three-sectional MSAE system.

After a time of about 3 ms from the moment of detection of a simulated arc flash, a gating impulse is given to the T_{h2} section. Triggering the T_{h2} branch causes the I_{Th2} current to flow. The expected state is to turn off the T_{h3} section and current flow in the T_{h2} section branch. Research has shown that with the applied type of thyristors for currents exceeding several hundred amps, current absorption by the lower order branch (section) is usually only partial. This is evident in the form of the characteristic current drop I_{Th3} shown in Figure 9. An analogous situation occurs in 6 ms from the moment of simulated arc detection. Section T_{h1} is triggered by a triggering gating impulse. Triggering the T_{h1} branch causes I_{Th1} to flow. The voltage drop on a single conductive thyristor from the T_{h1} section is not sufficient to support the flow of current I_{Th3} in the T_{h3} branch, but it is sufficient to maintain the flow of I_{Th2} current through the T_{h2} branch. The process of control and current flow for a negative half-wave is identical to that described above, with the T_{h6}, T_{h5} and T_{h4} sections successively conducting the currents T_{h6}, T_{h5} and T_{h4}. The I_{Th} current flow recorded by the current probe and shown in Figure 9 is the sum of currents flowing in subsequent sections of the arc eliminator. The continuity of the I_{Th} current flow shown in Figure 9 indicates the continuous, effective operation of the arc eliminator.

5. Influence of Thyristor Conduction Voltage Values on Arc Eliminator Operation

The voltage-current characteristics in the conduction state of the TR51-40 and T00-150 [30,33] thyristors used in the- experiments described above are presented in Figure 10. With the increase in the value of forward current I_T, the value of the voltage drop U_T increases. Exponential curve shape causes a rapid increase in voltage U_T to a value of about 7 V at I_{TSM} limit currents with an effective value of about 1000 A. As described in Section 4 and shown in Figure 9, during current flow close to the limit values, the thyristors of the higher section are not completely switched off due to the large voltage drop at the lower order MSAE section. The solution to this problem may be to increase the required forward voltage of the higher order sections or to reduce the voltage drop of the lower order sections. The schematic diagram presented in Figure 6 and waveforms recorded in this system (Figure 8) show a situation where, during current conduction, voltage on one thyristor of the lower order section is not able to maintain the conduction of the higher order section built of a larger number of semiconductors connected in series (three thyristors in series). At the moment of taking over the conductivity by the lower bypass branch section there is practically an immediate loss of current in the higher order section. Because this solution is quite expensive and involves the need to increase the number of serially connected semiconductor elements, Figure 11 shows a schematic diagram of an arc eliminator with a semiconductor element with a lower conduction voltage than the thyristor voltage in the higher order section. In sections T_{h2}, T_{h1} and T_{h5}, the TR51-40 thyristors are used, whereas in section T_{h4} the T00-150 thyristor is used. At the limit currents of the TR51-40 thyristor the voltage drop is over 7 V, while for the same value of the flowing current on the T00-150 thyristor the voltage is about 2.4 V. Such a low voltage at the thyristor terminals in the higher order section causes thyristors to practically cease to conduct or the current value will be slightly above single amperes.

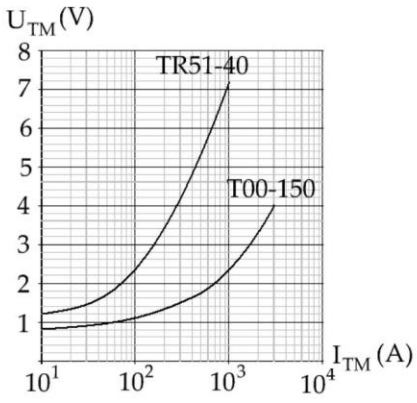

Figure 10. The voltage-current characteristics in conduction state for thyristors TR51-40 and T00-150-40.

Figure 11 shows a two-sectional arc eliminator in which sections T_{h2}, T_{h1} and T_{h5} were built using TR51-40 thyristors, while section T_{h4} was formed by T00-150 thyristor. The recorded waveforms of currents and voltages in this system for two maximum current values at 850 A and 1650 A are shown in Figure 12. For a positive half-wave, supply voltage may be conducted by the T_{h2} section, in which thyristors TR51-40 are used. At the moment when the current reaches a maximum of 850 A (I_{Th2} = 600 A effective current value), the T_{h1} section is triggered. The voltage on one conductive thyristor TR51-40 read from Figure 10 at current I_{TM} = 850 A is just over 6 V.

For bypass branches of a higher order (T_{h2}) the voltage is distributed approximately halfway per each thyristor. From the characteristics in Figure 10 it can be read that for such a voltage value effective current of over 150 A can flow through this branch. In Figure 12a, this can be seen in the form of a sharp reduction in the instantaneous flowing current I_{Th2} from the maximum value of 850 A to about 200 A. For the negative half-wave of the flowing current, conduction is taken over by the T_{h5} section built on the basis of TR51-40 thyristors. In the voltage amplitude, the T_{h4} section built of thyristor T00-150 is triggered. For the value of flowing current I_{T5} = 600 A (850 A of maximum value) the voltage

on the conductive thyristor T00-150 is about 2.2 V. For a bypass branch of a higher order (T_{h5}) this voltage is distributed approximately halfway per each thyristor. From the characteristics in Figure 10 it can be read that for a voltage of 2.2 V, thyristors can conduct current with the value of single amperes. In Figure 12a, this can be seen in the form of a total I_{Th4} current decay with a continuous flow of current I_{Th} through the AE. In the system presented in Figure 11, the application of semiconductors of equal voltage drop in the direction of conduction (T_{h2}, T_{h1}) and of semiconductors of different voltage drop for the negative voltage semi-wave (T_{h5}, T_{h4}) was a purposeful procedure. The differences in the operation of each shunt module are clearly seen in current characteristics shown in Figure 12. It can be observed in them how much lower the current flowing through the higher-order section is when the lower-order branch begins to conduct.

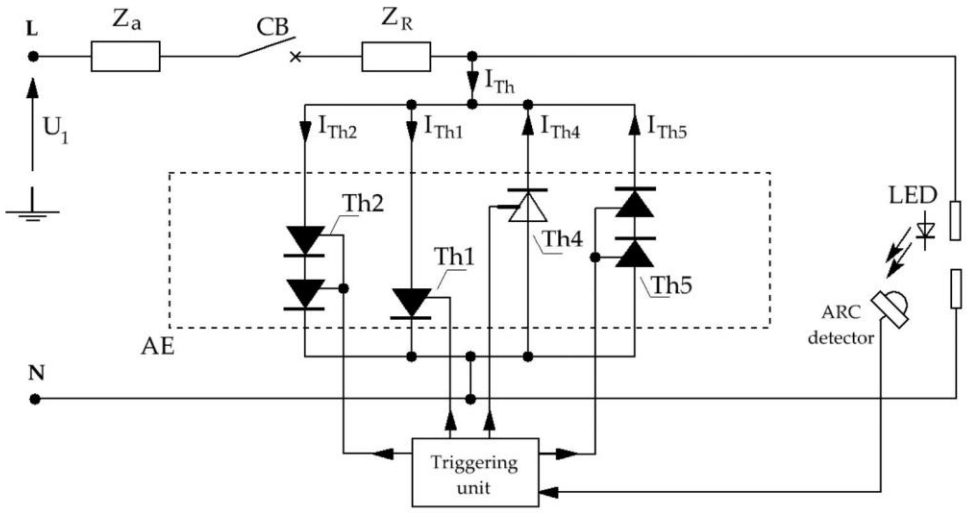

Figure 11. MSAE schematic diagram in a two-sectional system with T_{h4} semiconductor with a smaller voltage drop in the direction of forwarding.

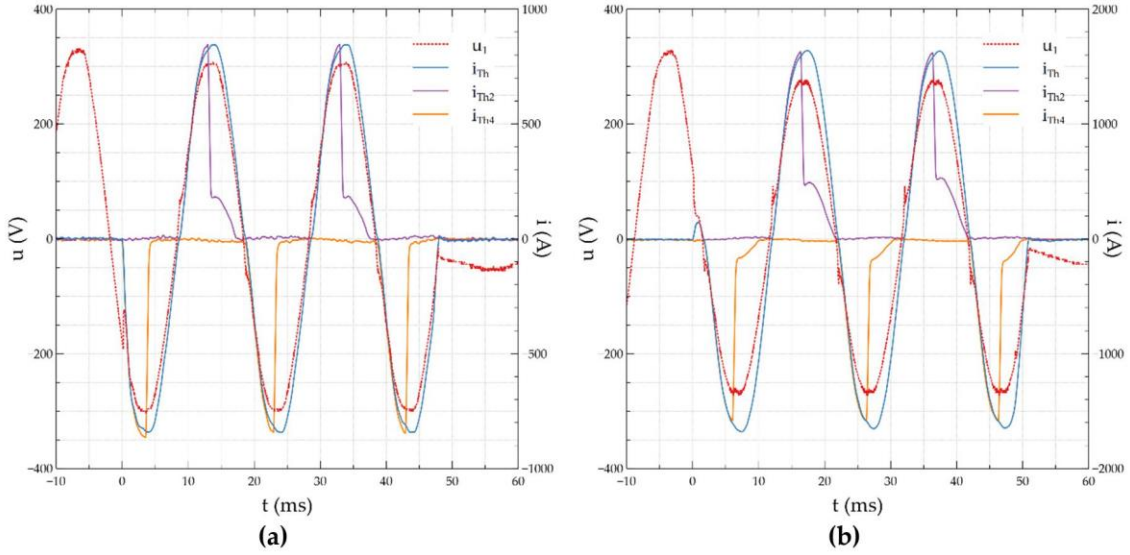

Figure 12. MSAE schematic diagram in a two-sectional system with T_{h4} semiconductor with a smaller voltage drop in the direction of forwarding: (**a**) I_{Thmax} = 850 A, (**b**) I_{Thmax} = 1650 A.

Figure 12b shows the waveforms at higher peak current. The current amplitude in this case was limited by Z_R impedance to about 1650 A. Voltage drop in the direction of conduction for thyristor TR51-40 is more than 7.2 V, which despite the operation of T_{h1} allows the current to flow through the

section of higher order (of the same type of thyristors) with the value of more than 500 A. In Figure 12b this can be seen in the form of a large value of the "stair" of I_{Th2} current. For the thyristor T00-150 with a current flow of $1600/\sqrt{2}$, the voltage drop across the semiconductor is 2.5 V. This voltage will cause a current of the order of 30 A to flow through the higher order branch built on basis of thyristors TR51-40.

The values of voltage drops in the above considerations are read from the voltage and current characteristics of a given thyristor based on the measured value of the current flowing through the AE. The values of currents quoted above for the readout of voltage drop in the direction of conductivity are much smaller than those recorded in the real circuit in Figure 11 and presented in Figure 12. The actual voltage drops on conductive semiconductor sections are larger. This is due to the additional series impedance in the semiconductor circuit. Its value is influenced by:

- wires connecting specific semiconductor sections,
- connections to semiconductor terminals,
- different distances of individual semiconductor sections from the power source.

6. Multi-Section Arc Eliminator in Real Arc Tests

Figure 3 shows a three-sectional AE working with positive and negative voltage polarity. Detection of arc disturbance in the positive half-wave of the flowing current triggers sections T_{h3}, T_{h2}, and T_{h1}, while sections T_{h6}, T_{h5} and T_{h4} are triggered when the fault in the negative half-wave occurs. In the presented experiment, thyristors TR51-40 were used with a maximum average forward current of 40 A and a unique peak conduction current of 900 A [31]. The current amplitude was limited to 1600 A due to available test values. The source of the arc are two cylindrical carbon electrodes facing each other with a diameter ϕ equal to 5.76 mm spaced 1 mm apart. A fuse element was placed between the electrodes, which initiates ignition of the electric arc after a pre-selected time delay (resulting from the diameter of the fuse element). For safety reasons, the arc generation system (electrodes with a fuse element and flash detector) was enclosed in an insulated enclosure equipped with openings to limit the pressure increase inside the enclosure. The presented experiment corresponds to a short-circuit occurring close to the arc elimination system (Z_R control impedance practically negligible).

Figure 13a,b show the waveforms of:

- the supply current i_1,
- the current in the arc branch i_a,
- the current in subsequent conductive sections i_{Th3}, i_{Th2} and i_{Th1},
- the total value of supply current $i_{Th} = i_{Th3} + i_{Th2} + i_{Th1}$,
- the voltage measured at the electrodes of the arc source u_a.

The recorded arc interference occurred during the positive half-wave of the flowing current. In order to facilitate the readings, the moment $t = 0$ s was assumed at the moment of arc ignition. When the current flow exceeds the permissible value for a fuse element, the arc ignition occurs between the carbon electrodes after approx. 1.5 ms. The arc voltage reaches the value of approx. 5.5 V at the moment of ignition.

When the electric arc ignites, the current drawn by the load from the power source is $i_1 = 1200$ A. The voltage on the resulting arc increases to a value of $u_a = 115$ V. When the detector detects an explosion of a fusible element, a thyristor section consisting of three serially connected thyristors is triggered.

For the system in Figure 3, this is the T_{h3} branch. Voltage u_2 is reduced to 32 V. This is the voltage on three serially connected semiconductor elements of the arc eliminator. The commutation of current by the T_{h3} thyristor branch does not cause a decrease in arc voltage u_a below the minimum arc burning value. A burning electric arc maintains current flow through the affected branch. The value of current i_a is 120 A in the initial phase and increases to 200 A with an increasing value of the supply voltage. After the programmed trigger time of the subsequent thyristor sections has elapsed,

the lower-third order branch, T_{h2}, consisting of two serially connected thyristors, is switched on. The flow of the i_{Th2} current through the T_{h2} branch lowers the arc voltage below the minimum value of the arc burning, which results in its extinguishing and reducing the i_a current to zero. In the last step, after the programmed time has elapsed, the branch of the lowest order T_{h3} built of one thyristor is switched on. Full commutation of the i_{Th3} current and a low voltage drop on the thyristor in the direction of conduction cause the complete switching off of T_{h3}, T_{h2} and i_{Th3}, i_{Th2} branches and the disappearance of i_{Th3} and i_{Th2} currents. In this case, the arc was already extinguished during the work of the second section (T_{h2}) of the MSAE.

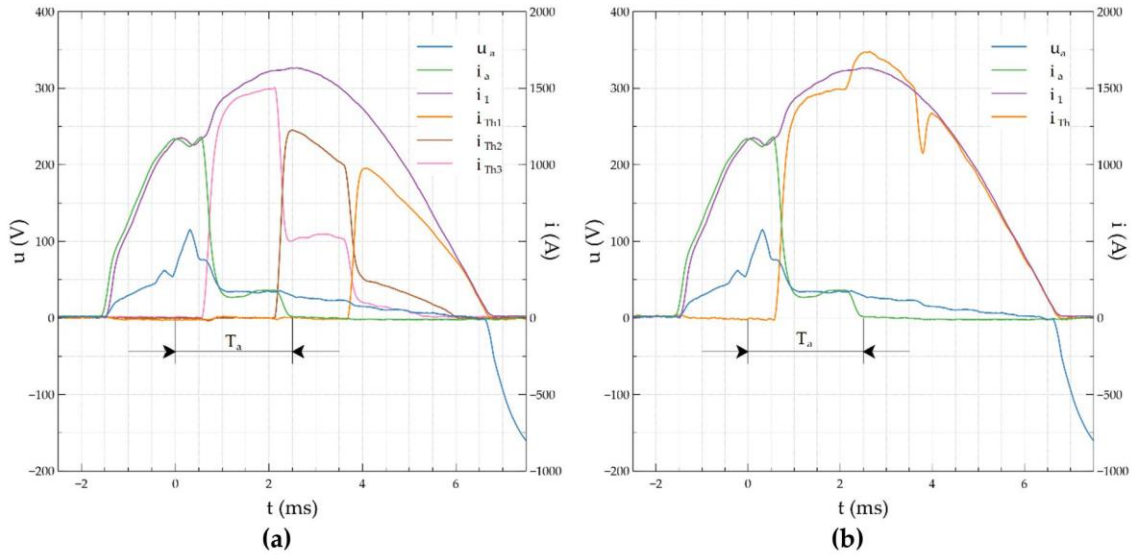

Figure 13. Waveforms of current and voltage of the arc in a circuit protected by the MSAE system: (**a**) partial currents; (**b**) current waveforms with the sum of I_{Th}.

Arc time T_a measured from the detection of the electric arc to the acquisition of full conduction by AE thyristor branches is 2.5 ms. The arc extinguishing time results from the delay in the detection of the electric arc and the delay in triggering the lower order bypass section. The voltage on the conductive thyristor branch T_{h3} is sufficient to sustain the free burning of an electric arc. This time can be shortened by triggering the lower order branch faster or by using semiconductor devices with a lower voltage drop in the direction of conductivity so that it is less than the voltage of the burning arc. Although it was shown in paper [15] that the time of extinguishing the electric arc in the AE built in the system of single oppositely connected thyristors is about 0.7 ms for the resistive load, the single-stage eliminator is characterized by a much lower current load capacity. It should also be emphasized that despite the extension of the arc burning time and the flow of arc current through the place affected by the fault, the value of current i_a decreased six times compared to the value at the time of the arc fault. This means that the effects of the arc burning are significantly reduced. Figure 13b shows the summed-up values of the currents of the individual MSAE bypass branches.

Figure 14 shows the situation in which arc detection triggers MSAE operation. From now on, the MSAE operation has been programmed as switched off. In the area affected by the failure, the arc is extinguished after T_a = 2.8 ms. Favorable thermal conditions and a short distance between the electrodes (arc generator) cause reignition of the discharge between the measuring electrodes. The arc ignites again for a negative half-wave of the supply voltage. The current in the arc branch starts increasing rapidly to a peak of 1250 A. This experiment was presented deliberately to illustrate MSAE effectiveness and the effects of its inaction. The state-of-the-art solution shown, for example, in [14] may, due to the limit parameters of the thyristors, reduce the possibility of the thyristors reacting again for the next half-waves of the flowing current. The solution in Figure 3, for the same values of the interfering current and the use of identical thyristors as in work [15], allows the time of operation of the

arc eliminator to be three times longer. However, if the operating time is limited to one half-wave (as described above), the use of a 3-sectional shunting thyristor branch allows to increase the eliminated disturbing current $\sqrt{3}$ times while maintaining the required thermal parameters of the elements used.

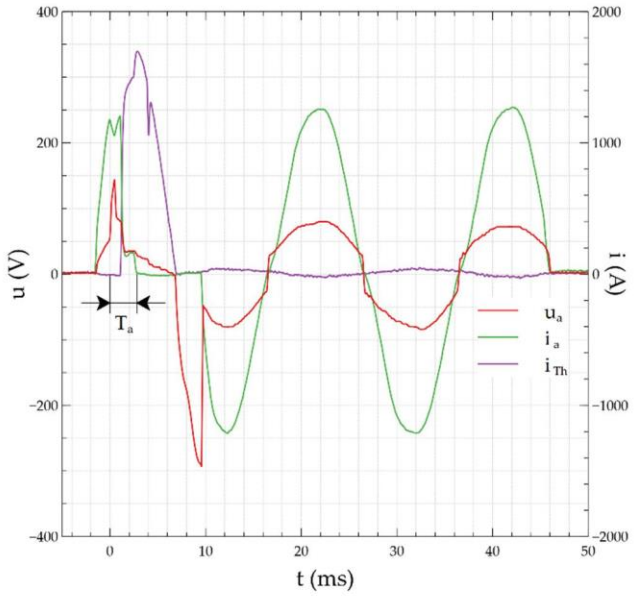

Figure 14. Current and voltage waveforms in the MSAE circuit with intentionally blocked operation in the second half-wave of the supply voltage.

Figure 15 shows the arc eliminator in a two-sectional solution. The purposefulness of using this solution with the multiplied number of elements of the higher order section is described in Section 4. Figure 16 shows the oscillograms of current and voltage recorded in the experimental circuit during arc fault.

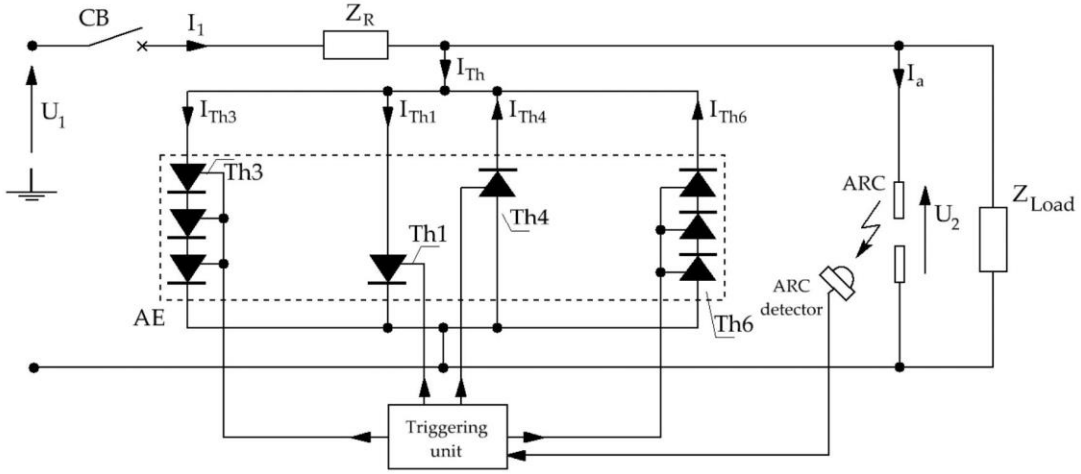

Figure 15. Circuit diagram of a test circuit with a two-sectional arc eliminator.

At $t = 0$ s, the voltage at the arc source terminals increases rapidly due to fuse element explosion. A triggered arc detector sends a thyristor trigger pulse. After approximately 0.7 ms, conduction of the first semiconductor section of the arc eliminator begins. The thyristor semiconductor branch T_{h6} commutates the current flow from the branch affected by the arc. The current in the arc branch decreases its value from 1200 A to 70 A. The voltage with the voltage drop value of the conductive T_{h6} thyristors sustains the burning electric arc, while the energy emitted on the arc decreases in such a

ratio as the value of current i_a. Tripping of the T_{h4} branch causes the total commutation of current from the T_{h6} branch and the affected branch. The electric arc goes out and the measured time T_a is 3.5 ms.

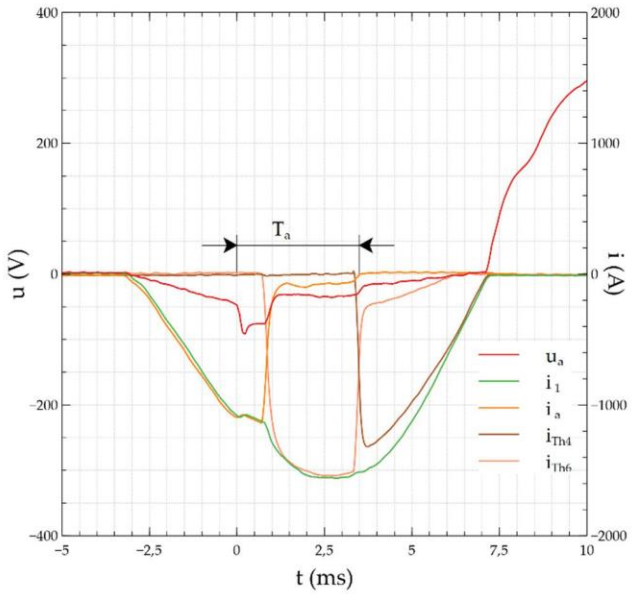

Figure 16. Current and voltage waveforms in a two-sectional arc eliminator system.

Figure 17 is a diagram of a two-sectional arc eliminator. In branches T_{h3}, T_{h1} and T_{h6}, TR51-40 thyristors are used, and in T_{h4}, thyristor T00-150 is applied, one with lower voltage drop in the direction of conduction. Such a solution, similarly to the system in Figure 15, allows to compare the efficiency of thyristor eliminators made of elements with different operating characteristics.

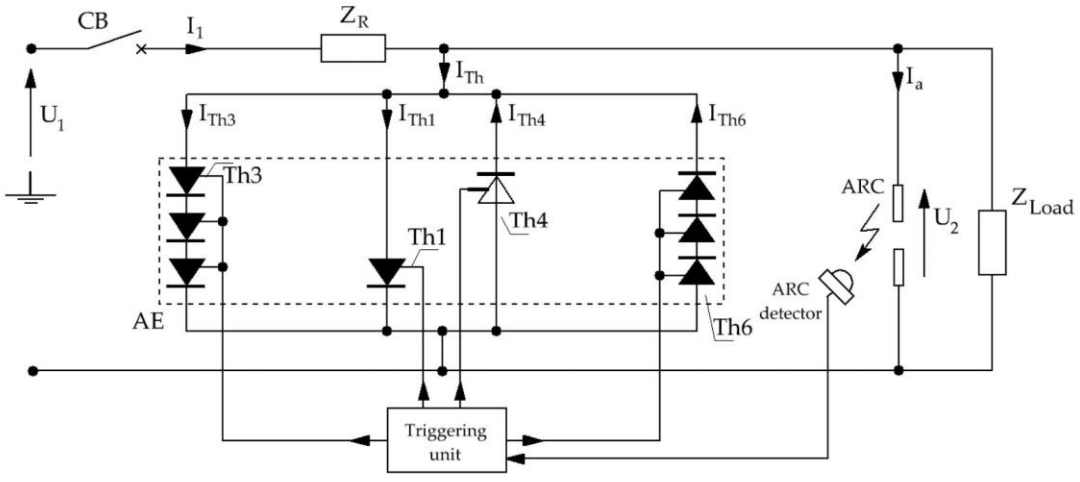

Figure 17. Schematic diagram of a two-sectional arc eliminator containing one of the thyristors with a smaller voltage drop in conduction direction T_{h4}.

Oscillograms of current and voltage waveforms recorded in the system presented in Figure 17 are shown in Figure 18. After the detector detects a disturbance, the first T_{h3} semiconductor section is triggered and the i_{Th3} current flow appears. After the set time is over, the lower order section T_{h1} and the current flow i_{Th1} are triggered. However, the arc is still not extinguished. Favorable thermal conditions and a short distance of the carbon electrodes cause another ignition of the arc in the negative half-wave of the supply voltage. The T_{h6} thyristor section and i_{Th6} current flow is switched on and, after a given time, conduction and i_{Th1} current flow is taken over by the lower order T_{h1}. In the T_{h1}

section, there is a thyristor with a smaller voltage drop in the direction of conduction, hence the faster shutdown of the higher order section and current loss in this section. The waveform u_a in the first part of the positive half-wave of the supply voltage illustrates the waveform recorded at the arc source terminals. Before ignition of the arc, it is the voltage on the conductive fuse element, while at the moment of ignition, the oscillogram shows the voltage on the arc. At the moment of triggering the first semiconductor section T_{h1}, the current in the branch of the arc i_a suddenly drops to zero, so it can be concluded that the arc is extinguishing. From this moment on, the recorded curve of the u_a shows the voltage course on the thyristor sections of the AE.

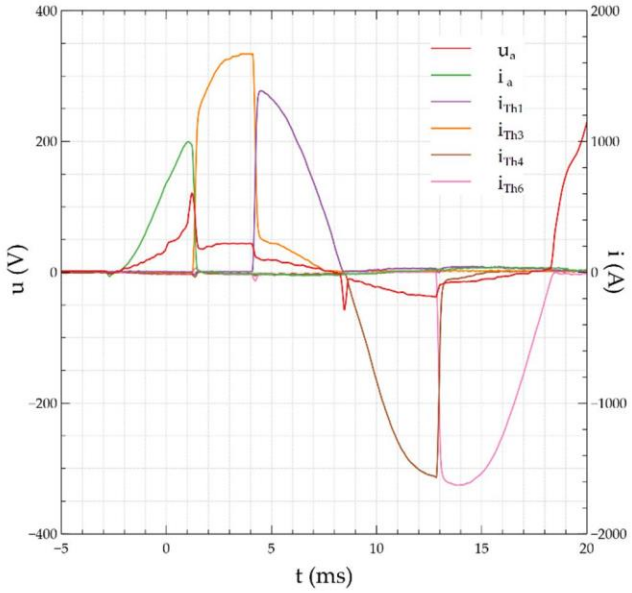

Figure 18. Current and voltage waveforms in a two-sectional arc eliminator system containing one of the thyristors with a smaller voltage drop in conduction direction.

7. Conclusions

After carrying out a number of studies and experiments presented in this paper, it can be concluded:

- there is a possibility of effective extinguishing of the arc fault in any semi-wave of current flow with the use of MSAE,
- the semiconductor bypassing systems enable very fast (faster than mechanical short-circuiting switches) bypassing of an electric circuit affected by arc fault, aiming at creating an alternative, privileged way for the flow of current. The result is a very fast elimination of electric arc and shortening of the fault current flow,
- there is a significant dependence of the effective (total) arc quenching on the selection of thyristor performance parameters. It is preferred that the thyristors in the lower (and particularly the lowest) branch have the lowest possible forward voltage. If this condition is not met, the eliminator system often works less efficiently. However, in each case, there is at least a reduction in the value of the arc current and the energy it emits,
- the MSAE system makes it possible to increase the current-carrying capacity of individual arc eliminator sections, and consequently to increase the permissible total current AE. The sequential division of the interference current into individual semiconductor branches enables the conduction of fault currents that are much larger than the allowable conduction currents of a single thyristor, usually given in catalogs for a conduction time of 10 ms,
- sequential (in each of the half-waves) switching on of current by individual bypass branches enables, admittedly, a significant increase in the current-carrying capacity of the arc eliminator,

yet it can cause an extension of the arc time. This voltage value may preclude the arc fault from extinguishing immediately. Despite the burning arc, the shunt semiconductor branch takes over much of the current from the branch affected by the arc. The value of the arc current is initially significantly reduced, and when the next semiconductor branch is activated, the arc extinguishes completely,

- through proper control of thyristor triggering impulses and their conduction time, it is possible to optimize the energy load degree of individual thyristors,
- the design and appropriate programming of MSAE enables the device to be used in circuits equipped with a short-circuiting switch with adjustable response times.

Author Contributions: Section 1 was prepared by K.N. and G.D. Section 2 was described by K.N. and J.J. Section 3 was prepared by all the authors. Sections 4–6 were prepared by K.N. and J.J. Conclusions (Section 7) were prepared jointly by all the authors. All authors have read and agreed to the published version of the manuscript.

Funding: This research was funded by the Polish Ministry of Science and Higher Education, grant number 04/41/SBAD/4408.

Conflicts of Interest: The authors declare no conflict of interest.

References

1. Berczynski, R.; Kulas, S.J. Analysis of the movement dynamics of contacts and contact-set of the making switches. *Prz. Elektrotech.* **2017**, *93*, 16–20. (In Polish)
2. Boren, S.G. Intelligence Automatic Bypass for a Motor Control Device Fault. US Patent No. US20040252423A1, 16 December 2004.
3. Bhargava, B.; Haas, R.G. Thyristor protected series capacitors project at Southern California Edison Co. In Proceedings of the IEEE Power Engineering Society Summer Meeting (PESS), Chicago, IL, USA, 21–25 July 2002; pp. 241–246.
4. Pulvirenti, F.; La Scala, A.; Pennisi, S. Low voltage-drop bypass switch for photovoltaic applications. In Proceeding of the IEEE International Symposium on Circuits and Systems (ISCAS), Seoul, South Korea, 20–23 May 2012; pp. 2283–2286.
5. Backman, M.; Demetriades, G.; Shukla, A. Hybrid Circuit Breaker. Patent No. EP2465129B1, 24 April 2013.
6. Liu, L.; Zhuang, C.; Wang, Z.; Jiang, Z.; Wu, J.; Chen, B. A hybrid DC vacuum circuit breaker for medium voltage: principle and first measurements. *IEEE Trans. Power Deliv.* **2015**, *30*, 2096–2101. [CrossRef]
7. Naidu, M.; Schoepf, T.J.; Gopalakrishnan, S. Arc fault detection scheme for 42-V automotive DS networks using current shunt. *IEEE Trans. Power Electr.* **2006**, *21*, 633–639. [CrossRef]
8. New Circuit Breakers Prevent Electrical Fires. Available online: https://phys.org/news/2012-10-circuit-breakers-electrical.html?utm_source=TrendMD&utm_medium=cpc&utm_campaign=Phys.org_TrendMD_1 (accessed on 10 November 2019).
9. Hatsagi, B. Electromagnetic Modelling and Testing of a Thomson Coil Based Actuator. Master's Thesis, KTH Royal Institute of Technology, Stockholm, Sweden, 2017.
10. Pei, X.; Smith, A.C.; Shuttleworth, R.; Vilchis-Rodriguez, D.S.; Barnes, M. Fast operating moving coil actuator for vacuum interrupter. *IEEE Trans. Energy Convers.* **2017**, *32*, 931–940. [CrossRef]
11. Kay, J.A.; Kumpulainen, L. Maximizing protection by minimizing arcing times in medium-voltage systems. *IEEE Trans. Ind. Appl.* **2013**, *49*, 1920–1927. [CrossRef]
12. Bissal, A.; Eriksson, A.; Magnusson, J.; Engdahl, G. Hybrid multi-physics modeling of an ultra-fast electro-mechanical actuator. *Actuators* **2015**, *4*, 314–335. [CrossRef]
13. Tirmizi, A.A. Pyrotechnic Circuit Breaker. Patent No. US7239225B2, 3 July 2007.
14. UFESTM Ultra-Fast Earthing Switch. Available online: https://new.abb.com/medium-voltage/apparatus/arc-fault-protection/ultra-fast-earthing-switch-ufes (accessed on 20 November 2019).
15. Nowak, K.; Janiszewski, J.; Dombek, G. Thyristor arc eliminator for protection of low voltage electrical equipment. *Energies* **2019**, *12*, 2749. [CrossRef]
16. Zhang, Z.; Ma, B.; Friberg, A. Thyristor working as arc eliminator protecting electrical apparatus in low voltage power system. In Proceedings of the IEEE International Conference on Industrial Technology (ICIT), Seville, Spain, 17–19 March 2015; pp. 1216–1219.

17. Kazmierczak, M. Arc faults - operational experience in Polish professional and industrial power engineering. *Autom. Elektroenerg.* **2011**, *2*, 98–109. (In Polish)
18. Volger, J. Arc fault protection as seen by employers' liability insurance associations. In *The Arc-Fault Demonstration in the Head Office of the Moeller*; GmbH: Bonn, Germany, 2008.
19. Hussain, G.A. Method for Arc-Flash Protection in Medium Voltage and Low Voltage Switchgear. Ph.D. Thesis, Aalto University, Helsinki, Finland, 2015.
20. Dugan, T. Reducing the flash hazard. *IEEE Ind. Appl. Mag.* **2007**, *13*, 51–58. [CrossRef]
21. Rojek, A.; Skrzyniarz, M. Contact arc time—Important parameter of DC high-speed circuit-breakers. In Proceedings of the International Scientific and Practical Conference Energy-Optimal Technologies, Logistic and Safety on Transport (EOT), Lviv, Ukraine, 19–20 September 2019; pp. 1–7.
22. Guo, X.; Cui, X.; Qi, L.; Cai, L.; Yang, Z. Bridge Arm Bypass Protection Circuit of Modularization Multi-Level Converter Aiming at Direct Current Short Circuit Fault. Patent No. CN106602531 (A), 26 April 2017.
23. Garzon, R.D. Arcing Fault Protection System for a Switchgear Enclosure. Patent No. US006141192A, 31 October 2000.
24. Nowak, K.; Janiszewski, J. Hybrid Short-Sircuiting Switch. Patent application No. P.427947, 2018.
25. Nowak, K.; Janiszewski, J. Hybrid Short-Circuiting Switch. Patent application No. P.427948, 2018.
26. Wettengel, S.; Lindenmueller, L.; Laessig, F.; Bernet, S.; Stelte, M.; Drilling, C.; Leifeld, M.; Schiele, J.; Schenk, M. Rectifier design for frequency converters using thyristor or diode modules in parallel connection, Intelligent Motion, Renewable Energy and Energy Management. In Proceedings of the International Exhibition and Conference for Power Electronics, Intelligent Motion, Renewable Energy and Energy Management (PCIM), Shanghai, China, 26–28 June 2012; pp. 79–85.
27. SCR in Parallel. Available online: https://www.daenotes.com/electronics/industrial-electronics/SCR-parallel-connection-operation (accessed on 8 January 2020).
28. *Thyristor Theory and Design Considerations. Handbook*, 1st ed.; ON Semiconductor: Phoenix, AZ, USA, 2005; pp. 10–25.
29. TME Electronic Components. Available online: https://www.tme.eu/pl/katalog/tyrystory-pojedyncze_100181/ (accessed on 8 November 2019).
30. The Catalogue of Power Semiconductor Devices: Thyristors. Available online: http://delibra.bg.polsl.pl/Content/30503/BCPS_34289_1986_Tyrystory---przyrzad.pdf (accessed on 3 July 2019).
31. Pawelski, W. *Thyristor Control*; Scientific and Technical Publishing House: Warsaw, Poland, 1974; pp. 77–86. (In Polish)
32. Nowak, K. Thyristor microprocessor controller. *Pozn. Univ. Technol. Acad. J. Electr. Eng.* **2018**, *95*, 77–86. (In Polish)
33. The New Catalogue of LAMINA Power Semiconductor. Available online: http://laminasi.com.pl/katalogi_en.htm (accessed on 3 March 2019).

Publikacja III

Karol Nowak, Jerzy Janiszewski, Grzegorz Dombek: „The Possibilities to Reduce Arc Flash Exposure with Arc Fault Eliminators”. *Energies 2021,* 14(7), 1927; https://doi.org/10.3390/en14071927

energies

MDPI

Article

The Possibilities to Reduce Arc Flash Exposure with Arc Fault Eliminators

Karol Nowak *, Jerzy Janiszewski and Grzegorz Dombek

Institute of Electric Power Engineering, Poznan University of Technology, Piotrowo 3A, 60-965 Poznan, Poland; jerzy.janiszewski@put.poznan.pl (J.J.); grzegorz.dombek@put.poznan.pl (G.D.)
* Correspondence: karol.nowak@put.poznan.pl; Tel.: +48-61-665-2584

Abstract: This paper presents a method to limit the arc energy and hence the hazard risk category value according to IEEE 1584 by using a system of two oppositely connected multi-sectional thyristor branches. A test circuit for testing the effectiveness of a thyristor arc eliminator was designed and constructed. Arc ignition inside electrical switchgear can be a source of danger for technical personnel. The arc energy calculated according to the algorithms in IEEE 1584 can be significantly reduced by using multi-sectional arc eliminator MSAE. For the actual measuring object, the calculation of the hazardous arc flash zone and the hazard category was carried out for the system not equipped with an arc eliminator, and then the same was performed in a system with an arc eliminator. In parallel, the pressure inside the closed polyvinyl chloride (PVC) electrical box enclosure was measured and then compared with the calculated pressures that could occur during an arc fault. It was found that a Multi-Sectional Arc Eliminator (MSAE) effectively protects devices supplied from low voltage networks against the effects of short circuit or arc fault, such as the sudden increase of gas pressure inside the switchboard, which may cause it to break, significantly reduce the loss of electrode material, limit the spread of hot electrode material outside the switchgear, and also significantly reduces the energy of the electric arc.

Keywords: arc eliminator; arc protection; IEEE 1584; arc fault energy; the pressure of arc gas

Citation: Nowak, K.; Janiszewski, J.; Dombek, G. The Possibilities to Reduce Arc Flash Exposure with Arc Fault Eliminators. *Energies* **2021**, *14*, 1927. https://doi.org/10.3390/en14071927

Academic Editor: Pavol Bauer

Received: 15 February 2021
Accepted: 29 March 2021
Published: 31 March 2021

1. Introduction

For many years, the term "electric arc" has been used in the electrical technical vocabulary. Since then, making electric arc calculations has remained a challenge for many power systems engineers and designers. Calculating incident energy levels and arc flash boundary distances to estimate the hazard risk category HRC [1] to which a worker would be exposed when working with electrical equipment is not easy. The calculations of the electric arc can tell us a lot about the behavior of the system in the short-circuit state [2]. They also give us an excellent opportunity to optimize the system in terms of safety and, above all, to try to prevent the occurrence of a hazard.

"Guide for Performing Arc-Flash Hazard Calculation" is known as the IEEE 1584 study [1–5]. This document includes algorithms for calculating the arc energy, the Flash Protection Boundary FPB, and the algorithms for calculating the value of the short-circuit current in the short-circuit circuit during the arc burning, verified by measurement results [6–9]. When an electric arc is generated, the electric energy supplied from the outside is converted into the incident energy, defined as its density on the unit surface at a given distance from the source. The density of this energy is expressed in joules (or calories) per square centimeter (1 inch/cm^2 = 4.184 J/cm^2) [10,11]. Very often, arc faults occur as a result of improper operation of switchgear devices, poor design solutions, or environmental conditions in which electrical devices operate [12–14].

The consequence of an emergency arc is the appearance in the vicinity (up to several meters) from the arc source [15–19]:

- a very high temperature,
- a blinding flash of light,
- the rapidly spreading plasma and hot air surrounding the discharge,
- shock wave with high-pressure impulse,
- high-intensity sound wave,
- ejection of hot shards and molten metal particles in all directions,
- large amounts of toxic gases.

The consequence of these phenomena is the destruction of equipment elements located near the arc [20] and the risk of health and life to the operating personnel [21,22]. It should be noted that a person does not have to touch anything to be injured by an electric arc. In the event of the conscious undertaking of live work on elements of electric circuits by a human being, the protection is much more difficult, and the type of protection must be preceded by a thorough analysis of the electric arc hazard category [23,24]. The result of such analysis is the determination of the arc incident energy value and the flash protection boundary FPB. Consequently, it is important how the arc hazard risk category can be reduced if the analysis shows that under normal conditions it is very large or when it is forbidden to perform any work under voltage [1,2,7].

The reduction of arc burning time and its fast elimination using a Multi-Sectional Arc Eliminator (MSAE) has been described in detail in [25,26]. The results of the conducted experiments have shown that for a resistive receiver, the electric arc is extinguished in less than 1 ms. The shortening of the arc time results in the reduction of the arc energy. The authors decided to check the effectiveness of MSAE in relation to the guidelines from the IEEE 1584 "Guide for Performing Arc-Flash Hazard Calculation" [1–5]. The experimental tests and mathematical calculations presented in the article allow to estimate the hazard categories in systems equipped with MSAE and those equipped with standard, commonly used protection devices. In addition, the authors focused on measuring the pressure inside a hermetically closed electrical box in which an electric arc burned. The shortening of the arc time (with the use of MSAE) undoubtedly results in a lower pressure increase inside the electrical box and thus the likelihood of the installation box casing bursting. Opening the installation junction box in which the electric arc burns is very dangerous. The heated parts of the electrodes coming out pose a real danger to people in the vicinity and can also ignite materials in the vicinity and cause a fire. The voltage, current and pressure waveforms recorded and presented in the article have been enriched with photographic recording by means of a high-speed camera. The photographic record allows the precise analysis of electric arc ignition, its development and extinction as a function of time.

This paper is organized as follows: Section 2 describes the arc incident energy estimation method based on the "IEEE 1584 Guide for Performing Arc-Flash Hazard Calculations". On this basis, the Hazard Risk Category HRC is determined. Section 3 describes research object and methodology. Section 4 describes the method of determining the energy balance of an electric arc. In this section, the operation of the MSAE system is explained for further analysis. Section 5 describes an approximate calculation of the pressure resulting from the ignition of an electric arc inside a closed electrical installation box. Section 6 presents the exact results of the experiments with MSAE. There are presented oscillograms of current and voltage waveforms recorded during the extinguishing of the electric arc. Additionally, photos recorded with a fast camera showing the moment of ignition and extinction of the electric arc are provided. Section 7 describes the comparison of the calculated values of pressure in a closed electric can with the measured values recorded during the experiment. Section 8 presents the calculation results of the hazard risk category in a circuit without an arc eliminator and in a circuit equipped with a high-speed solid-state arc eliminator MSAE. Finally, Section 9 presents our conclusions.

2. Electric Arc Hazard Risk Category

The electric arc hazard risk category is closely related to the arc energy value. There are several methods [4,5,27–29] using which it is possible to estimate the value of this

energy and other parameters characterizing the effects of the arc at the site of analysis. One of the most universal and allowing to obtain results considered to be the most consistent with reality is the method described in the "IEEE 1584 Guide for Performing Arc-Flash Hazard Calculations". According to the recommendations included in the aforementioned study [1,2,4,5,30], the arc incident energy density (expressed in J/cm^2) can be calculated from the equation:

$$E = 4.184 \cdot C_f \cdot E_n \cdot \left(\frac{t}{0.2}\right) \cdot \left(\frac{610^x}{D^x}\right) \quad \left(\text{J/cm}^2\right), \tag{1}$$

where C_f is a calculation factor equal to 1.5 for voltages below 1 kV and 1 for voltages above 1 kV, E_n is normalized incident energy (J/cm^2) (from Equation (3) below), t is arc duration (s), D is a distance from the worker's torso to the source of the arc (mm), and x is a distance exponent specified in Table 1.

Table 1. Equipment type and his distance exponent x.

Equipment Type	Distance Exponent D
Low voltage (0.208–1 kV) open air	2.000
Low voltage (0.208–1 kV) switchgear	1.473

The normalized arc energy E_n (J/c contained in Equation (1) is calculated assuming the arc duration time of 0.2 s (and the distance between the employee's body and the arc source is 610 mm) from the equation:

$$log_{10}E_n = K_1 + K_2 + 1.081 \cdot log_{10}I_a + 0.0011 \cdot G \quad \left(\text{J/cm}^2\right), \tag{2}$$

After conversion, we get:

$$E_n = 10^{K_1 + K_2 + 1.081 \cdot log_{10}I_a + 0.0011 \cdot G} \quad \left(\text{J/cm}^2\right), \tag{3}$$

where I_a is a arcing current (kA), K_1 is a coefficient equal to -0.555 when the analyzed object is closed in a casing and -0.792 when the arc burns in open space, K_2 is a coefficient equal to 0 when the analyzed system is not grounded and -0.113 for a grounded system, and G is a distance between current paths in the analyzed device (arc gap) (mm).

After calculating the value of the incident energy E and converting it into values expressed in (cal/cm^2), it is possible to determine the category of electric arc hazard and propose employee protection measures adequate to the level of risk. Table 2 lists the arc incident energy levels and the corresponding hazard risk categories.

Table 2. Arc incident energy values and hazard risk categories [1,2,4,5].

Arc Incident Energy (cal/cm^2)	Hazard Risk Category
0–1.2	0
1.2–4.0	1
4.0–8.0	2
8.0–25.0	3
25.0–40.0	4

If the arc incident energy is calculated to be greater than 40 cal/cm^2, all live work is prohibited as there are no measures in place to protect the worker from the effects of such an arc. In this situation, it is necessary to take measures to reduce the arc energy value, and thus reduce the hazard risk category.

The Flash Protection Boundary (FPB) is the distance during the incident energy of an event is 1.2 cal/cm^2, which is the amount of heat needed to cause burns of at least a

second degree. The distance of the border of the arc damage zone can be calculated from the equation:

$$D_B = [4.184 \cdot C_f \cdot E_n \cdot \left(\frac{t}{0.2}\right) \cdot \left(\frac{610^x}{E_B}\right)]^{\frac{1}{x}} \quad (\text{mm}), \tag{4}$$

where D_B is a flash protection boundary (mm), and E_B is the desired incident energy at the boundary (usually 1.2 cal/cm^2).

3. Research Object and Methodology

The experimental test was performed in a model system powered from a low voltage power grid. The arc generator (source of the arc) is placed in the surface-mounted junction box shown in Figure 1. The electrical junction box is made of thermoplastic material, which is characterized by high resistance to mechanical impact. The degree of protection provided by the junction box is International Protection (IP) Rating 55. The rubber seal and grommets (membranes) enable the protection level to be maintained at the level assumed by the producer. The actual dimensions of the can are 81.5 × 81.5 × 45.3 mm. According to the manufacturer's data, the junction box may operate within the temperature range from −25 °C to +85 °C, and its resistance to the glow wire test is 650 °C. The electrical junction box will be referred to as the electrical switchgear or junction box in the rest of this paper. The lockable cover and rubber membranes, in addition to sealing, indirectly protect against sudden pressure increase inside the switchgear (during an arc fault) and prevent catastrophic explosion in case of its excessive increase. Figure 1 show the view of the junction box housing the experimental arc disturbance source. Wires led into the interior of the can through conduits made of polyvinyl chloride (PVC). An electric arc detector was placed in one of the pipes. A filter made of plastic with the high light transmission (glass filter) provided insulation between the flash detector and the electrodes of the arc source. Next to the flash detector, a series 21G pressure sensor (Keller, Winterhur, Switzerland) was installed. Parameters of used pressure sensor was shown in Table 3.

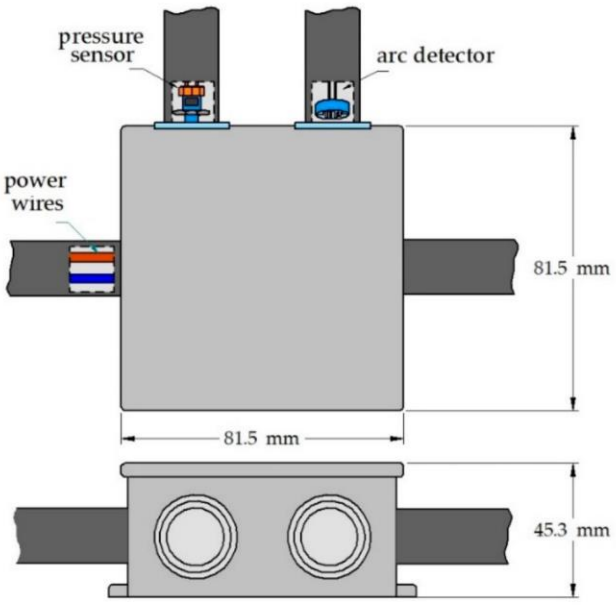

Figure 1. Electrical installation box which is a housing for an arc fault source.

Table 3. Parameters of the Keller 21G pressure sensor (Adapted from [31]). Reproduced from [31], Keller: 2020.

Parameters	Value
Types	Absolute or sealed gauge
Pressure ranges	from 0 to 5 bar
Electrical configuration	2 wire
Output	from 4 mA to 20 mA
Excitation	from 8 V to 28 V
Linearity (BSFL)	Typical 0.25% FS
Error band	from −40 °C to 80 °C typical 1.0% FS

The measuring part of the sensor through a sealing rubber diaphragm was placed inside the installation box. Figure 2 shows a model source of the emergency arc affected by the arc disturbance. The figure shows a burning electric arc and mass emission of the electrode material in the form of glowing drops.

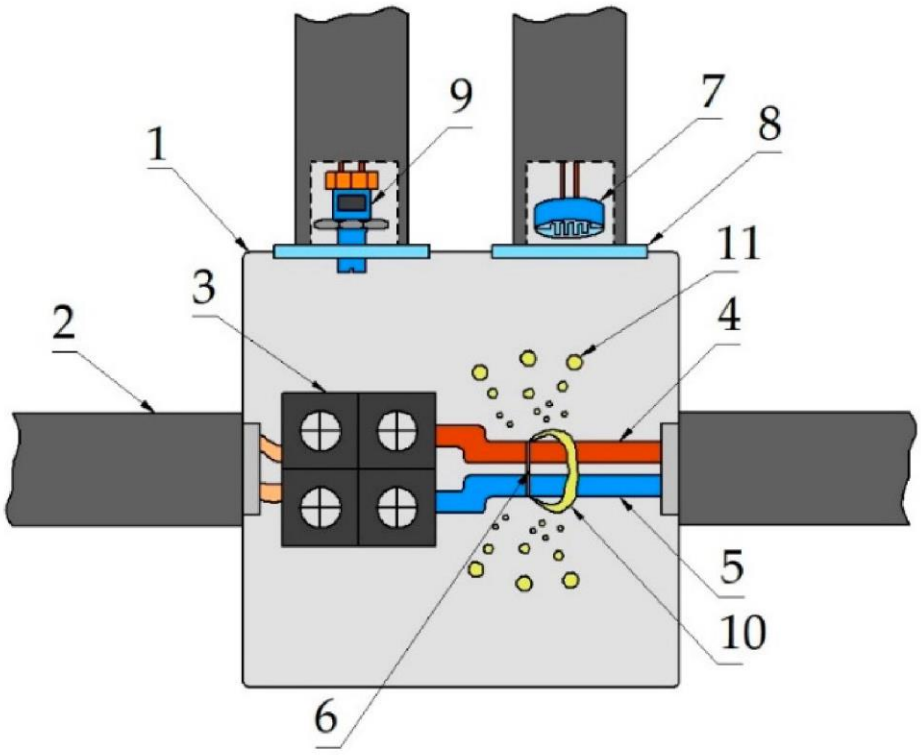

Figure 2. Construction of the arc generator: 1—Surface mounted electrical junction box; 2—PVC tube for electrical installations (φ = 16 mm) for entry and exit of the supply lines, as well as sensors; 3—Terminal strip for quick replacement of the arc generator electrodes; 4—Phase power wire; 5—Neutral power wire; 6—Fusible wire initiating the ignition of the arc; 7—Arc flash detector; 8—Glass, insulating protection of the flash detector; 9—Gas pressure sensor inside the electrical junction box; 10—Arc fault; 11—Drops of glowing material, which constitute the weight loss of the measuring electrodes.

4. The Balance of Energy Supplied to the Electric Arc Fault

The heat energy released in the emergency electric arc can cause, and often causes, significant damage to equipment inside and outside the area affected by the arc fault. It is also a serious threat to people and devices near an electric arc. If an electric arc occurs in the electrical switchgear or electrical junction box, there are mechanical risks associated with the possibility of tearing the casing walls (unsealing the housing) or breaking other switchgear elements (doors, partitions, etc.). It is related to the sudden increase in pressure

inside the place affected by the electric arc, proportional to the energy absorbed by the arc from the electrical supply network (Equation (6)).

Figure 3 shows the equivalent diagram of the tested AC circuit in which the electric arc was ignited between the electrodes of the arc generator and an example of sequential taking over current by shunting paths in the order in which thyristors are triggered. The MSAE [25,26] presented in Figure 3a is a multi-sectional arc eliminator which belongs to the family of bypass circuits affected by the failure. Its task is to quickly eliminate interference (electric arc, emergency current), preventing further development of irregularities. The system's operation consists in the sequential taking over the current by multi-sectional cascading bypass branches when a failure occurs in the protected electrical circuit (Figure 3b). The undoubted advantage of this solution is a significant increase in the allowable arc eliminator currents. The sequential division of the interference current into individual semiconductor branches enables the conduction of fault currents much larger than the allowable conduction currents of a single thyristor, usually given in catalogs for a conduction time of 10 ms. An additional advantage of arc eliminator is short-circuit current commutation in MSAE branches without arc and shortening the time of thermal effects' interaction in the protected circuit.

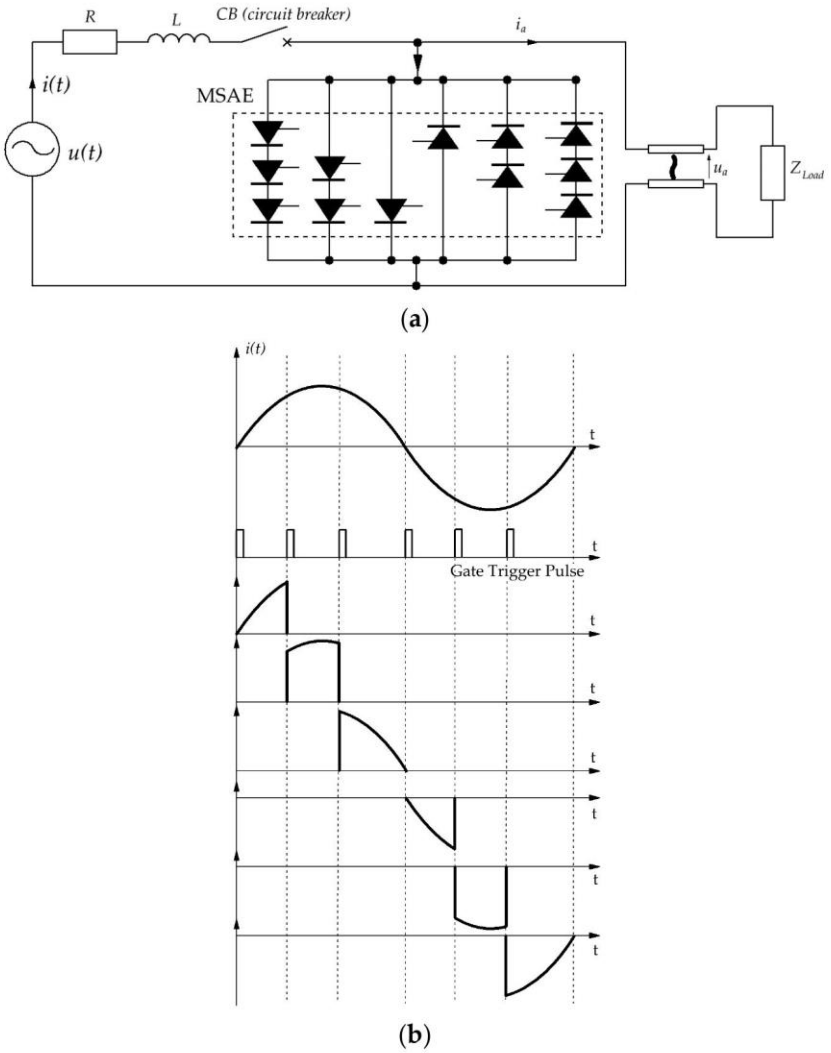

Figure 3. Multi-sectional structure of thyristors and operation of the MSAE: (**a**) Electrical scheme for an AC circuit with arc and MSAE made by the thyristors, (**b**) an example of sequential taking over current by shunting paths in the order in which thyristors are triggered.

The voltage balance in the circuit with the arc can be determined from the equation:

$$u(t) = R \cdot i_a + L \cdot \frac{di_a}{dt} + u_a \tag{5}$$

where R is a circuit equivalent resistance, L is a circuit equivalent inductance, u_a is the instantaneous value of the arc voltage, and i_a is the instantaneous value of arc current.

When an emergency arc occurs, the current through the Z_{LOAD} working load is usually negligible. The energy supplied to the arc from the supplying electric circuit can be determined from the Equation (5) after multiplying both sides by the formula $i_a dt$:

$$u_a \cdot i_a dt = \left(u(t) \cdot i_a - i_a^2 \cdot R\right) dt - L \cdot i_a di_a \tag{6}$$

Integrating Equation (6) within the arc burning time (t_1—arc ignition moment, t_2—arc extinguisher moment), we will obtain the formula for the energy supplied to the arc:

$$E = \int_{t_1}^{t_2} u_a \cdot i_a \cdot dt = \int_{t_1}^{t_2} q_a(t) \cdot dt \tag{7}$$

where the variables are instantaneous values of arc voltage u_a, arc current i_a, and power consumed by the arc q_a.

The instantaneous value of the power q_a is calculated from the dependence:

$$q_a(t) = u_a \cdot i_a \tag{8}$$

The observed actions and effects of a burning arc depend on the value of the current and the duration of the arc fault, as well as on the possibility and speed to move of the electric arc. Hence, one of the important methods of limiting the effects of emergency short circuits is shortening the short-circuit duration. Estimation of the basic energy parameters of the emergency arc during the arc fault ta enables the assessment of the hazards risk category, presented in Section 2.

5. Gas Pressure in a Hermetic Casing with an Existing Emergency Arc

The pressure rise inside the switchboard is primarily a function of the energy $e(t)$ taken from the network by the arc and converted into heat. The presence of apparatus and equipment near the electric arc, on the other hand, slightly reduces the temperature and pressure inside the covers of switchgear compartments. The following part of the paper presents an assessment of the impact of arc faults on the pressure increase in sealed casings, not equipped with safety flaps, but with floating membranes in the event of a sudden pressure increase inside the switchgear compartments (electrical junction box). The authors also attempted to verify the measured pressure increases about the calculated increases. The course of the pressure increase $\Delta p(t)$ in a tight, thermally insulated casing in which the free arc burns and all its energy $e(t)$ (in the form of heat) is evenly transferred to the surrounding air (in the form of heat), it is possible to calculate from the formula [32,33]:

$$\Delta p(t) = k_t \cdot \frac{K-1}{V_g} \cdot E_a(t) \quad \text{(Pa)} \tag{9}$$

where k_t is a heat transfer coefficient (value calculated experimentally [32] for copper electrodes Cu-Cu k_t = 0.48, for Al-Al k_t = 0.63, and for Fe-Fe k_t = 0.36), V_g is a net gas volume inside sealed electrical switchboard (m^3), K is adiabatic exponent (value read from the adiabatic diagram of selected gases)—For air it is K = 1.088 [32], and E_a is electric arc energy [J].

6. Emergency Arc Which Burns on Copper Electrodes

The experiment was carried out in the arrangement shown in Figure 3 for copper measuring electrodes with a diameter of φ = 2.21 mm (4 mm^2 wires). The system is powered by alternating voltage with an effective value of 230 V. For safety reasons, the amplitude of the current in the circuit shown in Figure 3 has been limited to 1300 A. The first stage of the tests was performed in a short-circuit electrical circuit with an inactive arc eliminator (MSAE OFF). The protection of the tested system is the circuit breaker CB (main switch).

The ignition of the electric arc and its subsequent effects were recorded with a Chronos 1.4 high-speed camera (Kron Technologies Inc., Burnaby, BC, Canada). The device is a 1.4 gigapixel-per-second handheld high-speed camera. It records 1280 × 1024 video at 1057 fps and can record at up to 38,565 fps at a lower resolution. Such a large number of frames allows you to analyze the previously recorded electric arc explosion with an accuracy of 26 µs for each photo. This gives great cognitive opportunities during research on the effectiveness of MSAE. Parameters of the high-speed Chronos 1.4 camera are listed in the Table 4.

Table 4. Parameters of a Chronos 1.4 high-speed camera (Adapted form [33]). Reproduced from 33], Krontech: 2018.

Parameters	Values
Color camera imaging	from 1280 × 1024 1057 fps to 336 × 96 38.565 fps
Camera memory	8 GB
Lens mount	CS mount, C mount with the included adapter
Camera IR Filter	650 nm, 18 × 18 × 1.1 mm
Camera display	5″ 800 × 480 capacitive touchscreen
Video formats	H.264 industry-standard mp4 files at bitrates up to 60 Mbps cinemaDNG Raw Standard Adobe
Image sensor	speed 1.4 Gpx/s—Full throughput down to 336 pixel image width dimensions 8.45 × 6.76 mm pixel pitch 6.6 µm shutter electronic global shutter, 1/fps to 1 µs (1/1,000,000 s)

The waveforms recorded in the tested circuit are shown in Figure 4. In the moments t_1 = 0 ms and t_6 = 7.1 ms, the first and second ignition of the electric arc takes place successively. The disturbance related to the electric arc ends at time t_8 = 15.5 ms. The total burning time of the electric arc for both half-waves of the flowing current was t = 13.8 ms. The recorded waveforms in Figure 4 present in turn:

- Figure 4a voltage waveform $u_{power} = f(t)$, voltage on the arc $u_a = f(t)$ and current in the branch with the arc $i_a = f(t)$,
- Figure 4b the course of the measured pressure $p_a = f(t)$ inside the electrical box in which the arc disturbance occurred and the design pressure value (9) $p_{obl} = f(t)$ for the installation electrical box in which there was no opening, and the arc burns during two half-waves of flowing electric current,
- Figure 4c waveforms of the calculated values of the power (8) consumed by the arc from the power network $q_a = f(t)$ and the energy (7) released in the arc $e_a = f(t)$.

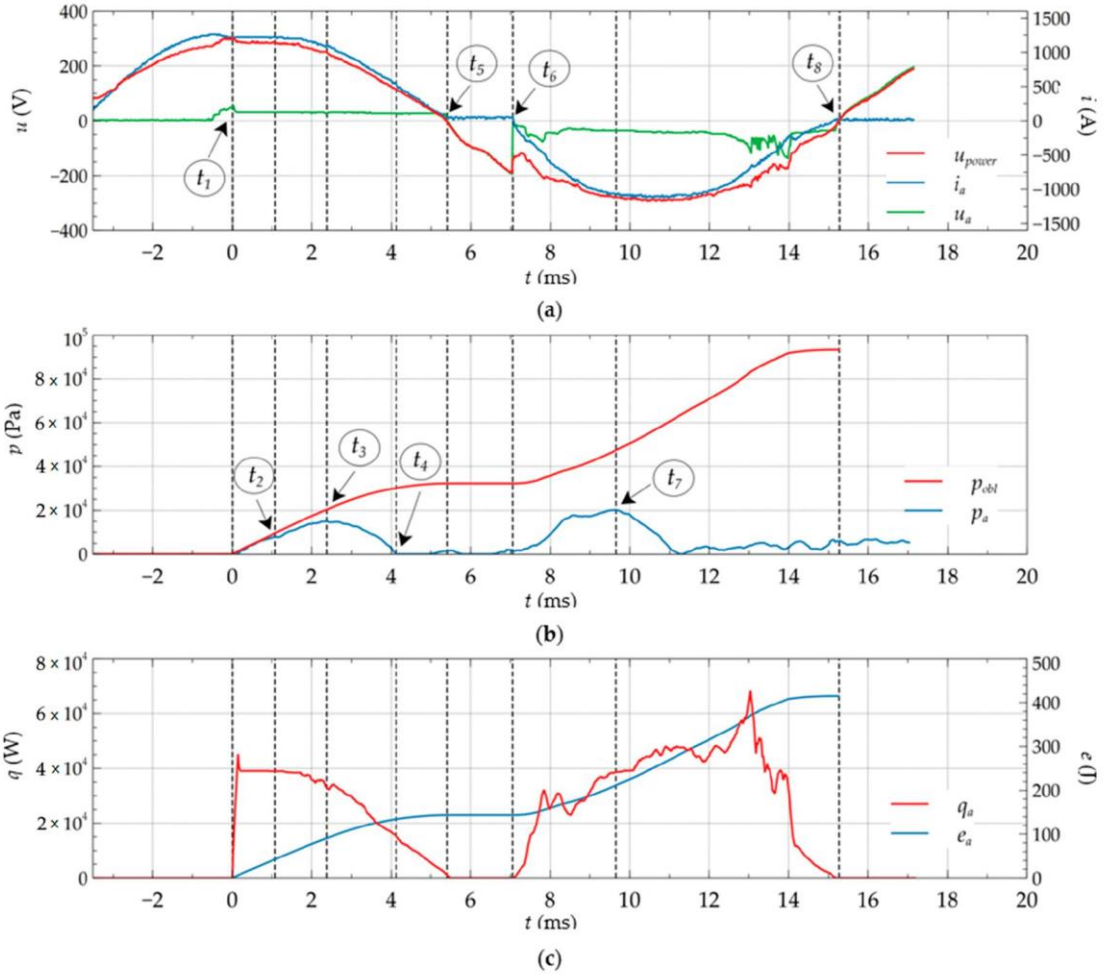

Figure 4. Waveforms as a function of the arc fault duration: (**a**) supply voltage u_{power}, arc voltage u_a and current in the arc branch i_a; (**b**) measured and calculated pressure p_a and p_{obl} inside the junction box casing; (**c**) power consumption by the arc q_a, and energy released on the arc e_a as a function of the duration of the arc fault. Points t_1–t_8 correspond to the successive photographic images a–h presented in Figure 5.

For the waveforms presented in Figure 4, several characteristic points were determined. For the same points using a Chronos 1.4 high-speed camera recorded images shown in Figure 5. The interpretation of the individual points is as follows:

(1) Figures 4a and 5a—At the moment t_1 = 0 ms inside the electrical junction box, the first electric arc ignition takes place. In the photo captured with a fast camera, a flash of an electric arc can be seen through a small viewfinder located on the side of the housing,
(2) Figures 4b and 5b—When t_2 = 1.15 ms the junction box is opened and the gas pressure inside the installation box is slightly reduced. On the recorded pressure oscillogram, the opening moment of the electrical junction box is visible in the form of a recess in the characteristic. For the same time moment, the camera registered a visible opening of the electric junction box by lifting one of the edges of the installation box lid, which is resiliently attached to the housing catches,
(3) Figures 4b and 5c—At the time t_3 = 2.3 ms the measured pressure reaches its local maximum, and in the next step it starts to decrease its value, which suggests the process of unsealing the electrical junction box,
(4) Figures 4b and 5d—At the time t_4 = 4.1 ms the pressure reduces its value to the value of the pressure before ignition of the electric arc. The burning electric arc inside the electrical junction box and the hot particles of the electrode material escaping outside,

visible in the photo, prove a significant opened of the casing and a strong, erosive effect of the arc inside it,

(5) Figures 4a and 5e—At the moment t_5 = 5.4 ms, the zero-crossing of the electric current causing the extinguishing of the first electric arc (in Figure 5e it is revealed by the weakening of the glow inside the box),

(6) Figure 4a,b and Figure 5f—At the time t_6 = 7.1 ms the electric arc is re-ignited, and the measured pressure inside the installation box increases. The photo captured with a fast camera shows the moment of elastic closing of the installation box cover and burning hot particles of electrode material thrown outside, resulting from the previous ignition of the electric arc,

(7) Figures 4b and 5g—At the time t_7 = 9.6 ms the measured pressure locally reaches the next maximum (for the second ignition of the arc). The photo for the same time moment shows the flap of the installation box opening again and the hot copper drops (electrode material) escaping outside,

(8) Figures 4a and 5h—At the moment t_8 = 15.3 ms, the electric arc is finally extinguished. The lid of the electric junction box closed by the elasticity of fastenings, as well as the heated internal elements and the remnants of the hot loss of electrodes inside the box, cause a slight increase in pressure, which can be observed on the recorded oscillogram (Figure 4b). Despite the arc extinguishing and the practically closed switchgear, the camera registered incandescent material that had managed to escape outside the electrical junction box.

Full photographic recording of the effects of emergency arc ignition, shown in Figure 5, is attached to this paper in the form of a time-lapse movie [34]. It shows the recorded film frames just before the ignition of the electric arc, through the ignition of the first and second arcs, and its end falls on the extinction of the remaining incandescent material losses from the measuring electrodes.

The evaluation of the measured and calculated pressure changes in the volume of the electrical junction box with the analyzed emergency arc can be performed based on the waveforms shown in Figure 4b. At the time t_1 = 0 ms, the electric arc is ignited for the flow of a positive current half-wave. In the photo recorded with a fast camera (Figure 5a), a flash of an electric arc inside the installation box can be seen through a small viewfinder located on the side of the electrical junction box. In the time from t_1 = 0 ms to t_2 = 1.15 ms, the pressure inside the closed junction box, due to the burning electric arc, reaches a critical value, sufficient to open the installation cover of the electrical box. Shortly after the casing is opened, the measured pressure drops slightly—Figure 4b.

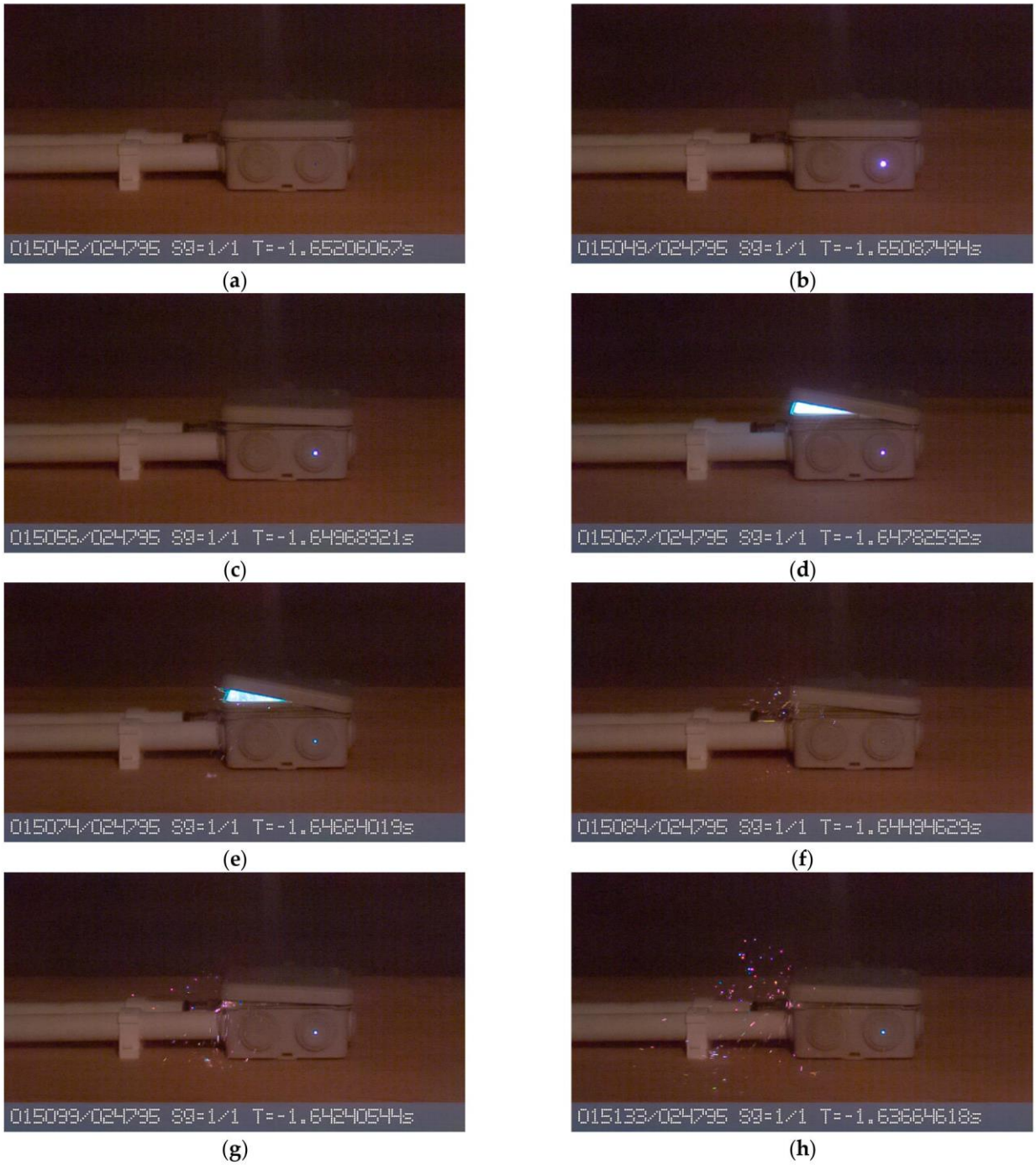

Figure 5. Photographic registration of the effects of the emergency arc in the electrical junction box (**a**) t_1 = 0 ms electric arc ignition; (**b**) t_2 = 1.15 ms switchgear opened; (**c**) t_3 = 2.3 ms pressure maximum for the first period time of arc ignition; (**d**) t_4 = 4.1 ms the pressure reduces to that before the ignition of the electric arc; (**e**) t_5 = 5.4 ms start of electric arc extinguishing; (**f**) t_6 = 7.1 ms electric arc re-ignition; (**g**) t_7 = 9.6 ms maximum pressure in the second period, the arc is burning; (**h**) t_8 = 15.3 ms final electric arc extinguishing (I_m = 1300 A, U = 230 V, Cu-Cu electrodes).

Since the instantaneous arc power is never negative, negative pressure gains can't occur. It follows that at time t_2 there was an elastic opening of the cover closing the junction box and the pressure drop through the created gap. This conclusion is also confirmed by the image recorded with a fast camera. The pressure built up inside, calculated according to Equation (9) at the moment of unsealing the can, is 9.75 kPa. The measured pressure value

for the same time instant reaches the value of 7.9 kPa. The increase in the measured pressure Δp_a in the initial phase of the arc disturbance until the electrical junction box is opened largely coincides with the increases in the calculated pressure curve Δp_{obl}. The conclusion is that knowing the arc energy characteristics $e_a(t)$ and knowing that the pressure increase is primarily a function of this energy, it is possible to determine the pressure curve inside the sealed switchgear with high accuracy. The course of the pressure increased calculated $p_{obl}(t)$ and measured $p_a(t)$ cease to coincide over time from the moment of opening the switchgear. A further attempt to compare both values does not give reliable results. However, further calculation of the increment of $p_{obl}(t)$ for the subsequent ignition of the arc allows estimating the value of the pressure in the tightly closed electrical junction box. The lack of ventilation flaps or safety membranes causes a further increase in the overpressure value as a function of the arc energy. In Figure 4b, the calculated pressure after t_7 = 15.3 ms, corresponding to the total arc burning time, could reach 94 kPa inside the junction box. After t_3 = 2.3 ms, the gas pressure inside the junction box reaches a maximum of 15 kPa. The energy supplied to the arc is then 88 J, and the power input from the power network needed to sustain the burning arc is 35.5 kW. The lid closing the junction box is opened and from that moment the primary and secondary products of the emergency arc in the form of metal vapors from electrode erosion, hot and toxic gases, smoke, etc. begin to escape into the environment from its interior. The described condition is well illustrated in Figure 5 and the time-lapse movie is recorded with a fast-speed camera [33]. At the time t_4 = 4.1 ms, the measured pressure reaches a value close to the initial (atmospheric) pressure, which is related to the considerable opening of the installation box cover—Figure 5c. In general, this situation continues until the current crosses zero (or is turned off). In the previously analyzed case, after the arc was extinguished, the can lid was closed, causing the apparent sealing again. The favorable thermal conditions and the small distance between the electrodes cause another arc ignition, this time for the negative half-wave of the supply voltage. At the time t_6 = 7.1 ms, the electric arc re-ignites, and the pressure of gases inside the closed installation box increase further. The second ignition of the arc and high temperature (next heating after the previously existing first electric arc) cause an increase in pressure at the time t_7 = 9.6 ms, up to 20.3 kPa, arc power energy up to 210 J, and power input from the power network up to 38.2 kW. In the next milliseconds of burning electric arc, the pressure of gases inside the junction box begins to decrease its value due to the subsequent opening of its cover. At t_8 = 15.3 ms, when the arc is extinguished, the pressure inside the switchgear decreases and fluctuates within 5 kPa. The high temperature inside the arc source housing, the flying in the air residual material loss from the electrodes and the re-closed installation box lid maintains the overpressure inside the box for some time.

Figure 6 shows the interior view of the electrical junction box and the effects of ignition of an electric arc burning for the time of 8.9 ms. It can be seen that even for such a short arc time, there is intense destruction of the electrodes and elements inside the electrical box. This is especially dangerous from the point of view of fire protection. Most of the part energy generated in the arc can initiate ignition of flammable elements in the vicinity of the electric arc.

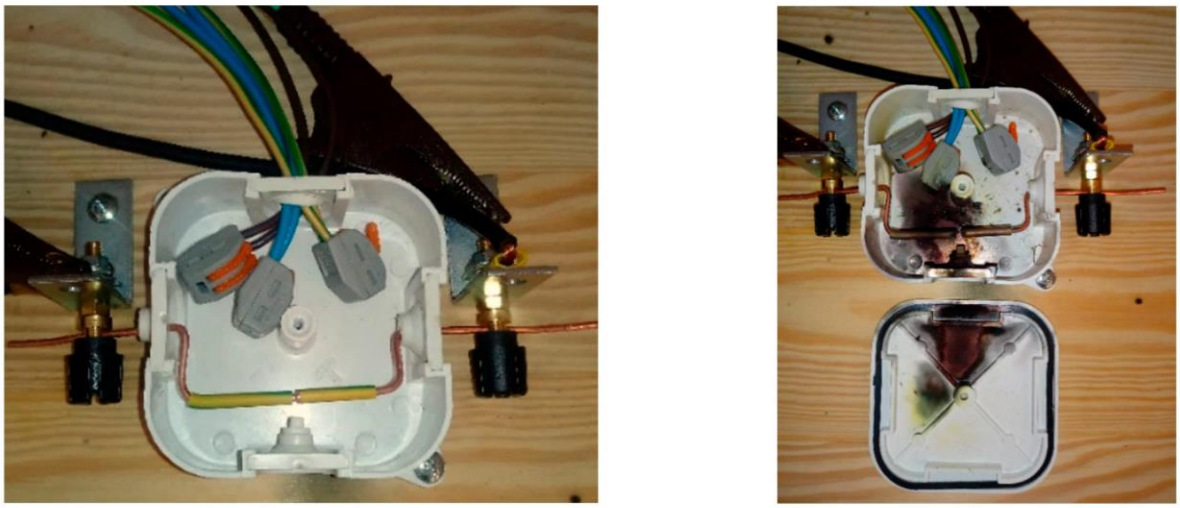

(**a**) (**b**)

Figure 6. View of the inside of the electrical junction box before (**a**) and after (**b**) the arc fault test; supply voltage 230 V; the arc current 1000 A; the electric arc duration time 8.9 ms.

The selected photos shown in Figure 7 were recorded during the ignition of the electric arc in the unsealed casing of the electrical junction box. The deliberate removal of the rubber insulating membranes made it possible to observe the direction of travel of the products of the electric arc explosion. The emission of hot gases that travel along the conductors can damage the insulation and further ignite the arc inside the electrical bushings. Despite the possible exit route for gases through the passages on its sidewall, it was found that the large and rapid increase in pressure inside the installation box still caused the arc source housing to unseal and the gases to be emitted outside.

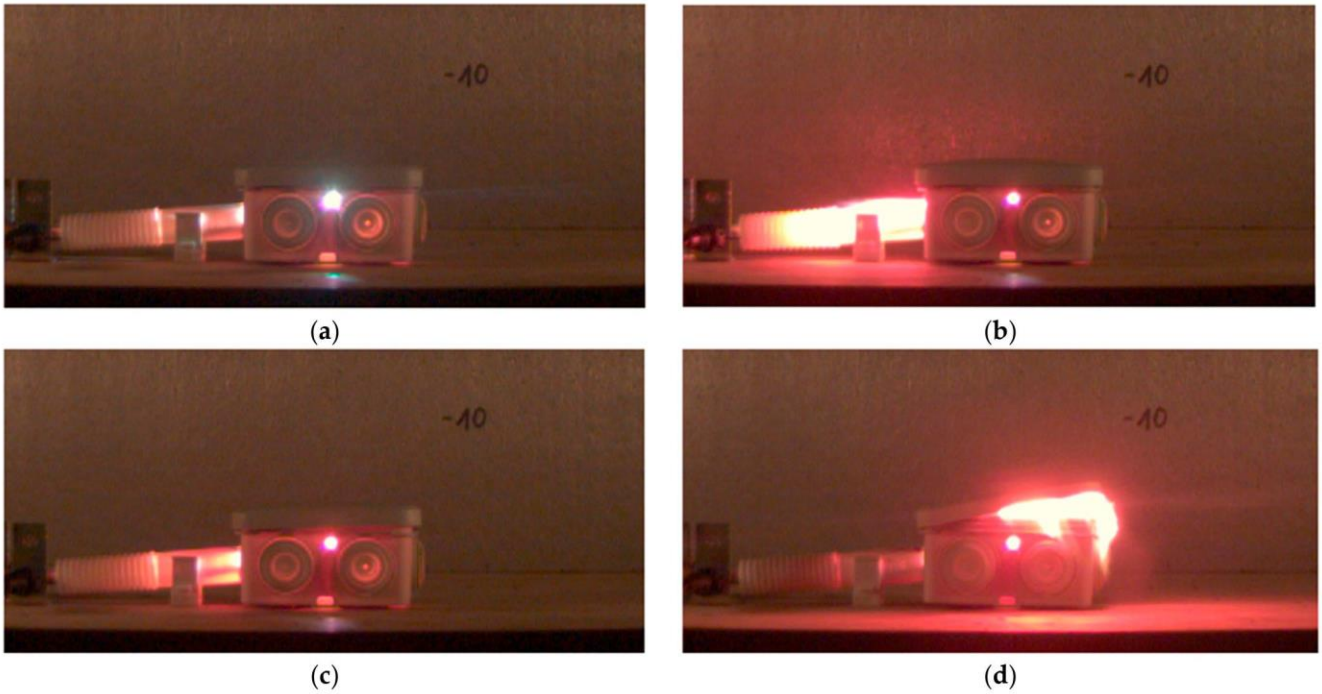

(**a**) (**b**)

(**c**) (**d**)

Figure 7. Evolution and product release of plasma and emergency arc products within the elements of a non-hermetic installation junction box (**a**) t = 0.5 ms; (**b**) t = 1.5 ms; (**c**) t = 2.5 ms; (**d**) t = 3.5 ms (I_m = 1250 A, U = 400 V, Cu-Cu electrodes).

Figure 8 shows an arc current and voltage oscillogram for three half-waves of the arc disturbance. The waveforms were recorded in the arrangement of Figure 3 without MSAE. The receiver is supplied with a phase-to-phase voltage of 400 V, and the electrodes of the arc source are made of aluminum wires with a diameter of φ = 2.38 mm.

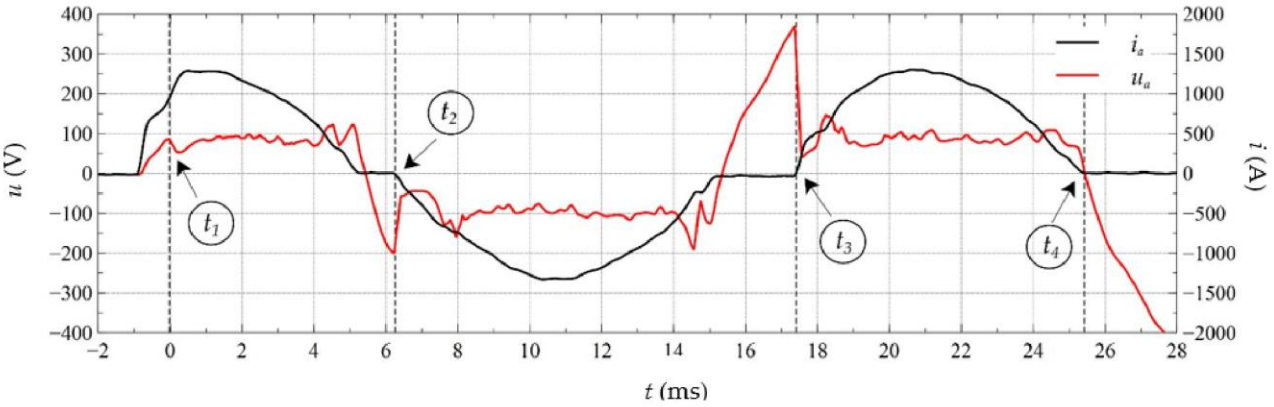

Figure 8. The waveform of the arc current $i_a(t)$ and the arc voltage $u_a(t)$ for three half-waves of the arc disturbance).

Four characteristic points are marked on the waveforms in Figure 8:

- first ignition of the electric arc t_1 = 0 ms,
- second ignition of the electric arc t_2 = 6.25 ms,
- third ignition of the electric arc t_3 = 17.4 ms,
- end of arc fault t_4 = 25.4 ms.

The arc duration time is t_a = 25.4 ms.

The photos presented in Figure 9 show the image of the arc at the time moments of the first, second, and third ignition of the electric arc. For an interfacial short circuit and much greater arc energy, the increase in pressure inside a closed junction box enclosure is capable of tearing off and ejecting the lid of the enclosure for several tens of centimeters. This is accompanied by the creation of a deafening acoustic wave, a rapid temperature rise, and the ejection into the environment of the primary and secondary products of the emergency arc in the form of metal vapors and droplets from the erosion of aluminum electrodes.

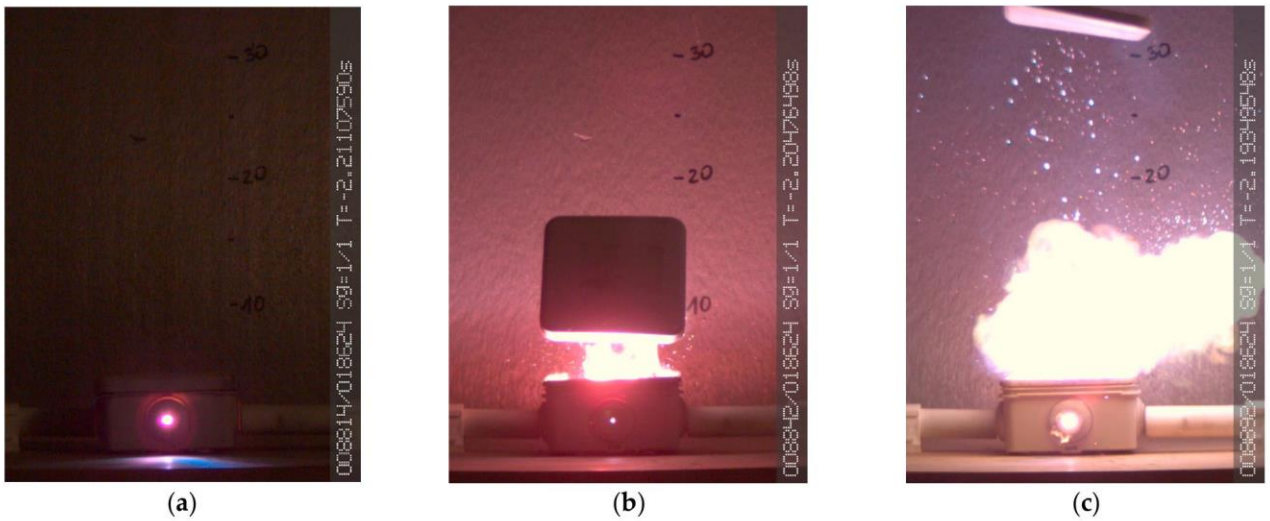

(**a**) (**b**) (**c**)

Figure 9. Development of the arc discharge for three successive ignitions of the electric arc: (**a**) first ignition of the electric arc t_1 = 0 ms, (**b**) second ignition of the electric arc t_2 = 6.25 ms, (**c**) third ignition of the electric arc t_3 = 17.4 ms (I_m = 1250 A, U = 400 V, Al-Al electrodes).

Figure 10 shows a sequence of selected frames of film recording for an arc burning between electrodes made of aluminum. The time of the disappearance of the electric discharge t_4 = 25.4 ms does not mean the end of the danger posed by the occurrence of the emergency arc. The exploding material from the electrodes poses a real danger of burns and fire even after 500 ms from the moment when the electric arc is extinguished, which is proved by the last frame of the presented recording, which shows still hot drops of aluminum. The height markers visible in the photos (clearly visible in Figure 10 at t = 20 ms) were scaled in centimeters. In the registered frames of the video, it can be seen that the heated aluminum droplets float above the last marker located at a height of 30 cm.

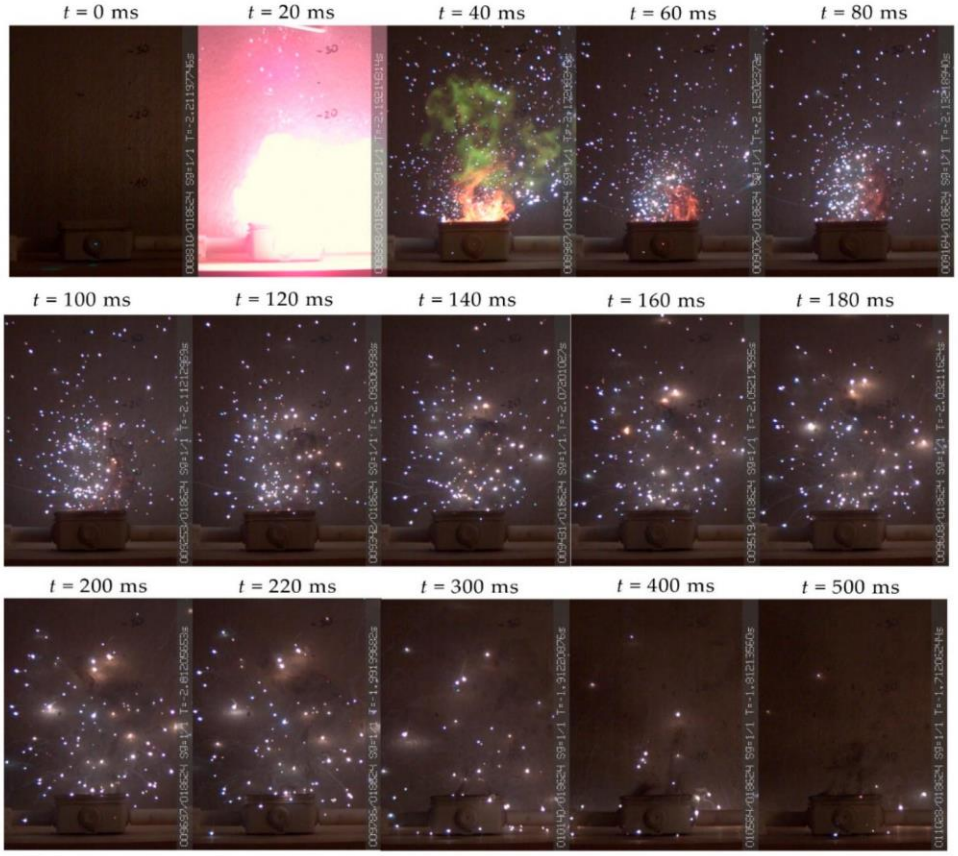

Figure 10. Selected frames of recording the effects of an emergency arc from its ignition to the almost complete extinction of the exploding, glowing remains of drops of electrode material (I_m = 1250 A, U = 400 V, Al-Al electrodes).

Full photographic recording of the effects of emergency arc ignition, shown in Figure 10, is attached to this article in the form of a time-lapse movie [35]. It shows the recorded frames of the film from the moment the arc ignited, through the subsequent ignitions of the arc, until the moment the remaining glowing loss of material from the aluminum electrodes expired.

The unsealing of the electrical junction box occurred 2.72 ms after the arc was ignited. The measured pressure value just before unsealing the casing was 48 kPa, the energy in the arc was 266 J, and the power input from the power network was 85 kW. If the housing had not been opened, the calculated value of pressure in the closed installation box, in the final phase of the arc, would have reached the enormous value of 310 kPa at arc energy of 1750 J. The use of the Chronos 1.4 high-speed camera made it possible to record the moment of unsealing of the electrical installation box. Figure 11a shows the moment just before it unseals. In the next photo from the film, Figure 11b, recorded after 0.225 ms, one can see the initial unsealing of the junction box (lifting of the electrical box lid) and the arc glow up

flash on the back wall of the arc source casing. This allows for accurate determination of the time of unsealing the housing.

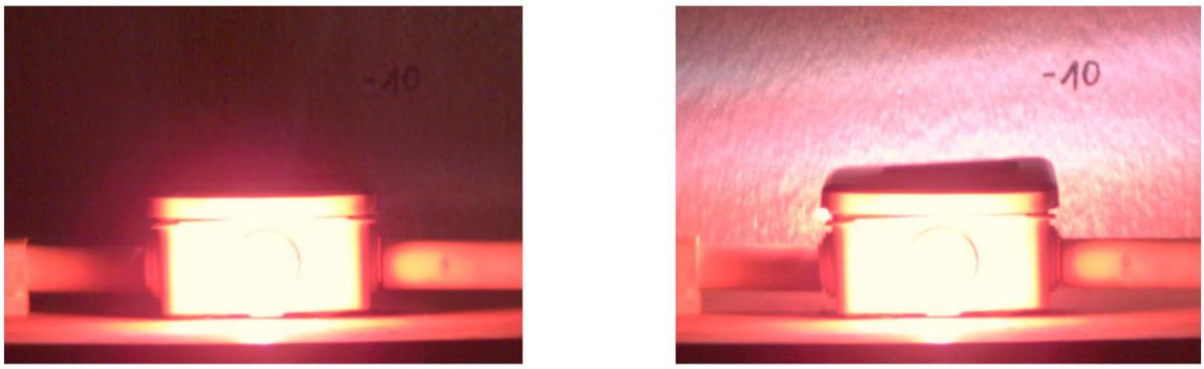

(**a**) (**b**)

Figure 11. Subsequent frames from recording the behavior of the test object: (**a**) just before unsealing the electrical installation box, (**b**) immediately after opening the electrical installation box; 225 µs time interval.

7. Testing the Effect of the Emergency Arc in a System with an Arc Eliminator

The experiment was carried out in the system shown in Figure 3 for copper measuring electrodes with a diameter of φ = 2.21 mm (4 mm^2 wire). The system is powered by phase voltage with an effective value of 230 V. The current amplitude in the circuit from Figure 3 was limited (as in previous tests) to a value of 1300 A. The tests were carried out to verify the effectiveness of reducing the effects of the emergency arc by using a thyristor multi-sectional arc eliminator (MSAE), the operation of which is presented in the work [25]. The waveforms in Figure 12 represent in turn:

(1) voltage waveform on the arc $u_a = f(t)$, current in the branch with the arc $i_a = f(t)$, the current flowing through the shunting system MSAE $i_T = f(t)$, and the arc flash detection pulse $imp_{wyz} = f(t)$,
(2) the course of the measured pressure $p_a = f(t)$ inside the installation electrical box in which the arc fault occurred and the calculated pressure value $p_{obl} = f(t)$ (9) for the arc duration,
(3) the course of the calculated value of the power (8) consumed by the arc from the power network $q_a = f(t)$ and the energy (8) released on the arc $e_a = f(t)$ calculated for the arc duration.

Analyzing the waveforms shown in Figure 12a, five-time characteristic points can be distinguished:

- at time t_1 = 0 ms the electric arc is ignited,
- at time t_2 = 0.05 ms the arc flash is detected and the thyristors of the MSAE are triggered,
- at time t_3 = 0.69 ms full conduction is taken over by the shunt branch of MSAE,
- at the time t_4 = 0.9 ms the electric arc is extinguished,
- at the time t_5 = 1.2 ms the measured pressure locally reaches the first maximum.

During the flow of current in the circuit at the time t_1 = 0 ms, a disturbance in the form of ignition of the electric arc occurs. The flash detector placed close to the arc generates a pulse that triggers the thyristors of the MSAE system after only 0.05 ms (at time t_2). The time delay of the thyristor triggering system, resulting from the internal structure and the semiconductor elements used, causes that after 0.64 ms from the moment of flash detection, at t_3 = 0.69 ms, the shunting MSAE system begins to conduct. MSAE semiconductor elements take over the current flow from the branch affected by the arc fault. The complete absence of current in the arc-affected branch occurs 0.21 ms after the MSAE is triggered.

The arc time t_a = 0.9 ms passes from the moment the arc appears until it is completely extinguished.

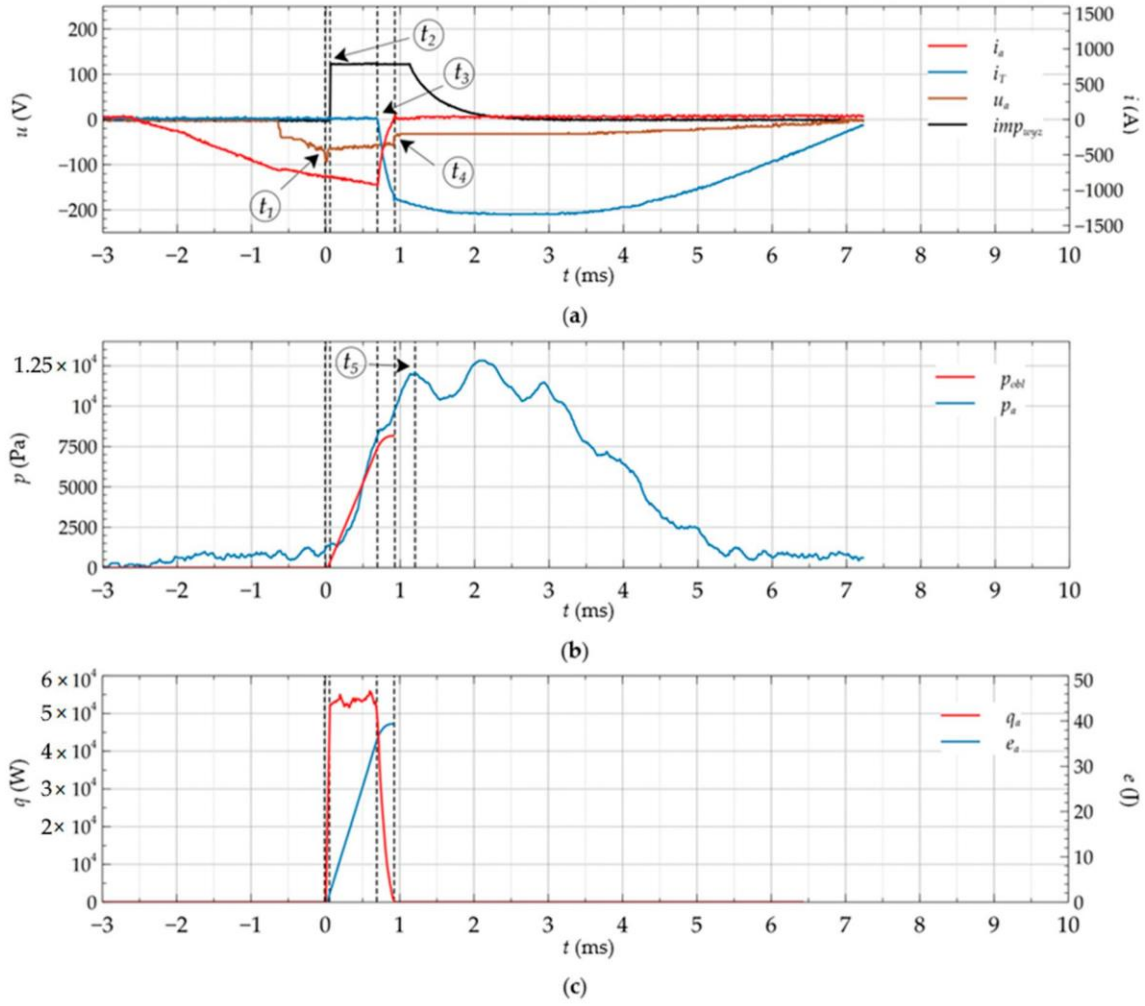

Figure 12. Waveforms as a function of the arc fault duration: (**a**) arc voltage u_a, current in the arc branch i_a, current in the MSAE i_T branches, arc flash detection pulse imp_{wyz}, (**b**) measured pressure pa and calculated P_{obl} inside the electrical junction box, (**c**) arc power q_a and arc energy e_a as a function of the arc disturbance duration.

The increase of the measured pressure Δp_a inside the closed casing of the junction box in the time from the moment of arc ignition (t_1 = 0 ms) to the complete taking over of the conduction by the bypass MSAE system (t_4 = 0.9 ms) is collinear with the increase of the calculated pressure value Δp_{obl}. When the conduction is fully taken over by the MSAE shunt, the measured pressure is p_a = 9.7 kPa, and the calculated pressure is p_{obl} = 8.1 kPa. The calculated pressure p_{obl} reaches 8.1 kPa and does not increase any further because the arc does not burn (the current in the arc branch does not flow, and thus the energy released in the arc is 0).

The short-term increase in pressure inside the electrical box while the arc is burning did not unseal it. The waveform presented in Figure 12b shows that the measured value of pressure pa continues to increase and reaches its maximum at 12.5 kPa despite the no longer burning electric arc. This increase may result from the heating of the air in the enclosure of the closed installation box, which is maintained by the heat dissipation of the heated copper arc electrodes, the walls of the enclosure, and the equipment. As a result, there was a slight open of the junction box, but it happened after the electric arc was extinguished. The power consumed from the mains, needed to sustain the burning arc,

reaches the value of 55 kW, and then when the MSAE is fully activated, it reduces its value to zero. The arc energy reaches its maximum at the level of 40 J and stops growing when MSAE is triggered because the arc does not burn.

The key frames of the disturbance recording in Figure 12 are shown in Figure 13. The tripping of MSAE significantly reduces the arc duration, which in turn reduces the arc energy and pressure inside the electrical box. No opening of the electrical box during arc ignition, shortening of the arc duration, reduction of arc energy causes:

- reduction of the loss of electrode material,
- limiting the temperature rise inside the switchgear,
- no emission of plasma, hot gases, smoke, and metal drops to the environment,
- no deafening sound wave.

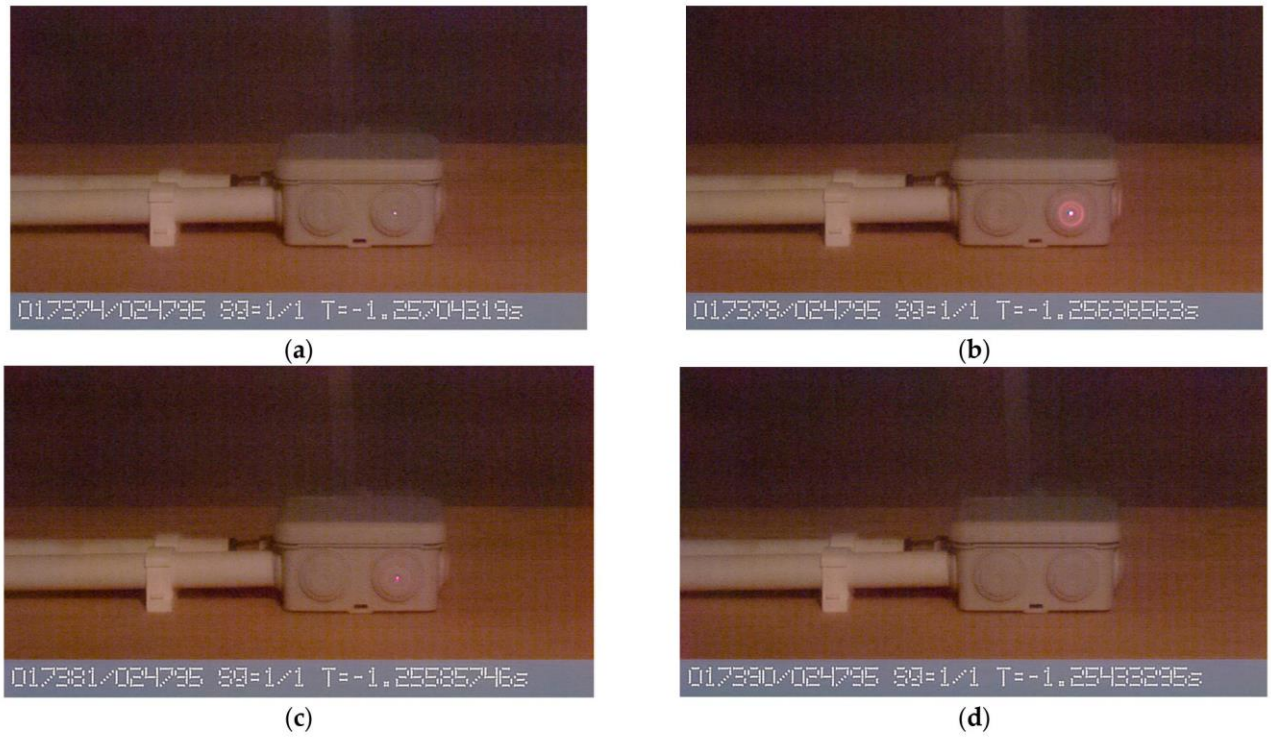

Figure 13. Images of the state of the installation box during an arc fault in a system equipped with an MSAE emergency arc eliminator: (**a**) t_1 = 0 ms electrcial arc initiation phase, (**b**) t_3 = 0.69 ms beginning of conduction through MSAE, (**c**) t_4 = 0.9 ms full conduction by MSAE, (**d**) t = 2.65 ms electrcial arc extinction phase (I_m = 1300 A, U = 230 V, Cu-Cu electrodes).

The junction box status images from Figure 13 recorded during an arc fault in a system equipped with an MSAE arc eliminator show in turn:

- at the moment t_1 = 0 ms the arc fault initiation phase,
- at the moment t_3 = 0.69 ms start of electric arc extinguishing by activation of MSAE. The energy emitted in the arc reaches its maximum, and in the photo, you can see intense illumination inside the installation box. The analysis of the recorded photos after time t_3 (MSAE on) shows that the intensity of the "glow" inside the installation box decreases considerably,
- at the time t_4 = 0.9 ms, MSAE is fully conducted, which forces the electric arc to extinguish. The shining point visible in the photo is not the effect of a burning electric arc, but the remnants of an exploding fuse material made of copper wire,
- the photo taken at the time t = 2.65 ms from the moment of initiation of the electric arc was registered during the flow of the maximum value of the supply current.

Full photographic recording of electric arc ignition in the system equipped with MSAE in Figure 13 is attached to this article in the form of a time-lapse movie [36]. It shows the recorded frames of the film from the moment of ignition of the electric arc, through the stage of MASE activation, to the complete extinction of the electric arc.

8. Calculation of the Hazard Risk Category

The effects of a burning arc depend on the value of the current and the duration of the arc disturbance. The arc burning time is directly related to the energy released in the electric arc. Reducing the arc fault time will reduce the arc energy and the amount of heat re-leased during arc burning. Reducing the arc fault time will also reduce the value of the electric current flowing in the arc circuit. The estimation of the basic energy parameters of the emergency arc enables to assess the degree of the hazard risk category, during the du-ration of the short circuit t_a.

On the basis of authors' experience, one of the most effective ways to reduce the effects of an electric arc flash is to reduce the arc burning time. In the work [25] and Section 7, the effectiveness of full MSAE activation within 0.9 ms from the appearance of the elec-tric arc was demonstrated. To calculate the hazard risk category, based on the Equations (1)–(3) caused by an electric arc according to IEEE 1584 [1,2,4,5], two variants based on actual measurement results were adopted. The first variant includes calculations and measurements for the facility without an MSAE system, which was presented in Section 6, the second one includes calculations for the MSAE protected system, which was presented in Section 7.

Assumptions for the conducted experiment:

- copper electrodes placed inside the installation electrical box,
- system supplied with 230 V single-phase voltage,
- arc current I_a [kA] (arcing current) read from the recorded waveforms,
- arc burning time t_a = 15.3 ms for a system without MSAE,
- arc burning time t_a = 0.9 ms when MSAE is activated,
- distance between parallel current paths in the analyzed circuit G = 3 mm,
- distance of the person's body from the source of the arc D = 50 mm—We assume that the person is in direct contact with the installation box (e.g., by performing checking activities),
- K_1 coefficient equal to −0.555 when the analyzed device is closed in sealed switchgear and −0.792 when the arc burns in an open space (the switchgear is opened),
- the exponent of distance x for an arc burning in an open space is 2 and 1.473 for an arc burning in a closed junction box.

Table 5 presents the results of calculations of the arc energy, fire zone, and hazard risk category for the experiment without MSAE (MSAE OFF) and in the system where MSAE was active (MSAE ON). The hazard risk category is directly related to the energy value of E (J/cm^2). In a situation where the facility is not MSAE equipped, the only way to reduce the risk is to increase the worker's distance from the source of the arc. The Arc Flash Hazard Assessment for the experiment presented in Section 6, assigned a category 1 to this disturbance.

Table 5. The results of calculating the arc energy, flash protection boundary, and hazard risk category for the experiment without MSAE (MSAE OFF) and in the system with MSAE (MSAE ON).

Type of Work	t_a (ms)	E_n (J/cm^2)	E (J/cm^2)	E (cal/cm^2)	D_B (mm)	HRC
MSAE OFF	15.3	0.22	16.02	3.83	89.52	1
MSAE ON	0.09	0.38	0.43	0.10	9.45	0

The designated hazard risk category 1 requires the use of personal protective equip-ment [1,2,4,5]:

- safety glasses,
- earplugs,
- protective helmet,
- helmet visor certified for min. 4 (cal/cm^2),
- leather safety shoes,
- leather gloves or leather gloves on electrical insulating gloves,
- underwear made of non-flammable materials,
- clothing (long trousers + long sleeve blouse or overalls) arc protection certified to min. 4 (cal/cm^2).

The boundary of the arc damage zone calculated from the Equation (4) is 89.52 mm. It means that a person within the assumed distance D = 50 mm is exposed to the direct effects of an electric arc.

Arc Flash Hazard Assessment in a system with an arc disturbance equipped with an MSAE device and described in Section 7, has shown that it falls under hazard category 0. The use of the MSAE arc eliminator shortens the arc time and thus reduces the arc flash hazard and significantly shortens the arc flash zone boundary to 9.45 mm. The safe operating distance of the device has increased almost tenfold, and the assumed working limit of the personnel D = 50 mm is five times safer than the permissible 9.45 mm.

Figure 14 shows in graphical form the dangerous extent of the arc discharge. The arc ignition occurs between two parallel conductors with the current. For a circuit not equipped with an MSAE, the range of the arc flash zone reaches almost 90 mm from the electric arc ignition point. Activation of the MSAE arc protection system reduces the range of the hazardous zone to 9.45 mm. The MSAE system has reduced the zone of possible arc flash hazard for technical personnel by 10 times.

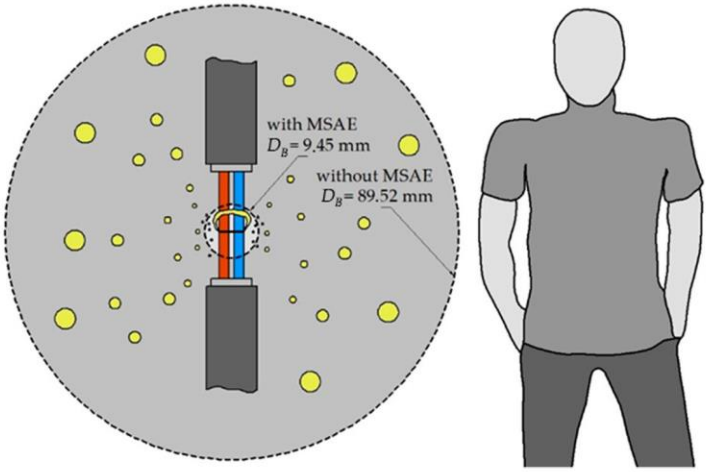

Figure 14. The emergency arc damage zone with MSAE (MSAE ON) and without MSAE (MSAE OFF).

The expected calculation parameters (according to IEEE 1584) and experimental parameters of the zones and hazard categories for the exemplary values of the arc current of 1.3/10/20 kA are presented in Table 6. For comparison with the previous calculations, the same assumptions were made:

- $C_f = 1.5$,
- $G = 3$ mm
- $K_1 = -0.792$,
- $x = 2$,
- D = 50 mm,
- three values of the arc current I_a = 1.3 kA /10 kA /20 kA were adopted,

- the duration of the arc hazard in the circuit without MASE is t_a = 100 ms and results from the own tripping times of the current breaker (CB),
- the arc hazard duration in the circuit equipped with MASE is t_a = 1 ms.

Table 6. The expected calculation parameters (according to IEEE 1584) of the FPB and hazard categories for the three arc current values.

t_a (s)	I_a = 1.3 kA				I_a = 10 kA				I_a = 20 kA			
	D_B (mm)		HRC		D_B (mm)		HRC		D_B (mm)		HRC	
	MSAE ON	MSAE OFF	MSAE ON	MSAE OFF	MSAE ON	MSAE OFF	MSAE ON	MSAE OFF	MSAE ON	MSAE OFF	MSAE ON	MSAE OFF
0.001	22.5	22.5	0	0	67.7	67.7	1	1	98.4	98.4	2	2
0.005		50.2		1		151.3		3		220.0		3
0.010		71.0		1		214.0		3		311.2		
0.020		100.4		2		302.6				440.1		
0.030		123.0		2		370.6				539.0		
0.040		142.0		3		427.9				622.4		
0.050		158.8		3		478.4				695.8		
0.060		174.0		3		524.1				762.3		
0.070		187.9		3		566.1				823.3		
0.080		200.9		3		605.2				880.2		
0.090		213.1		3		641.9				933.6		
0.100		224.6		3		676.6				984.07		
	NO ARC FAULT		NO ARC FAULT		NO ARC FAULT		NO ARC FAULT	DANGEROUS!	NO ARC FAULT		NO ARC FAULT	DANGEROUS!

The undoubted advantage of using MSAE is a significant reduction of the arc time. In the present work and the work [25], it was shown that for a resistive circuit this time can be about 1 ms. The fast tripping of the MSAE significantly reduces the energy released on the arc and thus reduces the dangerous hazard risk zone. Extending the burning time of the electric arc results in increased energy in the arc, and thus enlarges the danger zone for technical personnel.

The examples of arc flash zone and calculations of hazard risk category shown in Table 6 are intended to show the superiority of the application of the multi-sectional arc eliminator (MSAE) over the traditional time-delayed circuit breaker. The long actuation time of commonly used safety devices (to 100 ms), in many cases causes the arc energy to increase to values that threaten human life. The energy values are assigned to the appropriate categories from 0 to 4. Category 0 allows working in the vicinity of an arc fault with basic personal protection. A category increase above a value of 4 categorically prevents work in the vicinity of the arc (DANGEROUS in Table 6). In this case, the use of personal protective equipment will not adequately protect personnel from the undesirable effects of the energy released from the arc. That is why it is so important to strive to minimize the Hazard Risk Category HRC. The use of MSAE meets this requirement (reduces HRC), which significantly increases the safety of technical personnel who may be exposed to the effects of an electric arc. The use of MSAE also protects the components of the switchgear in which the electric arc was started.

The calculation results presented in Table 6 were made in accordance with the "IEEE 1584 Guide for Performing Arc-Flash Hazard Calculations" [1–5] and the assumptions adopted in this study. The example for 1.3 kA current has been experimentally verified and its results are described above.

Analysing the calculated and presented values in Table 6, it can be noticed that for the assumed current values from 1.3 kA to 20 kA, the use of MSAE (i.e., activation of the arc eliminator protection during 1 ms) significantly reduces the hazard category. Such a time of reaction MSAE operation, which for resistive circuits is shorter than 1 ms, in many cases will significantly reduce damage inside the switchgear in which the arc fault occurred and may even save human health or life. For the currents of 10 kA and 20 kA, and a circuit not equipped with MSAE, the developing arc disturbance in time causes a significant increase

of the arc energy to values exceeding the data of the category table. With energy above 40 cal/cm^2 (category 4), the presence of technical personnel in the area of the device in which the electric arc was ignited is prohibited. For the same values of currents and the circuit protected by the MSAE system, the arc energy is limited, and the value of the hazard category (1 for I_a = 10 kA and 2 for I_a = 20 kA respectively) allows to select of appropriate protective clothing and to designate a safe zone outside the arc zone.

Figure 15 shows the characteristics of flash protection boundary D_B as a function of the arc fault duration ta for the different current values. The calculation results from Table 3 have been presented in Figure 15 in such a way that the differences in the application of the MSAE system can be easily noticed. The curves marked with a dashed line refer to the system in which the arc fault develops for 100 ms until the main breaker is tripped. The same colour (solid line), for easy comparison, shows the range of the dangerous shock zone for the circuit protected with the MSAE system.

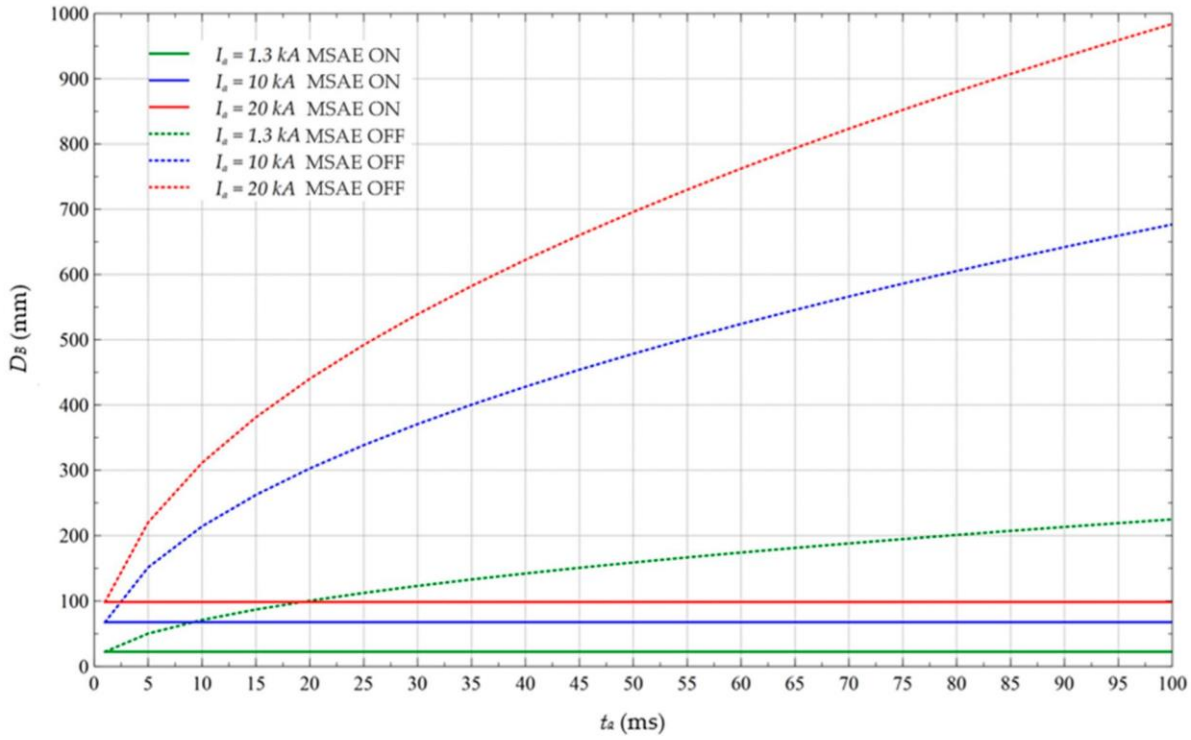

Figure 15. Characteristics of the arc flash boundary as a function of the duration of the arc disturbance for different values of the current in the circuit with the MSAE system and its absence.

When analysing Figure 15, it is important to note that triggering the MSAE in approximately 1 ms causes the arc to be extinguished. Eliminating the arc so quickly does not increase the energy and reduces the hazard risk.

9. Conclusions

The subject of the current publication and the research described in it are the results of experiments to check the effectiveness of the semiconductor module used as an electric arc eliminator. The author's project is a device enabling very quick shunting of the electric circuit affected by the arc disturbance, to create an alternative—a privileged path for the current flow. The result of this is a very fast elimination of the arisen electric arc and reduction of possible damage resulting from the developing arc disturbance.

Experimental studies presented in works [25,26] showed that in circuits affected by an arc fault, sections of anti-parallel connected thyristors working as an electric arc eliminator extinguish the arc in less than 1 ms. Reducing the duration of the arc fault significantly

reduces the amount of energy released in the arc, resulting in a reduction of the gas pressure inside the affected switchgear. The energy reduction also significantly reduces the loss of material from the arc electrodes, and thus reduces the risk of burns to people in the vicinity of the electric arc. The results of tests and calculations confirm the effectiveness of the thyristor system as an electric arc eliminator.

The experiments carried out in similar conditions for a system without MSAE and equipped with MSAE protection clearly showed the advantages of using thyristor branches as arc protection. The arc burning time from 15.3 ms in the system without MSAE was reduced to 0.9 ms, which gives the ratio t_{MSAE_OFF}/t_{MSAE_ON} = 17. The arc energy of 3.83 cal/cm^2 by reducing the arc time decreased to a value of 0.1 cal/cm^2. By reducing the energy by 38 times, the risk of injury from a burning arc is reduced and consequently, the hazard risk category is reduced to level 0. The use of MSAE reduced the arc range by more than 9 times, from 89.52 mm to 9.45 mm.

The values unmeasured in this work are the loss of electrodes of the arc source and the intensity of the emitted sound. Arc flares and the shipment of the electrode material droplets were recorded with a high-speed camera. In the case of many experiments, the heated remains of the electrode material are visible in the recorded photos after more than 0.5 s from the moment the arc is extinguished. After such a long time, burn marks at the base of the junction box were observed. As a result, a fire may start for surrounding materials and a flammable substrate. The triggering of the MSAE usually extinguishes the arc in less than 1 ms, which limits the loss of material from the arc source electrodes and prevents possible fires. Due to the lack of a measuring device, no reduction in the sound intensity level was recorded. These measurements will be presented in the next paper. However, the authors wish to share the information that the experiments in the system without MSAE had to be performed wearing protective earmuffs, while in the system with MSAE the sound accompanying the arc discharge, within the range of test currents used, did not occur inside the tested object.

The results of the tests of the Multi-Section Arc Eliminator (MSAE), presented in this article and in [25,26], confirm the undoubted advantages of using the system as a quick eliminator of the electric arc. The conducted experiments and the obtained results confirm this. The challenges that the authors set themselves are further tests of the MSAE operation for gradually increasing values of the current in the circuit. The test capabilities available to the authors are about 50 kA/50 Hz AC. In the final version, the MSAE system will cooperate with a mechanical short-circuiting switch, which in effect will constitute a hybrid short-circuiting switch. At the moment of detecting a disturbance with an electric arc, the semiconductor part of the hybrid short-circuiting switch takes over the current flow and allows time to close the contacts of the mechanical switch. A small voltage drop across the conductive sections of the MSAE will allow for arc-free closing of the high-current contacts of mechanical short-circuiting switch.

Author Contributions: Conceptualization, K.N. and J.J.; methodology, K.N. and J.J.; formal analysis, K.N., J.J. and G.D.; investigation, K.N. and J.J.; resources, K.N.; writing—original draft preparation, K.N., J.J. and G.D.; writing—review and editing, K.N., J.J. and G.D.; visualization, K.N.; supervision, K.N. and J.J. All authors have read and agreed to the published version of the manuscript.

Funding: This research was funded by the Polish Ministry of Science and Higher Education, grant number 0711/SBAD/4454.

Institutional Review Board Statement: Not applicable.

Informed Consent Statement: Not applicable.

Data Availability Statement: Not applicable.

Conflicts of Interest: The authors declare no conflict of interest.

References

1. IEEE. *IEEE Guide for Performing Arc-Flash Hazard Calculations*; IEEE Std 1584-2018 (Revision of IEEE Std 1584-2002); IEEE: New York, NY, USA, 2018; pp. 1–134. [CrossRef]
2. IEEE 1584-2018—IEEE Guide for Performing Arc-Flash Hazard Calculations. Available online: https://standards.ieee.org/standard/1584-2018.html (accessed on 17 January 2021).
3. Lippert, K.J.; Colaberardino, D.M.; Kimblin, C.W. Understanding IEEE 1584 arc flash calculations. *IEEE Ind. Appl. Mag.* **2005**, *11*, 69–75. [CrossRef]
4. Mohla, D.; Lee, W.; Phillips, J.; Marroquin, A. Introduction to IEEE Standard. 1584 IEEE Guide for Performing Arc-Flash Hazard Calculations—2018 Edition. In Proceedings of the 2019 IEEE Petroleum and Chemical Industry Committee Conference (PCIC), Vancouver, BC, Canada, 8–12 September 2019; pp. 1–12.
5. Mohla, D.; Lee, W.-J.; Phillips, J.; Marroquin, A. Introduction to IEEE Standard 1584: Guide for Performing Arc-Flash Hazard Calculations, 2018 Edition. *IEEE Ind. Appl. Mag.* **2020**, *26*, 64–76. [CrossRef]
6. Mohamed Abd Elwahab Ali_Lecture 07. IEEE 1584 Arc Flash Calculations.Pdf | Electric Arc | Electric Current. Available online: https://www.scribd.com/document/371508361/mohamed-abd-elwahab-ali-Lecture-07-IEEE-1584-Arc-Flash-Calculations-pdf (accessed on 17 January 2021).
7. IEEE 1584 Arc Flash Calculations—Electrical Diagnostic Surveys. Available online: https://arcflashtraining.net/ieee-1584-arc-flash-calculations/ (accessed on 17 January 2021).
8. Majd, A.; Luo, R.; Devadass, M.A.; Phillips, J. Comprehensive Overview and Comparison of ANSI Versus IEC Short-Circuit Calculations: Using IEC Short-Circuit Results in IEEE 1584 Arc Flash Calculations. *IEEE Trans. Ind. Appl.* **2019**, *55*, 5487–5493. [CrossRef]
9. Electrical Arc Flash Hazard Management Guideline. Available online: https://www.energycouncil.com.au/media/15808/eafhm_guideline_30_25-03-2019_web.pdf (accessed on 17 January 2021).
10. Simms, J.; Johnson, G. Protective Relaying Methods for Reducing Arc Flash Energy. *IEEE Trans. Ind. Appl.* **2013**, *49*, 803–813. [CrossRef]
11. Doan, D.R.; Sweigart, R.A. A summary of arc flash energy calculations. In Proceedings of the Record of Conference Papers. Industry Applications Society. Forty-Ninth Annual Conference. 2002 Petroleum and Chemical Industry Technical Conference, New Orleans, LA, USA, 23–25 September 2002; pp. 285–290.
12. Kazimierczak, M. ARC Faults: Operational Experiences in Industrial and Utility Power Plants. *Elektroenerg. Współczesność Rozw.* **2011**, *2*, 98–109.
13. Ventruella, D.J. Arc flash hazard—When over-estimating under-estimates a problem. In Proceedings of the 2017 Annual Pulp, Paper and Forest Industries Technical Conference (PPFIC), Tacoma, WA, USA, 18–23 June 2017; pp. 1–8.
14. Ventruella, D.J. Arc Flash Hazard—When Overestimating Underestimates a Problem. *IEEE Trans. Ind. Appl.* **2019**, *55*, 3287–3293. [CrossRef]
15. Lu, Q.; Ye, Z.; Zhang, Y.; Wang, T.; Gao, Z. Analysis of the Effects of Arc Volt–Ampere Characteristics on Different Loads and Detection Methods of Series Arc Faults. *Energies* **2019**, *12*, 323. [CrossRef]
16. Yin, Z.; Wang, L.; Zhang, Y.; Gao, Y. A Novel Arc Fault Detection Method Integrated Random Forest, Improved Multi-scale Permutation Entropy and Wavelet Packet Transform. *Electronics* **2019**, *8*, 396. [CrossRef]
17. Paul, S.; Jewell, W. Optimization Methodology for Minimizing the Arc Flash Incident Energy. In Proceedings of the 2018 IEEE Industry Applications Society Annual Meeting (IAS), Portland, OR, USA, 23–27 September 2018; p. 6.
18. Wu, H.; Li, X.; Stade, D.; Schau, H. Arc Fault Model for Low-Voltage AC Systems. *IEEE Trans. Power Deliv.* **2005**, *20*, 1204–1205. [CrossRef]
19. Kumar, P.; Kale, A.; Ranade, M. Internal arc fault simulation using CFD to predict thermal behavior in switchgear. In Proceedings of the 2017 6th International Conference on Computer Applications in Electrical Engineering-Recent Advances (CERA), Roorkee, India, 5–7 October 2017; pp. 236–241.
20. Short, T.A.; Eblen, M.L. Medium-Voltage Arc Flash in Open Air and Padmounted Equipment. *IEEE Trans. Ind. Appl.* **2012**, *48*, 245–253. [CrossRef]
21. Roscoe, G.; Valdes, M.E.; Luna, R. Methods for arc-flash detection in electrical equipment. In Proceedings of the 2010 Record of Conference Papers Industry Applications Society 57th Annual Petroleum and Chemical Industry Conference (PCIC), San Antonio, TX, USA, 20–22 September 2010; pp. 1–8.
22. Kumpulainen, L.; Hussain, G.A.; Rival, M.; Lehtonen, M.; Kauhaniemi, K. Aspects of arc-flash protection and prediction. *Electr. Power Syst. Res.* **2014**, *116*, 77–86. [CrossRef]
23. Catlett, R.; Lang, M.; Scala, S. Novel Approach to Arc Flash Mitigation for Low-Voltage Equipment. *IEEE Trans. Ind. Appl.* **2016**, *52*, 5262–5270. [CrossRef]
24. Hussain, G.A. *Methods for Arc-Flash Prediction in Medium Voltage and Low Voltage Switchgear*; Aalto University: Espoo, Finland, 2015; ISBN 978-952-60-6599-1.
25. Nowak, K.; Janiszewski, J.; Dombek, G. A Multi-Sectional Arc Eliminator for Protection of Low Voltage Electrical Equipment. *Energies* **2020**, *13*, 605. [CrossRef]
26. Nowak, K.; Janiszewski, J.; Dombek, G. Thyristor Arc Eliminator for Protection of Low Voltage Electrical Equipment. *Energies* **2019**, *12*, 2749. [CrossRef]

27. Wu, H.; Li, X. Calculation of Maximum Arc Energy for Low Voltage Power Systems. In Proceedings of the 2006 IEEE PES Power Systems Conference and Exposition, Atlanta, GA, USA, 29 October–1 November 2006; pp. 1627–1630.
28. Gammon, T.; Matthews, J. Conventional and recommended arc power and energy calculations and arc damage assessment. *IEEE Trans. Ind. Appl.* **2003**, *39*, 594–599. [CrossRef]
29. Anantavanich, K.; Pietsch, G.J. Calculation of Pressure Rise in Electrical Installations Due to Internal Arcing Taking into Account Arc Energy Absorbers. *IEEE Trans. Power Deliv.* **2016**, *31*, 1618–1626. [CrossRef]
30. Low Voltage Circuit Breakers "Arc Flash Hazards" ABB. Available online: https://electrical-engineering-portal.com/res/LV-Arc-Flash-Paper.pdf (accessed on 10 February 2021).
31. Keller Series 21 G Piezoresistive Pressure Transmitters. Available online: http://www.keller-druck.com.pl/produkty/przetworniki/pdf/21g_karta.pdf (accessed on 17 January 2021).
32. Kulas, S.J.; Supronowicz, H. Analiza łuku elektrycznego awaryjnego i sposoby ograniczania jego skutków. *Mech. Autom. Górnictwa* **2014**, *52*, 43–49.
33. High-Speed Camera Chronos 1.4—Datasheet. Available online: https://www.krontech.ca/wp-content/uploads/2019/03/FM-ENGR-50001-Chronos-1.4-Datasheet-Rv4-1.pdf (accessed on 10 February 2021).
34. Nowak, K. Photographic Registration of the Effects of the Emergency Arc in the Electrical Junction Box. Available online: https://chmura.put.poznan.pl/s/6SkIxmyG6uGYEy6 (accessed on 4 February 2021).
35. Nowak, K. Photographic Registration of Recording the Effects of an Emergency Arc from Its Ignition to the almost Complete Extinction of the Exploding, Glowing Remains of Drops of Electrode Material. Available online: https://chmura.put.poznan.pl/s/bcENdNAktD2svbJ (accessed on 4 February 2021).
36. Nowak, K. Photographic Registration of the State of the Electrical Box during an Arc Fault in a System Equipped with an MSAE Emergency Arc Eliminator. Available online: https://chmura.put.poznan.pl/s/4YYSGRYzPjuefee (accessed on 4 February 2021).

Publikacja IV

Karol Nowak, Jerzy Janiszewski, Grzegorz Dombek: „A New Short-Circuit Hybrid Device for the Protection of Low-Voltage Networks From the Effects of an Arc Fault". *IEEE Access 2022*, vol. 10, pp. 88678-88691;
https://doi.org/10.1109/ACCESS.2022.3199011

IEEE Access
Multidisciplinary | Rapid Review | Open Access Journal

Received 29 June 2022, accepted 30 July 2022, date of publication 16 August 2022, date of current version 29 August 2022.

Digital Object Identifier 10.1109/ACCESS.2022.3199011

RESEARCH ARTICLE

A New Short-Circuit Hybrid Device for the Protection of Low-Voltage Networks From the Effects of an Arc Fault

KAROL NOWAK, JERZY JANISZEWSKI, AND GRZEGORZ DOMBEK
Institute of Electric Power Engineering, Poznan University of Technology, 60-965 Poznan, Poland
Corresponding author: Karol Nowak (karol.nowak@put.poznan.pl)

This work was supported by the Poznan University of Technology under Grant 0711/SBAD/4560.

ABSTRACT A high-current electric arc inside an electrical switchgear can be a source of danger to electrical equipment and technical personnel. The article shows that the use of hybrid connectors as an arc eliminator significantly shortens the time of electric arc burning, and as a result reduces the electric arc energy. As a result, an effective device was obtained to protect low-voltage networks against the effects of short-circuit or arc fault, such as sudden increase in temperature, gas pressure, high-intensity sound wave, equipment destruction, material erosion of power rails, ejection hot debris and molten metal particles in all directions. Inside the closed switchgear, the proposed arc eliminator solution will significantly reduce the build-up of pressure and temperature.

INDEX TERMS Arc fault, short-circuit current, arc eliminator, effects of arc.

I. INTRODUCTION

In recent years, many designers of electrical power devices have paid great attention to the issue of safety in electrical assemblies, in relation to one of the most serious and destructive electro-physical phenomena, which is an electric arc [1].

Arc ignition causes the release of a huge amount of incident energy and its subsequent development, the creation of large pressure increases in the vicinity of the electric arc (e.g., inside metal-enclosed switchgear and control gear), and local temperature increases, which can cause high mechanical and thermal stresses in the device [2]. This happens when the voltage between two points exceeds the limit of the isolation strength (e.g., SF6 gas) [3]. Under favorable conditions, a plasma is formed between the conductive elements (electrodes), which conducts electric current until the protective device on the supply side is triggered.

The causes of electrical arc accidents are varied. The most common are human errors, bad connections, incorrectly selected devices, incorrectly designed power devices, lack of inspections and maintenance, aging and corrosion of insulating materials, overvoltage's, or even indirect participation of animals [4], [5]. One of the most common and dangerous accidents related to an electric arc occurs when maintenance workers are working on the maintenance or installation of equipment on an electrical switchboard [6]. This usually takes place with the door to the switch cabinet open. Since the cabinet door is open, the arc-proof structure of the switchgear cannot fulfil its task. Therefore, the use of a different arc protection system is a necessity for a modern switchgear design.

In the vicinity of electrical switchboards, large electrical machines, transformers or generators, there is a high short-circuit power, and thus also the incident energy associated with the electric arc resulting from the disturbance. How dangerous it is to stay in the vicinity of an electric arc can be illustrated by examples [7], [8], [9], [10]:

- pressure – it is estimated that a person standing at a distance of 0.6 (m) from the electric arc burning with the flow of 20 kA current is subjected to the force of 2206 (N), i.e., about 225 (kG),
- temperature – the arc environment can reach temperatures up to 2000 °C,

The associate editor coordinating the review of this manuscript and approving it for publication was Bernardo Tellini.

- arc movement speed – for currents in the range 15-20 (kA), the average speed of the arc movement along copper bars is from 200 to 250 ($m \cdot s^{-1}$),
- sound – the sound intensity level can reach even 160 (dB).

The electric arc can create dangerous hazards for people in its vicinity. Examples of effects resulting from the release of the huge amount of energy generated by the arc are [11], [12]:

- inhalation of toxic gases – vapors arise as a result of burning insulation materials or evaporation of structural elements of the apparatus and are formed by carbon particles suspended in the air and other solid substances, creating a dangerous gas cloud,
- burns of the body – are caused by the high temperature level of gases and ejected glowing material particles. Skin burns may also occur as a result of damaged protective clothing, which, while burning, may stick to the skin and cause dangerous burns.
- eye damage – the cause of the damage is ultraviolet and infrared radiation and high intensity of visible light,
- injuries caused by ejection of materials – arise as a result of damage to electrical apparatus and the ejection of elements from damaged electrical devices,
- hearing damage – occurs as a result of an increase in peak sound pressure (even up to 160 (dB)).

The impact of an arcing incident depends on the energy of the disturbance. The energy arc released depends on the voltage, current and duration of the arc fault, as well as the distance to the source of the arc. Most arc faults start as single-phase faults and then develop into three-phase faults, resulting in a significant increase in the energy released.

Practical principles of protection consist in increasing the distance from the arc or providing a mechanical barrier between the operator and the arc, reducing the disturbance duration, or reducing the arc current [13], [14], [15]. Safety of technical workers and the electrical installation itself, in the event of arcing inside the LV switchgear, can be achieved by using passive protection or active protection [16].

Passive risk reduction measures include personal protective equipment, pull-out devices, and arc-proof switchgear with pressure-reducing devices. From a safety point of view, the arc-proof switchgear provides protection to personnel as long as the switchgear door is closed. If the switchgear door is opened, as is typical during maintenance or commissioning, then there will be no protection against injury [17].

Active protection consists in limiting the short-circuit (arc) current or limiting the duration of the arc discharge. The current limitation at the fault location can be achieved by selecting transformers with higher impedance or by using current limiting chokes. The biggest disadvantage of such protection is the increased production cost and energy losses. Fuses are a more widely used method that provides not only current limitation, but also rapid elimination of the fault. A major disadvantage of current-limiting fuses is that their speed of operation depends on the value of the flowing current. A burning arc at rated currents can cause a significant increase in the tripping time of the fuse [18] or even its inactivity at rated currents. An advantageous solution from the point of view of the power circuit is an arc-time limiting method [19]. The use of the hybrid arc eliminator results in practically immediate elimination of the emergency arc in the affected circuit [20], [21], [22], [23].

The aim of the work is to present the possibility of using an innovative proprietary hybrid switch, which, in cooperation with sensors of electric arc detection, can be successfully used to work as a high-current electric arc eliminator (AE). The presented solution is an active protective system that is used to limit the effects resulting from the ignition of an electric arc.

II. OPTICAL DETECTION OF THE ELECTRIC ARC

A common parameter for each of the methods of protection against the effects of short-circuit current or the appearance of an electric arc is the time to remove the disturbance. Fig. 1 shows the arc incident energy levels of different protection method (calculated in accordance with IEEE Standard 1584 TM-2018) [24] depending on the time of failure removal.

The fastest arc detection is based on light detection. According to [25], the development of the arc can be traced directly by observing the intensity of the light. Light-sensitive flash detectors can detect the arc even from extraneous light sources of low power, which may cause undesirable switching on the short-circuiting section. To eliminate this inconvenience, in addition to lighting conditions, in most applications it is also required to detect voltage drop in the supply network and measure changes in the flowing current. The circuit breaker tripping can then be initiated within a few milliseconds [26].

When using integrated systems, the arc detector together with the circuit breaker (CB), the longest delay in arc protection is due to the trip time of the circuit breaker [27]. Maximum protection against the effects of burning arc can be achieved with arc eliminators (AE). Instead of interrupting the flow of short-circuit current with a delayed circuit breaker, these devices cause a deliberate short-circuit of the circuit above the affected arc fault location, extinguishing the arc in the shortest possible time.

The arc protection solutions based on light flash detection, voltage drop, and current measurement known from literature and industry [28], [29], [30], show that the total arc burning time consists of the fault detection time (0.5-15 (ms)) and the circuit breaker operation time (typically 50-80 (ms) for LV networks). In many situations, this time is too long to limit the destructive effects of the arc (e.g. an increase in temperature or pressure inside the switchgear) [7], [31]. The experimental studies presented, among others, in [20] show that even in difficult switching conditions, the use of the solution proposed by the authors, i.e., a hybrid arc eliminator, will allow to extinguish the electric arc in less than about 0.7 (ms), and consequently the importance of reducing the dangerous effects associated with an electric arc explosion. In addition to the speed of activation, the undoubted advantage of this

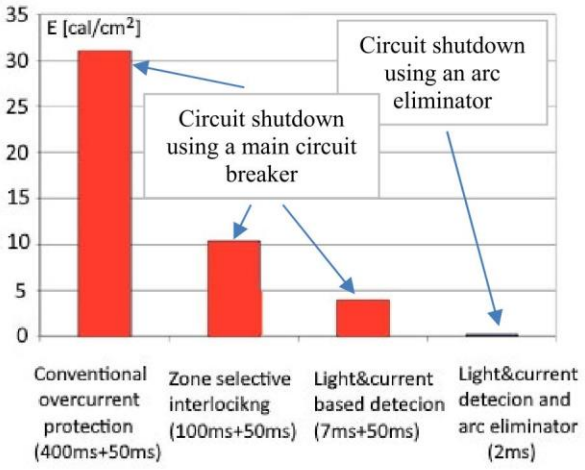

FIGURE 1. Examples of electric arc energy values for selected arc protection methods and various methods of electric arc detection [15].

solution is the possibility of activating the protection even with the door of the electrical switchgear open.

III. SHORT-CIRCUITTING SWITCH TO LIMIT SHORT-CIRCUIT EFFECTS

A. THE IDEA OF ACTION

In the pictorial block diagram of the use of a hybrid short-circuiting switch as an electric arc eliminator (AE) presented in Fig. 2 includes the most important components. The place of disturbance, at the moment of detection of an electric arc flash and measurement of the voltage drop in the supply network, is bypassed by virtually instantaneously switched-on system consisting of anti-parallel connected thyristors and a slow mechanical switch. As a result, the fault current flows through the hybrid switch, bypassing the part of the electrical network affected by the arc fault. This state continues until the entire circuit is switched off by the mains switch CB (Fig.2).

The main advantage of the semiconductor part of the hybrid switch is that the voltage drop on the conducting thyristors is smaller than the burning electric arc voltage, which in turn causes the electric arc to be extinguished. Delay closure of the high-current mechanical short-circuiting switch relieves the conductive thyristors and takes over the flow of the bypass current until the main circuit breaker is actuated. A small voltage drop on the conductive thyristors enables without arc closure of the contacts of the mechanical connector, thus limiting damage to the surface of its contacts.

The main difficulties faced by the authors were the appropriate and precisely planned control of multiple semiconductors (thyristors). For this purpose, a specialized microprocessor device has been developed. The microprocessor-based control system is designed to cooperate with arc detection systems, supply voltage zero detection, and determination of polarization of the flowing current. Precise determination of the polarization of the flowing current and its beginning of flow, enables both advanced control of the thyristor cascade triggering (including optimization and uniformity of the load of individual thyristor sections) and the activation time of the mechanical switch (at the lowest conduction voltage of semiconductor branches). The thyristor triggering system is galvanically separated from the control system. The use of semiconductor opto-isolators gives a high speed of response of thyristor blocks to control signals. In the remainder of this work, all items in Fig. 2 will be referred to as microprocessor control [32].

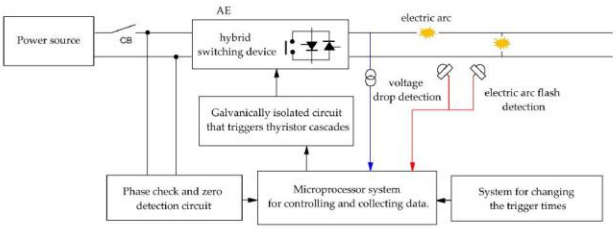

FIGURE 2. Block diagram of the use of a hybrid switching device as an electric arc eliminator (AE).

B. STRUCTURAL SOLUTION

Fig. 3 shows a schematic of the author's solution of a hybrid arc eliminator designed for single-phase powered circuits.

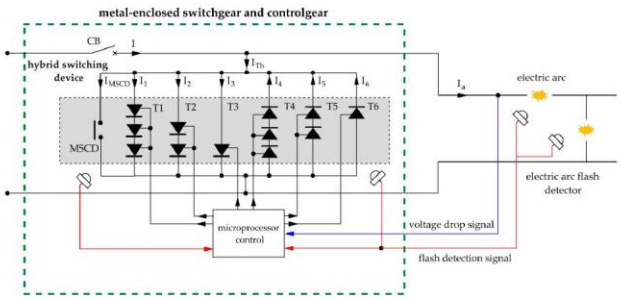

FIGURE 3. Practical solution of the arc eliminator (AE) built with a hybrid short-circuiting switch.

The scheme shown is a configuration of a multi-section hybrid arcing eliminator with one mechanism section and six thyristor sections, designated T1, T2, T3, and T4, T5, T6, switched on for positive or negative polarity of the flowing current, respectively. For each current polarization, the individual semiconductor shunt branches consist of a decreasing number of serially connected thyristors. The task of the series connected thyristors in the higher-order shunt branches is to maintain (in their conduction state) a voltage drop sufficient to drive the elements of the lower-order section. The activation of the hybrid switching device takes place in the first place by controlling the branch with the largest number of thyristors connected in series (T1 for positive polarization or T4 for negative polarization). Next, successive parallel branches are activated with a decreasing number of serially connected thyristors (T2 and T3 for positive polarization or T5 and T6 for negative polarization). The MSCD (mechanical short-circuiting device) branch of the mechanical

short-circuiting device is the last to close. The condition for taking the current conduction through the successive branches of the semiconductor shunt and the branch of the mechanical switch is appropriate control of the thyristor gates and the drive that releases the mechanism of closing the contacts of the mechanical switch.

The hybrid short-circuiting switching system, presented in Fig. 3, is equipped with DCR1910F14-1974 thyristors (Dynex Semiconductor) and ZZC-15 mechanical switch. The continuous on-state current I_T for a single thyristor is 2700 (A), while the surge (non repetitive) on-state current I_{TSM} is 30 kA. The mechanical short-circuit device has a switching capacity of 30 (kA). Due to the permissible current values of the elements of the hybrid short-circuit switch and for safety reasons (dangerous arcing effects), the value of the arc fault current amplitude has been limited to 30 (kA).

C. PRINCIPLE OF OPERATION

Fig. 4a and 4b show the current waveforms and the triggering pulses of the thyristors and the short-circuiting mechanical switch for a multisection hybrid short-circuiting switch. For example, if the detected initial fault current polarity is positive, the switching of individual elements of the semiconductor cascade takes place in the order T1, T2, T3 and then T4, T5, T6 (for Fig. 4a) or T4, T5, MSCD (for Fig. 4b). This corresponds to the conducted currents i_1, i_2, i_3 in sequence, then i_4, i_5, i_6 (or i_4, i_5 and i_{MSCD}). The task of such control is to flow the fault current through the semiconductor circuit for the time necessary to close the contacts of the MSCD. In this way, practically instantaneous tripping of the hybrid short-circuiting switch was achieved, successive relieving of its semiconductor actuators and final, arc-free current transfer by a mechanical switch with practically negligible transition resistance.

The waveforms presented in Fig. 4a refer to the case when the closing time of the mechanical closing contacts is long (more than 20 (ms)). The individual thyristor sections conduct until the actuation of a mechanical short-circuit device, whose own closing time for the considered course is equal to two periods of current flow or actuation of the main switch. Fig. 4b shows the waveforms of the currents both in the semiconductor part and after the contacts are closed in the mechanical short-circuit device (MSCD).

Fig. 5 shows the real-time waveforms of currents and voltages recorded in a circuit with an emergency arc, protected by the installation of a multi-sectional arc eliminator (MSAE).

Fig. 5a shows the recorded current waveform of the source i and the current waveform in the branch affected by the arc disturbance i_a. For the purposes of this presentation, in the presented case, the operation of the arc eliminator has been deliberately delayed to clearly show the current in the arc branch. Delayed activation of the arc eliminator by 1.2 (ms) caused the increase in the arc current to the value of 8 kA. It should be noted, however, that the actual operation time of the arc eliminator can be much shorter, and for resistive loads it can be as much as 0.32 (ms), as shown in [20]. Fig. 5b shows

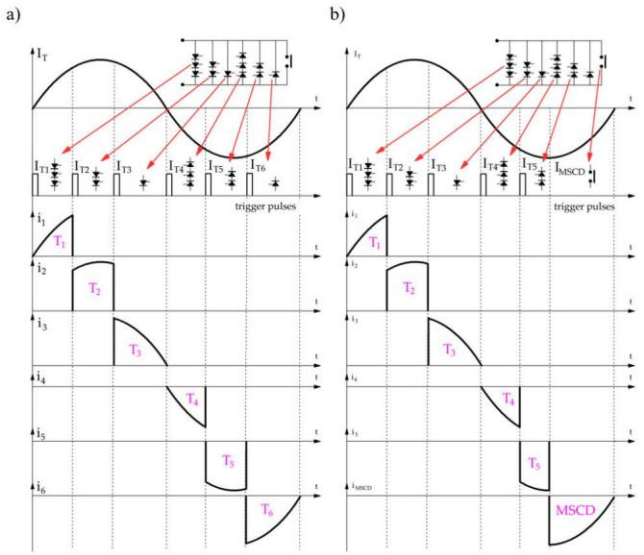

FIGURE 4. Time waveforms of currents, triggering pulses of thyristors and mechanical short-circuit device in the hybrid short-circuiting system shown in figure 3; a) the instantaneous values of the currents in the semiconductor branches of the arc eliminator, b) instantaneous values of the currents flowing through the thyristor sections and the mechanical short-circuit device (MSCD).

the current waveform in the branch of the i_{MSCD} mechanical short-circuit device and the voltage waveform u_a, which in the initial phase is the burning arc voltage. After the arc is extinguished (time 1.2 (ms)), the u_a waveform represents the voltage on the conducting thyristors, and in the final phase (after their switching off), the voltage on the contacts of the mechanical short-circuiting switch. The applied mechanical switcher is characterized by a relatively short activation time (about 18 (ms)), but also by unwanted contact bounce. At time $t = 13$ (ms), the mechanical switch contacts are closed for the first time. From then on, it takes over the flow of electricity. The voltage at its contacts is close to zero, which prevents the thyristors of the hybrid switch from triggering. After about 1 (ms), the switch contact bounces (reopening). One of the thyristor sections begins to conduct immediately, which causes the continuous flow of current through the hybrid short-circuiting switch, which prevents the electric arc from being started. At time t=18 (ms), the second and final closing of the mechanical switch contacts takes place and the last of the conducting branches of the thyristors is turned off. From this point on, the mechanical switch conducts the current until the contacts of the main circuit breaker (CB) are open. Fig. 5c shows the conduction currents of successive thyristor branches for the positive half-wave of the flowing current. Switching on individual elements of the semiconductor cascade (T1, T2, T3) enables the sequential acquisition of current by these cascades, which is shown in Fig. 5c by the waveforms i_1, i_2, and i_3. Similarly, Fig. 5d shows the conduction currents (i_4, i_5) of successive thyristor branches (T4, T5) and the mechanical short-circuit device (MSCD) for the negative half-wave of the flowing current i_{MSCD}. The lack

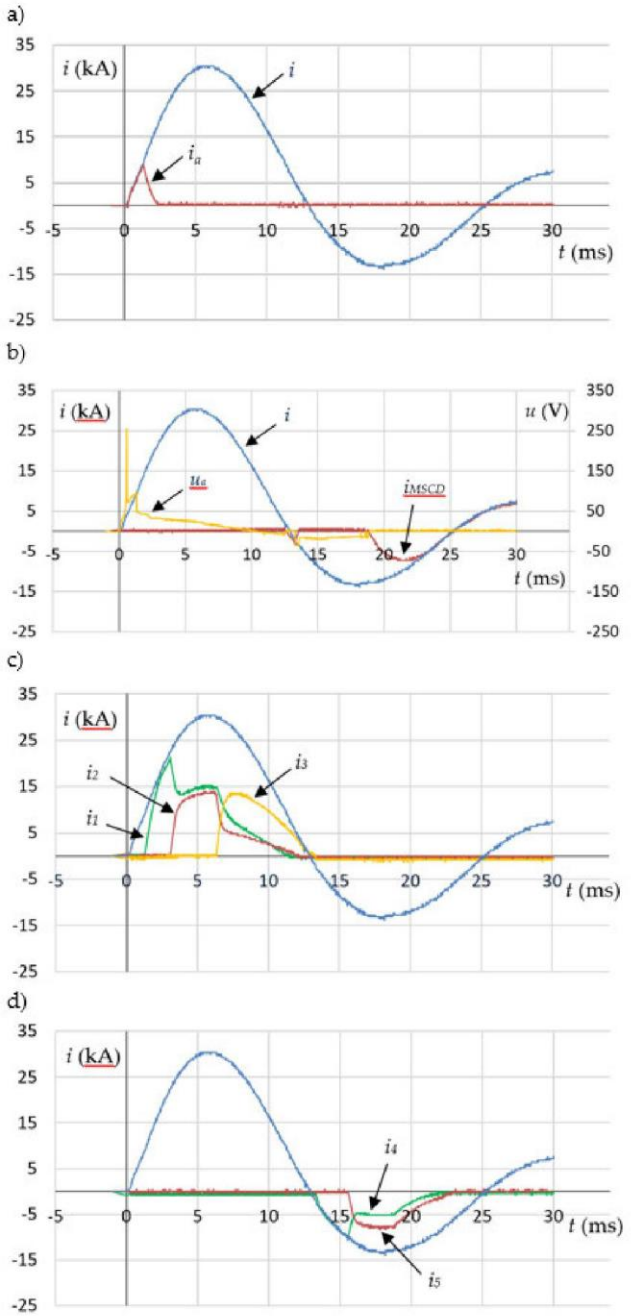

FIGURE 5. Time courses of currents and voltages in a three-section hybrid short-circuit device; a) source current, arc current, b) MSCD current, arc voltage, c) currents in the branches of thyristors for a positive current half-wave, d) currents in the branches of thyristors for negative half-wave current.

of the current waveform i_6 in Fig. 5d is the result of the full conduction of the mechanical short-circuiting switch.

D. HYBRID SHORT-CIRCUITING SWITCH IN A PRACTICAL SOLUTION

Fig. 6 shows a practical solution for a hybrid short-circuiting switch. The thyristor blocks were placed in pipes (Fig. 6a) made of hard insulating material. The arrangement of thyristors inside plastic covers is shown in Fig. 6c. The mechanical short-circuits device (MSCD) valve presented in Fig. 6b is connected in parallel to the thyristors block by means of appropriately selected wires with a large cross section.

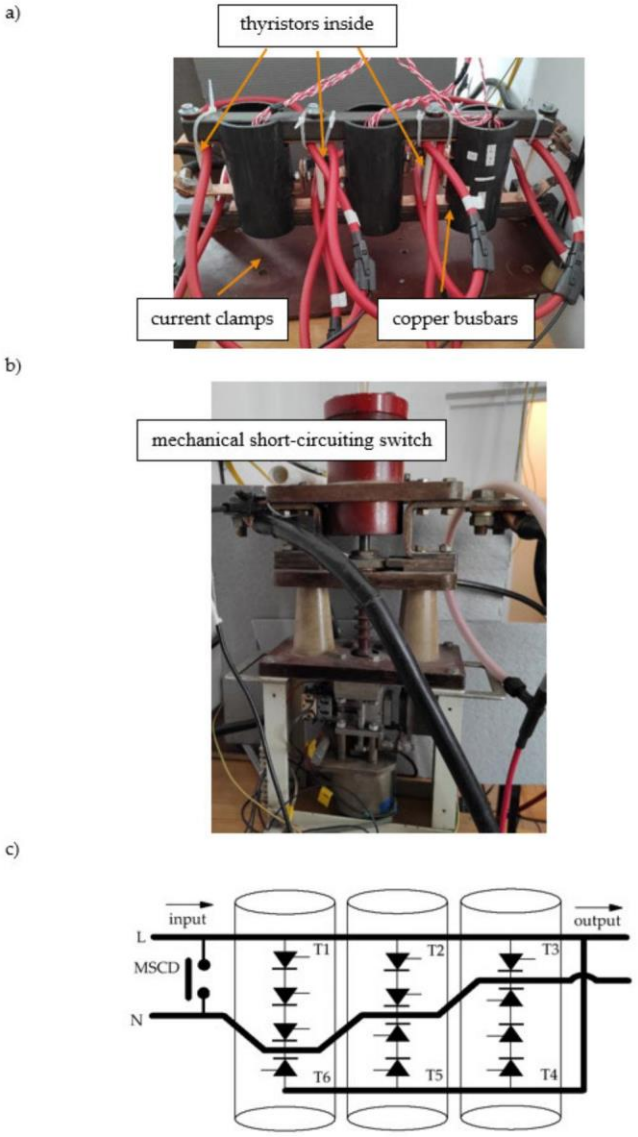

FIGURE 6. Hybrid short-circuiting switch in a practical solution; a) thyristor block, b) mechanical short-circuiting switch, c) arrangement of thyristors inside the plastic pipe.

IV. LIMITATION OF THE ELECTRODYNAMIC EFFECTS OF SHORT-CIRCUIT CURRENTS IN CIRCUITS PROTECTED WITH A HYBRID SHORT-CIRCUTING SWITCH

Electrodynamic interactions in current paths and electrical connector contact systems are caused by the electric current flowing through them [33]. The electrodynamic forces are greatest during the flow of short-circuit currents. The current flowing through the switch during a short-circuit may exceed hundreds of times the rated current, so electrodynamic forces may be tens of thousands of times greater than the forces occurring in rated operating conditions.

The subject of the analysis of electrodynamic interactions are, in particular, issues related to the calculation of [34]:

- forces and stresses in current paths when short-circuit currents flow through them,
- forces acting on the contacts of electric contactors.

The electrodynamic force results in bending stresses in rigid conductors and breaking stresses in supporting insulators. As far as flexible conductors are concerned, short-circuit forces can cause additional stretching and deflection of conductors and their equipment. The most visible and destructive effects of short-circuit currents occur in metal-enclosed switchgear, where the distances between conductors are smaller than in the case of typical overhead lines [35].

The maximum value of the force is of particular importance in the case of rigid conductors. The forces acting between two long parallel conductors can be expressed by the relation [36]:

$$F = \frac{\mu_0}{2\pi} \cdot \frac{i_1 \cdot i_2}{a} \cdot l, \tag{1}$$

where F is the force applied to the current track (N), l is the length of the current track (cm), i_1 and i_2 are instantaneous values of the flowing currents (kA), and a is the distance between the axes of the current tracks (cm).

The strength of the electrodynamic interaction can also be determined based on the measurement of the maximum deflection of the busbar, using the relationship [37], [38]:

$$F = \frac{384 \cdot E \cdot J \cdot \Delta}{l^3}, \tag{2}$$

where E is a modulus of elasticity of the busbar material, for Aluminum $E = 6.86 \cdot 10^6$ (N·cm^{-2}), J is a moment of inertia of the beam section (cm^4), and Δ is a maximum deflection (cm).

The deflection of the busbars due to the flowing current is the result of a force. By transforming formula (2), from the calculated value of the acting force (formula (1)), it is possible to determine the value of the maximum busbar deflection under the influence of the flowing short-circuit current:

$$\Delta = \frac{F \cdot l^3}{384 \cdot E \cdot J}. \tag{3}$$

Fig. 7 presents an attempt to assess the effectiveness of limiting the electrodynamic short-circuit effects in the hybrid short-circuiting switch action as an arc eliminator. During the experiment, two parallel aluminum current-carrying wires with a length of $l = 1000$ (mm) and diameter $d = 8$ (mm) were used, arranged at a distance of $a = 2$ (mm). Fig. 7a shows the test object prior to the short-circuit test. Fig. 7b shows the effect of electrodynamic effects during the flow of a short-circuit current with an amplitude of 10 (kA). The flowing currents have opposite directions, which causes the electrodynamic forces to repel the current-carrying wire, deforming them in opposite directions. At the time of the greatest impact of electrodynamic force on the current-carrying wire, its calculated value was 2013 (N). Fig. 7.b presents the effect of the electrodynamic force of this value is the deformation of the current-carrying wire. The distance

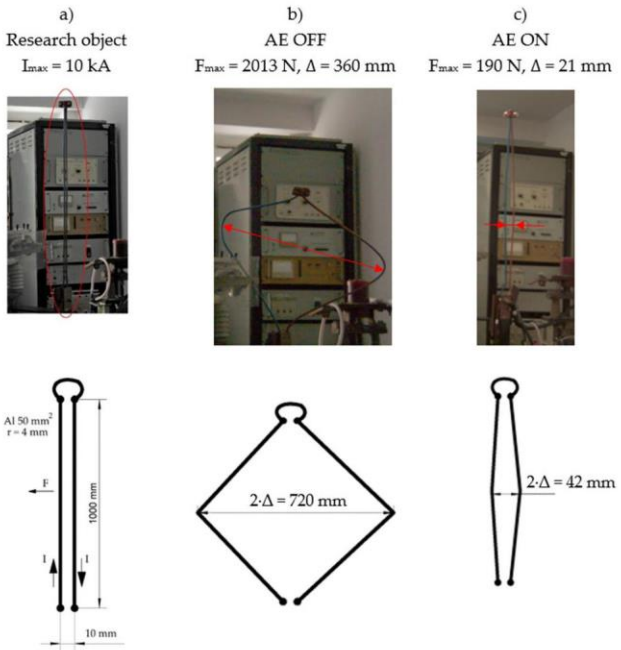

FIGURE 7. An attempt to evaluate the electrodynamic effects during the flow of a current with an amplitude of 10 kA in a system of parallel aluminum wire; a) research object, b) electrodynamic effects of AE OFF, c) electrodynamic effects of AE ON.

between the conductor centers, which before the short-circuit test was 10 (mm), increased to 720 (mm) due to the electrodynamic force with the peak value of 2013 (N). Assuming that the same force acts on both conductors, the maximum deflection for each of them is $\Delta = 360$ (mm). The calculated value of the deflection of formula (3) for the same conditions is $\Delta' = 379$ (mm). For the same test object and short-circuit conditions, in the system in which the hybrid short-circuiting switch was used, the calculated value of the acting force was only 190 (N). Under these conditions, the greatest deformation distance of the conductors between their centers was only 42 (mm) (Fig. 7c), the maximum deformation for a single conductor is $\Delta_{AE} = 21$ (mm). The calculated value of the deflection of equation (3) for the same conditions is $\Delta'_{AE} = 36$ (mm).

Due to the testing capabilities available for of the current source in the research laboratory, all calculations presented in Table 1 were performed in the range of peak currents of 5 to 30 (kA). Table 1 contains the calculated values of the electromagnetic forces acting on the current wire during the flow of the short-circuit current. The use of a hybrid short-circuiting switch makes it possible to significantly shorten the duration of the short-circuit disturbance, and thus to reduce the effects of electrodynamic influence. The calculations performed of the occurring electromagnetic forces during the current short-circuit showed that the application of the hybrid short-circuiting switch proposed by the authors results in a reduction of the electromagnetic impact on the current wire by about 90%. The measured value of the deformation of the current wire during the flow of the short-circuit current with

an amplitude of 10 (kA) confirms the effectiveness of the use of the hybrid short-circuiting switch, where the deformation (Δ_{AE}/Δ) decreased by approximately 94%.

TABLE 1. The value of the short-circuit current and the corresponding calculated value of the electromagnetic force acting on the current wires.

I_{max} (kA)	AE OFF F_{max} (kN)	AE ON F'_{max} (kN)	F'_{max}/F_{max} (%)
5	0.5	0.047	9.4
10	2.0	0.19	9.5
15	4.5	0.43	9.6
20	8.0	0.76	9.5
25	12.5	1.19	9.5
30	18.0	1.70	9.4

V. LIMIT THE EROSION OF THE CURRENT CIRCUIT SUBJECTED TO THE ACTION OF AN ELECTRIC ARC

The burning of an electric arc and the fault current flowing through the current circuit of electric power devices and apparatuses cause the occurrence of various physical and chemical phenomena. The thermal energy released in the emergency electrical arc can cause significant damage to devices inside and outside the switchgear, as well as pose a threat to the environment [39]. During normal operation, all types of current-carrying element must be resistant to such phenomena as:

- rise of temperature,
- oxidation,
- corrosion of the material.

A particularly dangerous unintentional situation is the erosion of material occurring in the event of an electric arc burning between the conductors or a component of the conductor and the enclosure wall, which may become perforated. Damage to the switchgear cover as a result, its unsealing, causes the emission into the environment of toxic chemical compounds, metal vapors, drops, etc., resulting from the direct impact of the arc on the apparatus, structures, and insulating elements [40].

Material erosion is generally understood to mean the weight or volume loss of electrode mass, as well as the degradation and change in the properties of the electrode surface as a result of various phenomena and processes related to the occurrence of an electric arc. Fig. 8 shows the model of material transport between electrodes during the burning of a high-current short arc.

The mass balance equations of the electrodes (anode and cathode separately), during the arc between them, can be written as follows:

$$\Delta m_A = \Delta m_{A1} + \Delta m_{A2}, \tag{4}$$

$$\Delta m_C = \Delta m_{C1} + \Delta m_{C2}, \tag{5}$$

where $\Delta m_A/\Delta m_C$ is the calculated mass of the molten evaporated anode/cathode material, $\Delta m_{A1}/\Delta m_{C1}$ is the mass of the material thrown into the environment in the form of vapors and drops from the anode/cathode, and $\Delta m_{A2}/\Delta m_{C2}$ is a mass of anode/cathode material transferred in the form of a stream of metal vapors and drops of material to the opposite electrode (so-called transport of material from one electrode to the other).

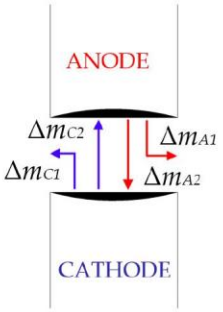

FIGURE 8. Model of material transport during the burning of a high-current disturbance of an electric arc.

Weight loss in the mass of contacts can be written with the following dependencies [41]:

$$\Delta m_{Awl} = \Delta m_{A1} + (\Delta m_{A2} - \Delta m_{C2}), \tag{6}$$

$$\Delta m_{Cwl} = \Delta m_{C1} + (\Delta m_{C2} - \Delta m_{A2}), \tag{7}$$

where Δm_{Awl} is the total weight loss (index *wl*) of the anode including material discharged into the environment and transport of material from one electrode to the other, Δm_{Cwl} is the total weight loss from the cathode including material discharged into the environment and transport between the electrodes.

Electrode weight loss occurs when the electrode material is removed to the outside in the form of charged particles, vapors of molten material, and liquid material (droplets). The electrode material can be removed from the surface of the electrodes during the flow of the fault current (electric arc) and after its termination. The condition for this is to supply the electrodes with a sufficiently high energy and to achieve the melting point or boiling point of the material on the electrode surface. Material loss influenced by many phenomena, including [42]:

- evaporation of contact material under the influence of high arc temperature,
- ejection of the liquid contact material outside under the influence of electrodynamic forces,
- transfer of material from one electrode to another by plasma streams,
- ejection of metal vapors into the environment by appropriately positioned plasma jets,
- the violent escape of gases from the solidifying metal which have been absorbed by the metal in its liquid state.

The dependence of the erosion rate E_r of the electrode material can be roughly described [43]:

$$E_r = \frac{\Delta m_e}{Q}, \tag{8}$$

where Δm_e is a total weight loss of the electrodes and Q is electric charge.

The total weight loss of the electrodes Δm_e consists of part of the electrode material lost due to melting Δm_m and part of the electrode material lost due to evaporation Δm_v [43], [44]:

$$\Delta m_e = \Delta m_m + \Delta m_v. \tag{9}$$

The electrical arc energy supplied to the electrodes is converted into heating the electrode material and into heat of change of aggregate state. The energy balance can be written as:

$$E_e = \Delta m_m \cdot C_p \cdot (T_m - T_a) + \Delta m_m \cdot C_p + \Delta m_v \cdot C_p \cdot (T_b - T_m) + \Delta m_v \cdot C_v, \tag{10}$$

where c_p is a specific heat capacity, for copper 386 (J · kg^{-1} · K^{-1}), c_m is a specific melting heat of the electrode, for copper 205 (kJ · kg^{-1} · K^{-1}), c_v is a specific vaporization heat of the electrode, T_a is a ambient temperature (293 (K)), T_m is a melting point (for copper 1358 (K)), and T_b is a boiling point (for copper 2835 (K)).

In papers [43] and [44] it was shown that for an arc that burns freely in the air, the loss of mass of copper electrodes due to evaporation is much lower in relation to the loss of mass by melting. Hence, the expression for the electric arc energy supplied to the electrodes can be simplified to the form:

$$E_e = \Delta m_e \cdot C_p \cdot (T_m - T_a) + \Delta m_e \cdot C_m. \tag{11}$$

Knowledge of the specific heat value, temperature difference and energy transferred to the electrodes will allow to determine the theoretical values of the maximum loss of electrode material due to the action of an electric arc. The dependency is as follows:

$$\Delta m_e = \frac{E_e}{c_p \cdot (T_m - T_a) + c_m}. \tag{12}$$

For example, for a high-current arc between copper electrodes, in a circuit without arc eliminator (AE OFF), the following was determined:

- total electric arc energy $E = 26.1$ (kJ),
- average value of the arc current $I_{av} = 15.9$ (kA),
- arc burning time $\Delta t = 14.2$ (ms),
- electrode weight loss $\Delta m_m = 2.45$ (g).

According to the results presented in [43] and [44], it was assumed that the electrode erosion rate was 19 (g/kC). For an average current value of 15.9 (kA) and an arc burning time of 14.2 (ms), the value of the electric charge is equal to $Q_{AE\_OFF} = 225$ (C). With these assumptions, the maximum weight loss of the electrodes is $\Delta m_e = 4.3$ (g). If we compare the measured and calculated weight loss ($\Delta m_m/\Delta m_e$), we find that the measured weight loss Δm_m is 57% of the total achievable value of the material loss Δm_e. It can be assumed that due to the high temperature and melting of copper, approximately 1.85 (g) of the liquid mass of the material still remained on the electrodes (which is not included in the measured loss), but changed its position.

If it is assumed, according to the work [45], that 25% of the arc energy is supplied to the electrodes, and the remaining 75% is dissipated to the environment, then the electric arc energy supplied to the electrodes is $E_e = 6.53$ (kJ), and the maximum calculated loss weight is at the level of $\Delta m_e = 10.7$ (g). The measured loss of mass of the electrodes Δm_m is in this case 23.8% of the maximum material erosion Δm_e (counted as $\Delta m_m/\Delta m_e$). It follows that about 7.85 (g) of the liquid mass of the material could still remain on the electrodes.

For the same measurement conditions, the experiment in the circuit with the arc eliminator (AE ON) was repeated, and the following was determined:

- total electric arc energy $E = 0.13$ (kJ),
- average value of the arc current $I_{av} = 3.12$ (kA),
- arc burning time $\Delta t = 0.7$ (ms),
- electrode weight loss $\Delta m_m = 0.0016$ (g).

For an average current value of 3.2 (kA) and an arc burning time of 0.7 (ms), the value of the electric charge is $Q_{AE\_ON} = 2.2$ (C). If we assume (as before [43], [44]) that the electrode erosion rate is 19 (g/kC), then the maximum weight loss of the electrodes is $\Delta m_e = 0.042$ (g). If we compare the measured and calculated weight losses $\Delta m_m/\Delta m_e$, then we find that the measured electrode weight loss Δm_m is 3.8% of the maximum material erosion Δm_e.

If we assume that 25% of the arc energy is supplied to the electrodes [45], and the remaining 75% is dissipated to the environment, then the electric arc energy supplied to the electrodes is $E_e = 0.033$ (kJ), and the maximum calculated loss $\Delta m_e = 0.053$ (g). The measured loss of mass of the electrodes Δm_m is 3% of the maximum erosion of the material (counted as $\Delta m_m/\Delta m_e$).

If, for an arc disturbance with a current amplitude of 25 (kA) and a mass loss of the electrodes at the level of 19 (g/kC), according to the equation:

$$Q_{\%} = \frac{Q_{AE\_ON}}{Q_{AE\_OFF}} \cdot 100\%, \tag{13}$$

the percentage share of the calculated values of the electric charge in systems with AE (Q_{AE_ON}) and without an eliminator (Q_{AE_OFF}), it amounts to less than $Q_{\%} = 1\%$. This means that the proposed hybrid short-circuiting switch action as an arc eliminator, according to the calculations, causes limits the maximum theoretical weight loss of the electrodes by over 100 times. Assuming that 25% of the energy is transferred to the arc, the loss is more than 200 times in favor of the arc eliminator system.

Table 2 summarizes the measured and calculated (maximum achievable) material erosion values based on the measurements of current, voltage, arc burning time, and electrode erosion. The results are presented for two measuring systems:

- without arc eliminator (AE OFF),
- with arc eliminator (AE ON).

In the system with the arc eliminator (AE ON), for current amplitudes in the range of 5 to 20 (kA), the measurement of material erosion was at the level of gauge error (±0.4 (mg)), and the photographic recording did not show visible changes on the electrode surface. For currents greater than 25 (kA) and the system without the arc eliminator (AE OFF), for safety reasons, the tests were not carried out.

TABLE 2. Calculated and measured erosions of the electrode material for various arc currents.

	I_{max} (kA)	5	10	15	20	25	30
AE OFF	$m_{m\_AE\_OFF}$ (g)	0.35	0.85	1.0	2.1	2.45	-
	$m_{19\_AE\_OFF}$ (g)	0.96	1.5	2.64	3.66	4.3	-
	$m_{25\_AE\_OFF}$ (g)	1.05	2.65	4.66	7.5	10.7	-
AE ON	$m_{m\_AE\_ON}$ (g)	<0.0004	<0.0004	<0.0004	<0.0004	0.0016	0.0045
	$m_{19\_AE\_ON}$ (g)	-	0.03	0.025	0.036	0.042	0.021
	$m_{25\_AE\_ON}$ (g)	0.023	0.03	0.035	0.046	0.053	0.081

I_{max} – amplitude of the expected current in the branch affected by the electric arc, m_m – measured material loss, m_{19} – calculated material loss assuming erosion of electrodes 19 (g/kC), m_{25} – calculated loss of electrode material, assuming that only 25% of the arc energy is transferred to the electrodes.

Fig. 9 shows examples of photos of two copper busbars between which an arc ignited. For a better visualization of the material loss from the electrodes, both the front and back of the current busbar are shown along with the anode A and cathode K markings. During the arc disturbance, the amplitude of the flowing electric current was 25 (kA), and the total incident energy emitted in the arc reached the value of 26.1 (kJ). The first current crossing through zero and favorable deionization conditions caused the arc to extinguish after 14 (ms). The measured material loss from the copper busbars was $\Delta m = 2.45$ (g) with a measurement error of ±0.4 (mg).

FIGURE 9. Erosion of the copper electrode material as a result of the high-current electric arc action.

It is reported in the literature [46] that with an arc energy value of up to 100 (kJ), there is only soot of the equipment inside the electrical switchgear without damaging busbars, and the methods of removing the damage consist of cleaning. Only when the arc energy exceeds 170 (kJ), there are traces of burnout of busbars and insulators, thermal damage, and the removal of the resulting damage consists in the replacement of structural elements, apparatuses, and devices. The test result presented in Fig. 9 with an arc energy of 26.1 (kJ), that is, 4 times lower (in relation to 100 (kJ)), it didn't end with the electrodes being dirty, but with a significant loss of material from the copper current busbars. Note that some of the material remained on the electrodes (which was not included in the measured loss), but only changed its position.

Fig. 10 presents the erosion of the copper electrode material for different arc energy values under two test conditions, with and without an arc eliminator, and their photographic documentation [20]:

- AE OFF (Fig. 10a-10e) – arc fault for a system without an arc eliminator. The arc is extinguished at the moment of the first passage of the current through zero (for the test circuit it is about 14 (ms)),
- AE ON (Fig. 10f-10g) – arc fault in the arc eliminator circuit. The time to extinguish the arc is within the range 0.32-4.6 (ms) depending on the nature of the receiver.

FIGURE 10. Erosion of the material of copper electrodes as a result of the action of an electric arc in a system without AE (AE OFF) and with (AE ON) an arc eliminator (I_{max} – measured value of the interference current, E – calculated electric arc energy, Δm – measured material loss of both electrodes).

In the configuration with an arc eliminator (AE ON), with currents ranging from 5 to 20 (kA), there was no visible damage to the electrodes, and the measurement of material erosion was at the error level of the measuring instrument (±0.4 (mg)). The material loss, clearly visible and measurable, occurred only for the current amplitude of 25 (kA) and more.

Comparing, for a current amplitude of 24.5 (kA), the results of the tests in the system with the arc eliminator (AE ON), in relation to the results from the system without the eliminator (AE OFF), one can observe the following:

FIGURE 11. Sample photos of electric arc ignition and erosion of copper busbar material.

- 200-fold reduction in arc energy,
- reduction in electrode material loss by more than 1500 times,
- visible, significant reduction in electrode surface degradation.

Measurements of electrode material loss in a system without an arc eliminator (AE OFF) were limited, for the safety of personnel and measuring equipment, to a current amplitude of 25 (kA). Already at this current value, the sound intensity and the number of hazardous vapors accompanying the ignition of the arc, as well as the material emission level in the form of glowing copper droplets, thrown in every direction from the place affected by the arc, were, in the authors' opinion, on the edge of the acceptable safe measurement values. Fig. 11 shows two selected photos from the measurement series, showing the erosion of the material of the copper electrodes as a result of burning an electric arc at a current of 25 (kA).

On the basis of many series of tests, it was found that the arc eliminator (AE) significantly reduces the risks posed by a burning electric arc. Therefore, the measurement was performed for the electric arc and the current of 29.6 (kA) with arc eliminator. For safety reasons, such a measurement was not performed in a system without an arc eliminator (AE OFF). The test results can be seen in Fig. 10g. Despite the much larger current amplitude, electrode erosion is still slight.

Fig. 12 shows two examples of the material loss volume calculated for comparable current values in the system without and with the arc eliminator. Comparing the calculated volume of material loss in the system with the eliminator V_{AE_ON} to the material loss in the system without the eliminator V, we obtain over 1500 times lower value of the loss in favor of the system with the arc eliminator (V_{AE_OFF}/V_{AE_ON}). To better show the difference in volumes, in Fig. 12, the material loss is presented in the form of spheres with radius r.

Fig. 13 shows the graphical dependence of the measured weight loss of copper electrodes as a function of the electric arc energy. In the case of a still arc that burned stably between the current busbars, the erosion of the electrodes is practically directly proportional to the energy of the electric arc. The material loss in the system with the hybrid short-circuiting switch, due to the small, measured values, is near the origin of the coordinate system (red circle). This section has been enlarged and shown on the right as a separate graph.

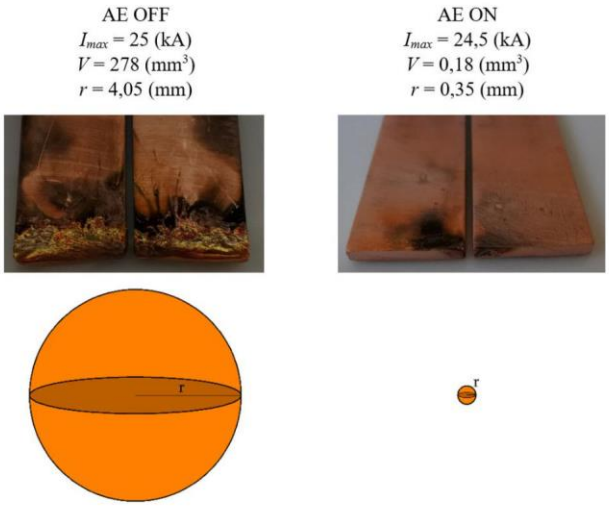

FIGURE 12. Graphical representation of the volume of material ejected from the electrodes into the environment.

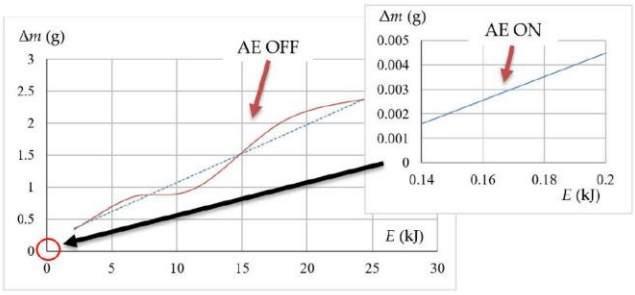

FIGURE 13. Dependence of the material loss of the copper electrodes as a function of the energy of the electric arc.

The dashed line is the trend line of the change in mass loss as a function of arc energy.

VI. LIMITING HAZARDS CAUSED BY THE ACOUSTIC INFLUENCE OF THE ELECTRIC ARC

The acoustic wave is described by the so-called sound pressure p (Pa), which is the pressure difference due to the wave motion and the constant atmospheric pressure. The pressure is a scalar quantity and is the quotient of the force F (N) acting on a given surface area A (m^2). The sound intensity is a measure of the amount of acoustic energy flowing through a unit of surface area. The measurement of sound intensity is performed most often in order to determine the sound power of sound sources and their location.

During the ignition of an electric arc and in the following moments of its burning, a sound wave is created as a result of a sudden increase in pressure, the intensity of which can damage or even cause hearing loss. An average arc with a current intensity of a few to several kiloamperes and a length of several to several dozen centimeters generates at a distance of 1 (m) from the arc, acoustic pressure with values up to 150 (dB), which is much more than the pain threshold level of 120 (dB) [47]. Even more dangerous is the acoustic

shock generated when the arc ignites in a sealed enclosure switchgear or cable fittings. These acoustic shocks are caused by the rapid escape of gases through a narrow discharge channel. The sound levels in such situations often exceed 160 (dB), that is, the level at which the human ear can suffer irreversible damage. Table 3 presents selected levels of sound intensity ranging from 60 to 160 (dB) that are generated by sound sources and the effects of the impact on the human body [48]. For humans, the safe limit of sound intensity does not exceed 85 (dB). After exceeding it, depending on the intensity level and duration of the sound, a person is first exposed to increasing pain and consequently, hearing loss.

TABLE 3. The level of sound intensity and the effect of the impact on humans [48].

Sound intensity β	The source of the sound and the effects of the impact on humans
60 (dB)	Normal conversation
70 (dB)	Heavy car traffic
80 (dB)	Loud radio, school classroom
100 (dB)	Noisy industrial plant, siren 30 meters away, possible hearing damage due to 8-hour exposure to noise
110 (dB)	Possible hearing damage caused 30-minute noise exposure
120 (dB)	Loud concert, jackhammer from 2 m away, pain threshold
140 (dB)	Jet aircraft at 30 m distance, severe pain, hearing loss
160 (dB)	Destruction of the eardrum

Due to the measuring range of the Sauter SW-1000 meter used (and the fear of exceeding it), the measurements of sound intensity were made at a distance of 3 (m) from the sound source generated by the electric arc. Knowing the intensity of the sound at a distance of 3 (m) from the sound source, intensity values were calculated for distances of 1.5 (m) and 0.75 (m), which may correspond to the actual working distances of the technical personnel. Fig. 14 shows the system for measuring the intensity of sound of the burning electric arc.

For fault arc current amplitudes ranging from 5 to 20 (kA), at a distance of 3 meters from the arc source, the sound intensity values were measured in the system without the arc eliminator (AE OFF) and in the system with a hybrid switching device as an arc eliminator (AE ON). The results of the sound intensity measurements are presented in Table 4.

The following designations are used in Table 4:

- $\beta_{AE\ OFF\ 3m}$ – measured sound intensity at a distance of 3 (m) from the source of the arc in the system without arc eliminator (AE OFF),

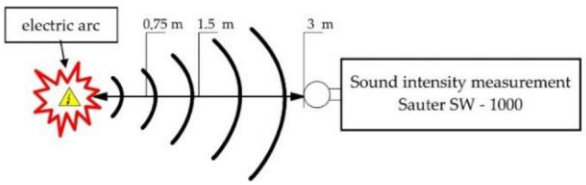

FIGURE 14. Measurement of the sound intensity from an electric arc.

- $\beta_{AE\ OFF\ 1.5m}$ – calculated value of sound intensity at a distance of 1.5 (m) from the source of the arc in the system without arc eliminator (AE OFF),
- $\beta_{AE\ ON\ 3m}$ – measured sound intensity at a distance of 3 (m) from the source of the arc in a system with an arc eliminator (AE ON),
- $\beta_{AE\ ON\ 1.5m}$ – the calculated value of sound intensity at a distance of 1.5 (m) from the source of the arc in a system with an arc eliminator (AE ON).

TABLE 4. Measured and expected values of sound intensity at a distance of 3 meters and 1.5 meters from the source of the arc in test systems without and with an arc eliminator.

I_{max} (kA)	AE OFF		AE ON	
	Measured value	Expected calculation values for a measuring distance of 1.5 m	Measured value	Expected calculation values for a measuring distance of 1.5 m
	$\beta_{AE\ OFF\ 3m}$ (dB)	$\beta_{AE\ OFF\ 1.5m}$ (dB)	$\beta_{AE\ ON\ 3m}$ (dB)	$\beta_{AE\ ON\ 1.5m}$ (dB)
5	121.0	127.0	110.0	116.0
10	123.0	129.0	113.0	119.0
15	124.5	130.5	116.5	122.5
20	126.5	132.5	119.5	125.5

The measured values of sound intensity for the system without the arc eliminator exceeded the level of 120 (dB), which is the pain threshold for the human body, and its prolonged exposure is very dangerous. For a system with a hybrid switch used as an arc eliminator, the recorded value of the level of sound intensity did not exceed 120 (dB). The sound intensity levels registered for this configuration still assume dangerous values for the human ear, but do not threaten its loss. It should be mentioned here that in the system with an arc eliminator, there is a Mechanical Short-Circuit Device MSCD (Fig. 3), the drive system of which and closing contacts generate the sound intensity at the level of 106 (dB) measured at a distance of 3 (m).

The average increase in sound intensity for the configuration without AE OFF in relation to AE ON is 9 (dB), to the disadvantage of the former. This value corresponds to the eight-fold change in the amplitude ratios of the two sounds' intensity, i.e., the perceived noise level in the AE ON system is 8 times lower in relation to the AE OFF system.

Disregarding the influence of disturbances introduced by objects of the testing laboratory equipment, a two-fold

reduction of the measuring distance (from 3 (m) to 1.5 (m)) is about a four-fold increase in sound intensity. For this distance, the expected (calculated) sound intensity values are given in Table 4. It should be emphasized that after exceeding the level of 130 (dB), there are no simple and effective hearing protection tools in the form of earmuffs or protective masks. For a system equipped with AE ON, the noise level is still 8 times lower, and therefore the exposure to hearing loss is much lower.

For a distance of 0.75 (m) from the electric arc, the situation is very dangerous because the calculated level of sound intensity is close to the limit of hearing loss. Still, the sound level with the arc eliminator will be at least 6 (dB) lower. The expected design values are summarized in Table 5.

TABLE 5. Expected values of sound intensity at the distance from the electric arc of 0.75 meters.

I_{max} (kA)	AE OFF $\beta_{AE\ OFF\ 0.75m}$ (dB)	AE ON $\beta_{AE\ ON\ 0.75m}$ (dB)
5	133.0	127.0
10	135.0	129.0
15	136.5	130.5
20	138.5	132.5

Since the expected calculation values (due to the conditions of the experiment) may be burdened with some inaccuracy, the authors, in the next part, evaluated the effectiveness of reducing the risk caused by the acoustic influence of an electric arc, focused on comparing the values of the measured sound intensity at a distance of 3 (m).

Table 6 shows the difference in sound intensity measurements at a distance of 3 (m) from the sound source for a system without arc eliminator (AE OFF) and in a system with the arc eliminator (AE ON) and the corresponding changes in the intensity ratios (I_2/I_1). It is worth noting that for the arc current amplitude of 5 (kA), the reduction in sound intensity was up to 11 (dB), which means a 13-fold reduction in the intensity of the sound wave. The successive differences in intensity are 10, 8, and 7 (dB), respectively, for the currents of 10, 15, and 20 (kA). This shows how effective the use of a multi-section arc eliminator is for suppressing noise generated by electric arc.

If one wanted to visualize the calculated values presented in Table 6 and show how much the use of the hybrid arc eliminator limits the sound intensity value, it can be done as in Figure 15. The vertical axis of the graph $\beta_{AE\ OFF\ 3m} - \beta_{AE\ ON\ 3m}$ is the difference between the measurement of the intensity of the sound at a distance of 3 (m) from the sound source in a system with arc eliminator, and the measurement over the same distance in a system without an arc eliminator. The axis of the graph I_2/I_1 is the conversion of the quantities expressed in (dB) to the appropriate multiplicity of this difference. In this way, the perceived difference in sound intensity can be assessed more quickly. For example, if the level of the

TABLE 6. Differences in sound intensity levels measured at a distance of 3 meters from the electric arc and the corresponding sound intensity ratios.

I_{max} (kA)	$\beta_{AE\ ON\ 3m} - \beta_{AE\ OFF\ 3m}$ (dB)	I_2/I_1
5	- 11	13
10	-10	10
15	-8	6.5
20	-7	5

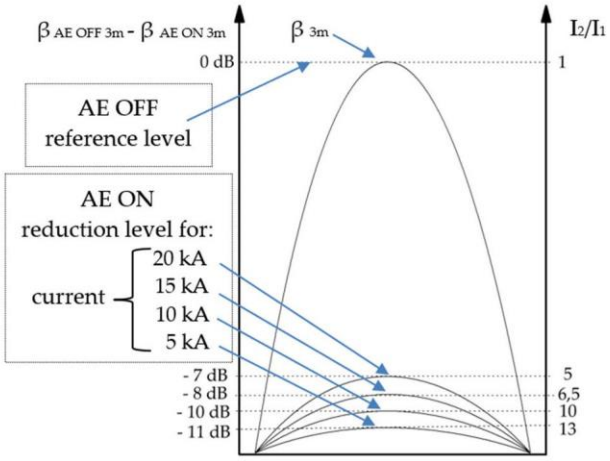

FIGURE 15. Dependence of the difference in sound intensity and the corresponding changes in the sound intensity ratios.

signal recorded in the AE ON configuration is lower than the sound intensity in the AE OFF system by 7 (dB), then the perceptible sound intensity is five times lower. The highest amplitude in Figure 15 corresponds to the measurement of the sound intensity at a distance of 3 (m) from the source in the system without arc eliminator and is taken as the reference level. All other curves represent the difference in sound intensity from the β_{3m} reference value for a given arc current value. The height of the amplitudes corresponds to the ratio of the intensity of the sounds in subsequent measurements.

VII. CONCLUSION

The subject of this publication and the research described there are the results of experiments that confirm the effectiveness of the hybrid short-circuiting switch used as an electric arc eliminator. The proprietary design is a device enabling a very quick shunting of an electric circuit affected by an arc disturbance, in order to create an alternative – privileged path for the current flow. This results in a very fast elimination of the arcing that has occurred and a reduction in the damage caused by the developing arcing disturbance. The high speed of operation of the hybrid short-circuiting switch was achieved by the use of thyristor short-circuiting branches that cooperate with the bypassing mechanical short-circuit device.

Experimental studies have shown that in circuits affected by an arc disturbance, sections of antiparallel connected thyristors working as an electric arc eliminator are able to

extinguish an electric arc with an intensity of 30 (kA) in less than 1 (ms). Shortening the arc disturbance duration significantly reduced the amount of energy released in the arc and thus significantly reduced the hazardous effects of the electric arc.

This resulted in the following:

- limiting electrodynamic effects of short-circuit currents,
- limiting the erosion of current circuit subjected to the action of an electric arc,
- reducing the risks caused by the acoustic effects of an electric arc,
- limitation of gas pressure inside a closed electrical switchgear,
- significant reduction of the time of thermal effects in the protected circuit,
- reduction of the dangerous arc flash zone.

The authors focused on demonstrating the effectiveness of the device in LV circuits, as a multi-faceted series of tests was performed in the low-voltage short-circuit laboratory at the Institute of Electrical Power Engineering of Poznan University of Technology. Ultimately, the device with the presented concept can also be installed in medium voltage high-current circuits/switchgears (using thyristors with a sufficiently high rated voltage), and even in DC traction circuits - with the use of thyristor blocks operating in one polarity. Both solutions - bipolar and unipolar - have been submitted to the Patent Office of the Republic of Poland.

The results of tests and calculations presented by the authors in a series of publications on the elimination of an electric arc with a hybrid short-circuiting switch confirm the effectiveness of the multi-section hybrid short-circuiting switch as an electric arc eliminator. The proposed device in an industrial solution may contribute to the protection of the health or life of people exposed to the action of an electric arc, and it will also significantly minimize material losses resulting from damage caused by the electric arc or short-circuit current.

Further research work will focus on the use of a short-circuit hybrid device in power supply systems and protection of electric vehicle charging stations and contact line systems. At the same time, research will also be conducted aimed at the protection of devices powered from the medium voltage network, where the main problem is the selection of thyristors with an appropriately high forward voltage. The solution to this problem may be the short-circuit hybrid device presented in this paper, which in its branches has a series connection of several thyristors enabling the increase of the forward voltage.

REFERENCES

[1] ABB. *Protection Against Electric Arc Integration Between Arc Guard System TVOC-2 and SACE Emax 2*. Accessed: Aug. 22, 2022. [Online]. Available: https://library.e.abb.com/public/fc33af751d664dad932e9c7344cffec0/1SDC007407G0203_revB_Protection%20against%20electric%20arc%20.pdf

[2] P. G. Slade, "Effect of the electric arc and the ambient air on the contact resistance of silver, tungsten, and silver-tungsten contacts," *J. Appl. Phys.*, vol. 47, no. 8, pp. 3438–3443, 1976.

[3] C. Li, J. Chen, W. Zhang, L. Hu, J. Cao, J. Liu, Z. Zhu, and S. Wu, "Influence of arc size on the ignition and flame propagation of cable fire," *Energies*, vol. 14, no. 18, p. 5675, Sep. 2021.

[4] M. Kaźmierczak, "Zwarcia łukowe—Doświadczenia eksploatacyjne w polskiej energetyce zawodowej i przemysłowej," *Elektroenergetyka-Współczesność i Rozwój*, vol. 2, no. 8, p. 16, 2011.

[5] J. Volger, "Arc fault protection as seen by employers' liability insurance associations," in *The Arc-Fault Demonstration in the Head Office*. Bonn, Germany: Moeller GmbH, 2008.

[6] M. Szadkowski, A. Warachim, and K. Dekarz, "Minimalizajca skutków zwarć łukowych w stacjach wnętrzowych SN," *Energetyka*, vol. 12, pp. 791–797, Jan. 2015.

[7] Z. Yin, L. Wang, Y. Zhang, and Y. Gao, "A novel arc fault detection method integrated random forest, improved multi-scale permutation entropy and wavelet packet transform," *Electronics*, vol. 8, no. 4, p. 396, 2019.

[8] S. Paul and W. Jewell, "Optimization methodology for minimizing the arc flash incident energy," in *Proc. IEEE Ind. Appl. Soc. Annu. Meeting (IAS)*, Sep. 2018, pp. 1–6.

[9] K. Kowalski-Trakofler and E. Barrett, "Reducing non-contact electric arc injuries: An investigation of behavioral and organizational issues," *J. Saf. Res.*, vol. 38, no. 5, pp. 597–608, Jan. 2007.

[10] *Fault Arcs on Busbar Sets and Switchboards*. Accessed: Aug. 22, 2022. [Online]. Available: https://www.studiecd.dk/cahiers_techniques/Fault_arcs_on_busbar_sets_and_switchboards.pdf

[11] G. Roscoe, M. E. Valdes, and R. Luna, "Methods for arc-flash detection in electrical equipment," in *Proc. Rec. Conf. Papers Ind. Appl. Soc. 57th Annu. Petroleum Chem. Ind. Conf. (PCIC)*, Sep. 2010, pp. 1–8.

[12] L. Kumpulainen, G. A. Hussain, M. Rival, M. Lehtonen, and K. Kauhaniemi, "Aspects of arc-flash protection and prediction," *Electr. Power Syst. Res.*, vol. 116, pp. 77–86, Nov. 2014.

[13] H. B. Land, C. L. Eddins, and J. M. Klimek, "Evolution of arc fault protection technology at APL," *Johns Hopkins APL Tech. Dig.*, vol. 25, no. 2, pp. 140–153, 2004.

[14] P. A. Scarpino, A. Reatti, and F. Grasso, "A.C. Arc flash analysis: A new derivation method," in *Proc. AEIT Int. Annu. Conf.*, Oct. 2018, pp. 1–4.

[15] L. Kumpulainen and S. Dahl, "Selective arc-flash protection," in *Proc. 20th Int. Conf. Exhib. Electr. Distrib. (CIRED)*, Jun. 2009, pp. 1–4.

[16] A. H. Ghulam, "Methods for arc-flash prediction in medium voltage and low voltage switchgear," Ph.D. dissertation, School Elect. Eng., Aalto Univ., Helsinki, Finland, 2015.

[17] R. A. Jones, D. P. Liggett, M. Capelli-Schellpfeffer, T. Macalady, L. F. Saunders, R. E. Downey, L. B. McClung, A. Smith, S. Jamil, and V. J. Saporita, "Staged tests increase awareness of arc-flash hazards in electrical equipment," in *Proc. Rec. Conf. Papers, IEEE Ind. Appl. Soc. 44th Annu. Petroleum Chem. Ind. Conf.*, Sep. 1997, pp. 313–322.

[18] T. Dugan, "Reducing the arc flash hazard," *IEEE Ind. App. Mag.*, vol. 13, no. 3, pp. 51–58, May 2007.

[19] J. A. Kay and L. Kumpulainen, "Maximizing protection by minimizing arcing times in medium-voltage systems," *IEEE Trans. Ind. Appl.*, vol. 49, no. 4, pp. 1920–1927, Jul. 2013.

[20] K. Nowak, J. Janiszewski, and G. Dombek, "Thyristor arc eliminator for protection of low voltage electrical equipment," *Energies*, vol. 12, no. 14, p. 2749, Jul. 2019.

[21] K. Nowak, J. Janiszewski, and G. Dombek, "A multi-sectional arc eliminator for protection of low voltage electrical equipment," *Energies*, vol. 13, no. 3, p. 605, Jan. 2020.

[22] K. Nowak, J. Janiszewski, and G. Dombek, "The possibilities to reduce arc flash exposure with arc fault eliminators," *Energies*, vol. 14, no. 7, p. 1927, Mar. 2021.

[23] Z. Zhang, B. Ma, and A. Friberg, "Thyristor working as arc eliminator protecting electrical apparatus in low voltage power system," in *Proc. IEEE Int. Conf. Ind. Technol. (ICIT)*, Mar. 2015, pp. 1216–1219.

[24] *IEEE Guide for Performing Arc-Flash Hazard Calculations*, IEEE Standard 1584, 2018.

[25] B. Melouki, M. Lieutier, and A. Lefort, "The correlation between luminous and electric arc characteristics," *J. Phys. D, Appl. Phys.*, vol. 29, no. 11, pp. 2907–2914, Nov. 1996.

[26] *ZL-4A—Arc Fault Protection*. Accessed: Aug. 22, 2022. [Online]. Available: https://www.spie-energotest.pl/en/products/zl-4a-arc-fault-protection.html

[27] D. Doan, "Designing a site electrical system with arc flash energy under 20 cal/cm^2," *IEEE Trans. Ind. Appl.*, vol. 45, no. 3, pp. 1180–1183, May/Jun. 2009.

[28] J. A. Kay and L. Kumpulainen, "Maximizing protection by minimizing arcing times in medium voltage systems," in *Proc. Conf. Rec. Annu. IEEE Pulp Paper Ind. Tech. Conf. (PPIC)*, Jun. 2012, pp. 1–8.
[29] A. Öberg, F. Chimento, J. Qin, L. Wang, and O. Jeppsson, "Bypass switch assembly," U.S. Patent 2 013 185 815, Dec. 19, 2013.
[30] *ABB's New Ultra-Fast Earthing Switch.* Accessed: Aug. 22, 2022. [Online]. Available: https://www.scribd.com/document/352246380/ABB-Review-2-2010-72dpi-pdf
[31] H. Wu, X. Li, D. Stade, and H. Schau, "Arc fault model for low-voltage AC systems," *IEEE Trans. Power Del.*, vol. 20, no. 2, pp. 1204–1205, Apr. 2005.
[32] K. Nowak, "Thyristor microprocessor controller," *Poznan Univ. Technol. Academic J. Elect. Eng.*, vol. 95, pp. 77–86, Mar. 2018, doi: 10.21008/j.1897-0737.2018.95.0008.
[33] J. Turowski, *Elektrodynamika Techniczna*. Warsaw, Poland: WNT, 1993, pp. 123–135.
[34] S. Kulas, *Tory Prądowe i Układy Zestykowe*. Warsaw, Poland: OWPW, 2008, pp. 95–117.
[35] M. Daszczyszak, "Narażenia mechaniczne izolatorów w czasie trwania zwarcia," *Prz. Elektroic*, vol. 3, pp. 51–53, Mar. 2007.
[36] *Short-Circuit Currents—Calculation of Effects—Part 1: Definitions and Calculations Methods*, IEEE Standard 60865-1, 2011.
[37] M. Pawłot, "The electrodynamic impact of fault currents on system of aluminum busbar connected by pressure," *Prz. Elektroic*, vol. 92, no. 7, pp. 132–135, 2016.
[38] *Copper for Busbars—Guidance for Desing and Installation*. Accessed: Aug. 22, 2022. [Online]. Available: https://electrical-engineering-portal.com/download-center/books-and-guides/power-substations/copper-for-busbars-guidance
[39] C. Królikowski, *Inżynieria Łączenia Obwodów Elektrycznych Wielkiej Mocy*. Poznań, Poland: WPP, 1998, pp. 51–57.
[40] S. Wapniarski, G. Król, and A. Mercik, "Łukoochronność rozdzielnic SN na przykładzie przeprowadzonych prób odporności na wewnętrzne zwarcia łukowe," *Bezpieczeństwo Pracy i Ochrona Środowiska w Górnictwie*, vol. 10, pp. 26–33, Jan. 2010.
[41] P. Borkowski, "Zjawiska cieplno-erozyjne w silnoprądowych zestykach z materiałów kompozytowych," Ph.D. dissertation, Dept. Elect. App., Lodz Univ. Technol., Łódź, Poland, 1999.
[42] S. Dzierzbicki, *Aparaty Elektroenergetyczne*. Warsaw, Poland: WNT, 1977.
[43] T. Øyvang, E. Fjeld, W. Rondeel, and S. T. Hagen, "High current arc erosion on copper electrodes in air," in *Proc. IEEE 57th Holm Conf. Electr. Contacts (Holm)*, Sep. 2011, pp. 1–6.
[44] W. R. Wilson, "High-current arc erosion of electric contact materials [includes discussion]," *Trans. Amer. Inst. Elect. Eng., III: Power App. Syst.*, vol. 74, no. 3, pp. 657–664, Jan. 1955.
[45] P. Borkowski, "Badanie migracji i degradacji łukowej styków," Erozja łukowa łączników elektrycznych, Lodz Univ. Technol., Łódź, Poland, Tech. Rep., 2013, pp. 150–160.
[46] I. L. Surówka. *Zwarcia Łukowe w Rozdzielnicach Elektroenergetycznych SN i nn*. Accessed: Aug. 22, 2022. [Online]. Available: https://leonardo-energy.pl/wp-content/uploads/2017/01/zwarcia-lukowe-w-rozdzielnicach-elektroenergetycznych-SN-i-nn.pdf
[47] B. Koch and J. Maksymiuk, *Łukoochronność Rozdzielnic Osłoniętych i Symulacja Zwarć Łukowych*. Warsaw, Poland: OWPW, 2007, pp. 126–127.
[48] *Noise Level Charts of Common Sounds With Examples*. Accessed: Aug. 22, 2022. [Online]. Available: https://boomspeaker.com/noise-level-chart-db-level-chart/

KAROL NOWAK was born in Poland, in 1982. He received the M.Sc. (Eng.) degree in the field of electrical engineering from the Rzeszow University of Technology, in 2007. Since 2016, he has been working with the Poznan University of Technology as a Research and Teaching Worker. He is the author or coauthor of over nine publications, the issues of which are mainly related to the electric arc and the flow of short-circuit current. His research interests include controlled semiconductor systems, elimination of electric arc, and limiting the effects of short-circuit current flow.

JERZY JANISZEWSKI was born in 1957. He received the M.Sc., Ph.D., and Habilitation degrees from the Poznan University of Technology, Poznan, Poland, in 1981, 1995, and 2013, respectively.

Since 2018, he has been the Head of the Department of Distribution Devices and Electrical Installations with the Poznan University of Technology. He is the author of more than 80 articles and holds ten patents. His research interests include electrical apparatus, switching processes, and switching arc phenomena, especially high-current vacuum arcs.

GRZEGORZ DOMBEK was born in Kostrzyn, Odra, Poland, in 1987. He received the B.Sc., M.Sc., and Ph.D. degrees in electrical engineering from the Faculty of Electrical Engineering, Poznan University of Technology, Poland, in 2010, 2011, and 2016, respectively.

From 2014 to 2016, he was a Research Assistant with the Institute of Electric Power Engineering, Poznan University of Technology. From 2019 to 2020, he was an Assistant Professor with the Faculty of Electrical Engineering, Poznan University of Technology, where he has been an Assistant Professor with the Faculty of Environmental Engineering and Energy, since 2020. He is the author of more than 60 articles and holds one patents. His research interests include high voltage insulation diagnostics, dielectric materials, nanoliquids, electric arc, and thermal field in transformers. Since 2020, he has been the Vice-Dean of the Faculty of Environmental Engineering and Energy, Poznan University of Technology.

mgr inż. Karol Nowak
Politechnika Poznańska
Wydział Inżynierii Środowiska i Energetyki
Instytut Elektroenergetyki
ul. Piotrowo 3a, 61-138 Poznań

Poznań 08.09.2022

Oświadczenie o współautorstwie

Potwierdzam udział w publikacjach:

1. Karol Nowak, Jerzy Janiszewski, Grzegorz Dombek: „Thyristor Arc Eliminator for Protection of Low Voltage Electrical Equipment". Energies 2019, 12(14), 2749;

2. Karol Nowak, Jerzy Janiszewski, Grzegorz Dombek: „A Multi-Sectional Arc Eliminator for Protection of Low Voltage Electrical Equipment". Energies 2020, 13(3), 605;

3. Karol Nowak, Jerzy Janiszewski, Grzegorz Dombek: „The Possibilities to Reduce Arc Flash Exposure with Arc Fault Eliminators". Energies 2021, 14(7), 1927;

4. Karol Nowak, Jerzy Janiszewski, Grzegorz Dombek: „A New Short-Circuit Hybrid Device for the Protection of Low-Voltage Networks From the Effects of an Arc Fault". IEEE Access 2022, vol. 10, pp. 88678-88691;

Mój udział w publikacjach 1,2 i 3 szacowany jest na 60% i obejmuje przygotowanie stanowiska badawczego, wykonanie i rejestrację wyników badań, analizę danych pomiarowych, opracowanie pierwszej wersji publikacji.
Mój udział w publikacji 4 szacowany jest na 80% i obejmuje opracowanie koncepcji i metodyki badań, wykonanie i rejestrację wyników badań, analizę danych pomiarowych, opracowanie pierwszej wersji publikacji.

……
Karol Nowak

dr hab. inż. Jerzy Janiszewski, prof. PP
Wydział Inżynierii Środowiska i Energetyki
Politechnika Poznańska
Instytut Elektroenergetyki
ul. Piotrowo 3a, 61-138 Poznań

Poznań 06.09.2022

Oświadczenie o współautorstwie

Potwierdzam udział w publikacjach:

1. Karol Nowak, Jerzy Janiszewski, Grzegorz Dombek: „Thyristor Arc Eliminator for Protection of Low Voltage Electrical Equipment". Energies 2019, 12(14), 2749;

2. Karol Nowak, Jerzy Janiszewski, Grzegorz Dombek: „A Multi-Sectional Arc Eliminator for Protection of Low Voltage Electrical Equipment". Energies 2020, 13(3), 605;

3. Karol Nowak, Jerzy Janiszewski, Grzegorz Dombek: „The Possibilities to Reduce Arc Flash Exposure with Arc Fault Eliminators". Energies 2021, 14(7), 1927;

4. Karol Nowak, Jerzy Janiszewski, Grzegorz Dombek: „A New Short-Circuit Hybrid Device for the Protection of Low-Voltage Networks From the Effects of an Arc Fault". IEEE Access 2022, vol. 10, pp. 88678-88691;

Mój udział w publikacjach 1,2 i 3 szacowany jest na 30% i obejmuje wsparcie naukowe, analizę danych, przygotowanie artykułu oraz opiekę merytoryczną.
Mój udział w publikacji 4 szacowany jest na 10% i obejmuje wsparcie naukowe, analizę danych oraz opiekę merytoryczną.

……
Jerzy Janiszewski

dr inż. Grzegorz Dombek
Wydział Inżynierii Środowiska i Energetyki
Politechnika Poznańska
Instytut Elektroenergetyki
ul. Piotrowo 3a, 61-138 Poznań

Poznań 30.08.2022

Oświadczenie o współautorstwie

Potwierdzam udział w publikacjach:

1. Karol Nowak, Jerzy Janiszewski, Grzegorz Dombek: „Thyristor Arc Eliminator for Protection of Low Voltage Electrical Equipment". Energies 2019, 12(14), 2749;

2. Karol Nowak, Jerzy Janiszewski, Grzegorz Dombek: „A Multi-Sectional Arc Eliminator for Protection of Low Voltage Electrical Equipment". Energies 2020, 13(3), 605;

3. Karol Nowak, Jerzy Janiszewski, Grzegorz Dombek: „The Possibilities to Reduce Arc Flash Exposure with Arc Fault Eliminators". Energies 2021, 14(7), 1927;

4. Karol Nowak, Jerzy Janiszewski, Grzegorz Dombek: „A New Short-Circuit Hybrid Device for the Protection of Low-Voltage Networks From the Effects of an Arc Fault". IEEE Access 2022, vol. 10, pp. 88678-88691;

Mój udział w publikacjach 1,2,3 i 4 szacowany jest na 10% i obejmuje wsparcie naukowe oraz opiekę merytoryczną.

……

Grzegorz Dombek